Report
P-17-22
February 2020

Äspö Hard Rock Laboratory

Äspö Pillar Stability Experiment

Three-dimensional mechanical discontinuum modelling of the de-stressing slot drilling at the APSE site

Diego Mas Ivars

SVENSK KÄRNBRÄNSLEHANTERING AB

SWEDISH NUCLEAR FUEL
AND WASTE MANAGEMENT CO

Box 3091, SE-169 03 Solna
Phone +46 8 459 84 00
skb.se

SVENSK KÄRNBRÄNSLEHANTERING

ISSN 1651-4416
SKB P-17-22
ID 1591652
February 2020

Äspö Hard Rock Laboratory

Äspö Pillar Stability Experiment

Three-dimensional mechanical discontinuum modelling of the de-stressing slot drilling at the APSE site

Diego Mas Ivars, Itasca Geomekanik AB

Abstract

At the Äspö Pillar Stability Experiment (APSE) site a large thermal loading field test has been performed (Andersson 2004). To enable the removal and mapping of the tested pillar, a de-stressing slot was drilled. There were no stress measurements while drilling this de-stressing slot. For this reason, and to better understand the previous field experiments conducted at the site, a three-dimensional mechanical numerical analysis of the redistribution of the stresses during the drilling of the de-stressing slot has been carried out with the distinct element code 3DEC.

The main objective of this modelling exercise was to assess the influence of the larger fractures in the study volume, by comparing a continuum simulation with a discontinuum simulation (explicitly representing the larger fractures in the study volume in the numerical model). An additional objective for this project was to serve as prediction of the current state of stress for core disking studies at the APSE site. For this reason, a last step was included in this numerical study in which the pillar was removed, and the stress field simulated. The results of this last step are presented in the appendix of this report.

The results show that the stress field is symmetric before, during and after the whole de-stressing period for the continuum model, as expected. On the other hand, there is a clear asymmetry in the stress field in every step of the simulation in the discontinuum case. In this case, the maximum stress in the near field surrounding the deposition hole DQ0066G01 is much lower, in every step, than that of the deposition hole DQ0063G01. This asymmetry is caused by the stress release induced by movements along fractures 08 and 14 (see figure below). The results support the conclusion that fractures 08 and 14 have played a significant role in the redistribution of stresses around the deposition holes at the APSE site.

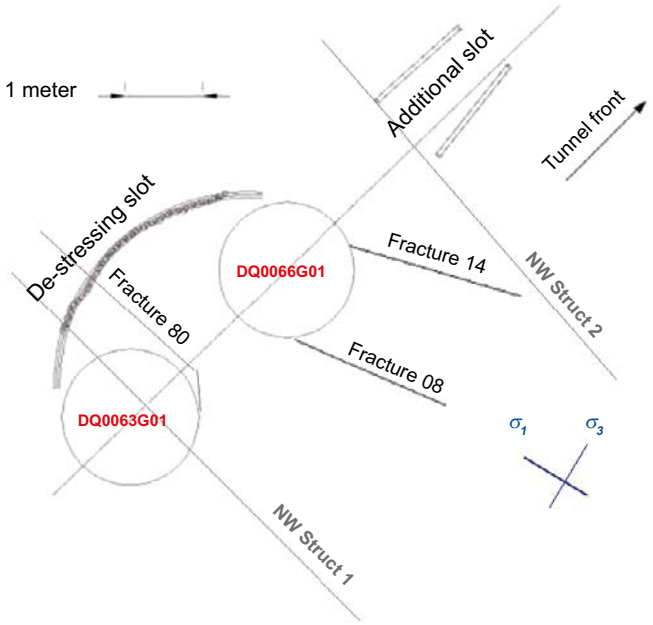

Layout of the HM data acquisition experiment (Mas Ivars 2005) (not to scale).

Sammanfattning

Ett stort termiskt belastningstest har utförts i Äspölaboratoriet, det så kallade ”Äspö Pillar Stability Experiment” (APSE) (Andersson 2004). För att möjliggöra en borttagning samt kartläggning av den testade pelaren borrades en avlastningsslits. Detta gjordes utan att spänningen mättes. På grund av detta samt för att få en bättre förståelse av tidigare resultat i fälttestet utfördes en tredimensionell numerisk analys av spänningsomfördelningar under borrningen av avlastningsslitsen. Detta gjordes med data-programmet 3DEC.

Huvudmålet med denna modellering var att bedömma hur mycket de större sprickorna påverkar det studerade området genom att jämföra en kontinuum-modell med en diskontinuum-modell (de stora sprickorna i det studerade området representeras explicit i modellen). Ytterligare ett mål för projektet var att ge en prognos av det nuvarande spänningstillståndet för studier av ”core disking” i APSE-tunneln. På grund av detta lades ett sista steg till den numeriska analysen, det när pelaren togs bort och spänningsfältet simulerades. Resultaten av detta sista steg presenteras i rapportens appendix.

Resultaten visar, som förväntat, på att spänningsfältet är symmetriskt före, under och efter avlastnings-perioden för kontinuum-simuleringen. Å andra sidan fås en klar asymmetri i spänningsfältet i varje steg av diskontinuum-simuleringen. I detta fall är den maximala spänningen i närfältet till deponerings hål DQ0066G01 mycket lägre i varje steg än den maximala spänningen vid deponerings hål DQ0063G01. Denna asymmetri beror på spänningsrelaxation på grund av rörelser längs med sprickorna 08 och 14 (se figuren nedan). Resultaten stödjer slutsatsen att spricka 08 och 14 har spelat en betydande roll i omfördelningen av spänningar runt deponeringshålen i APSE-tunneln.

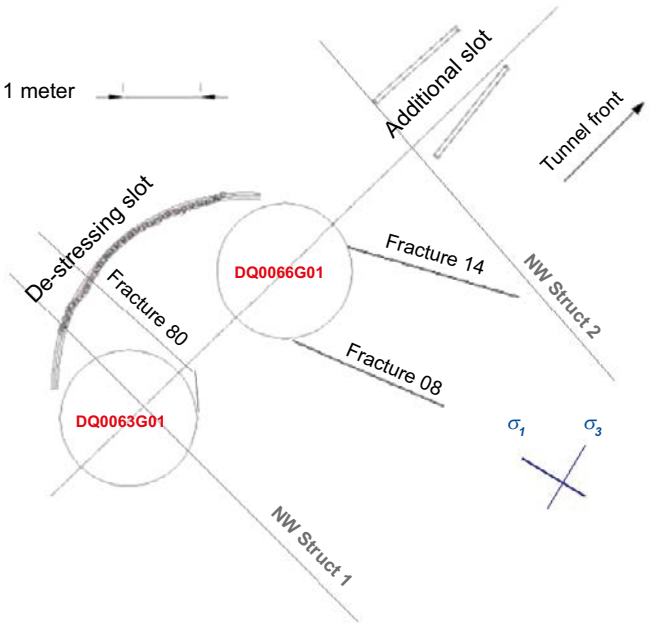

Layout of the HM data acquisition experiment (Mas Ivars 2005) (not to scale).

Contents

1 Introduction

One of the recent experiments performed by the Swedish Nuclear Fuel and Waste Management Co (SKB) has been the Äspö Pillar Stability Experiment (APSE). This experiment was designed to demonstrate the ability to predict spalling in a fractured rock mass, to consider the effect of backfill on the rock mass response, and to compare the capabilities of 2D and 3D numerical models. The experiment was carried out at 450 m depth at the Äspö HRL. High stresses were induced by excavating a tunnel with curved floor and by boring two vertical boreholes of deposition hole size (1.8 m diameter) close to each other (Figure 1-1). To further increase the stress, the rock volume between the boreholes was heated. The effect of confining pressure was also studied by applying a uniform pressure of 0.7 MPa from a rubber blather to the wall of the first hole drilled. The pressure was maintained during drilling of the second hole and the heating phase. After the heating, the pressure was stepwise reduced while the rock mass response was monitored by acoustic emission (Andersson 2004).

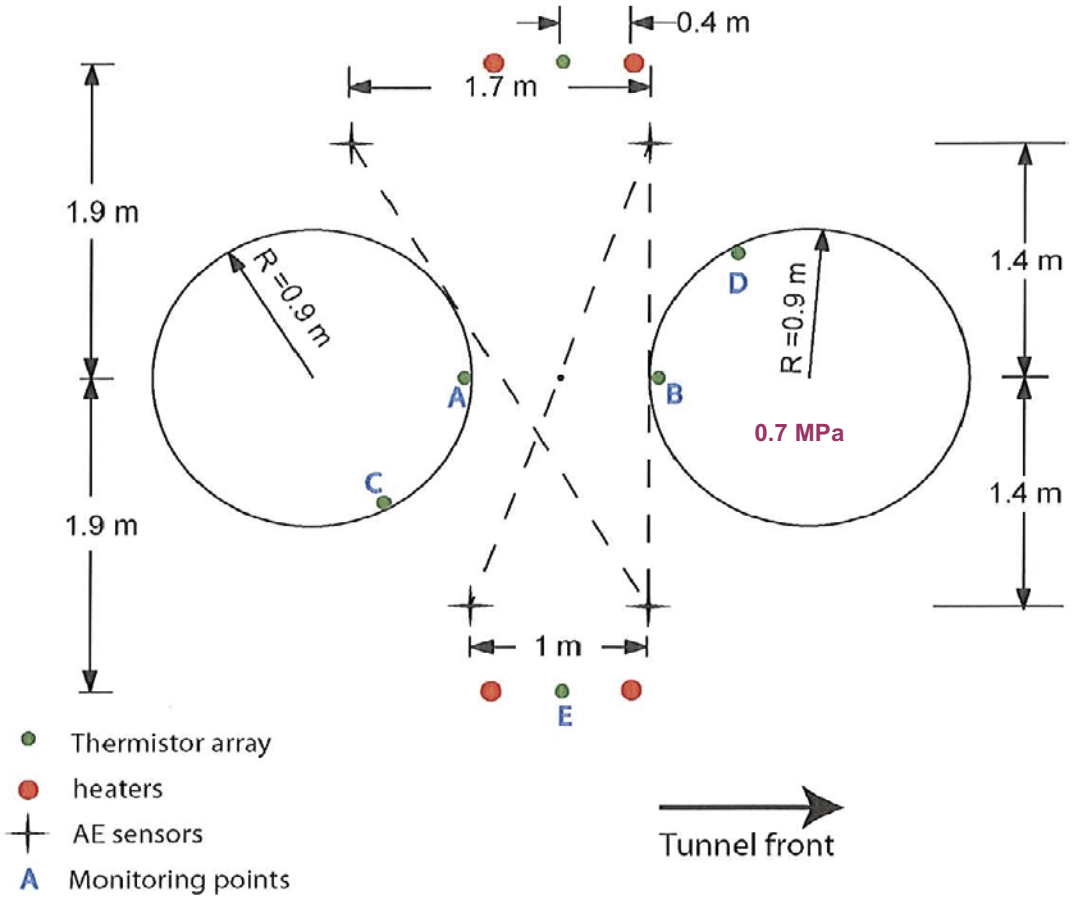

Figure 1-1. *Layout of the APSE experiment (Andersson 2004).*

One of the last phases of the APSE project involved the extraction of the pillar between the holes to study the effect of high stress concentrations obtained during the experiment. Before cutting and extracting the pillar, it had to be de-stressed. The de-stressing of the pillar was carried out by drilling a semi-circular array of boreholes (Figure 1-2). During this phase of the APSE project a large field experiment was conducted with the aim of acquiring hydro-mechanical data during the drilling of the de-stressing slot.The de-stressing of the pillar was expected to cause a number of coupled hydro-mechanical effects in two highly conductive sub-vertical fractures intersecting borehole DQ0066G01 (Figure 1-2). The effective normal stress acting on the fractures was expected to change, affecting the fracture aperture and consequently the inflow. In addition, the change in normal stress would affect the fracture shear strength, which, combined with the change in shear stress along the fracture, could lead to slip and dilation of the fracture. Therefore, fracture displacements, fracture inflow and total inflow into borehole DQ0066G01 were monitored during the drilling of the slot.

Fracture normal openings of up to 0.6 mm and shear displacements of up to 0.9 mm were registered during the drilling of the slot. The inflow coming from fracture 08 increased from 2.4 l/min to 4 l/min, and the inflow from fracture 14 increased from 6.1 l/min to 18 l/min. The water pressure was monitored at several locations during the experiment to be able to assess the influence of the drilling of the de-stressing slot on the hydraulic response of the surrounding rock mass. Strong responses were registered at several locations (Mas Ivars 2005).

There were no stress measurements while drilling the de-stressing slot. For this reason, and to better understand the previous field studies conducted at the APSE site, a three-dimensional mechanical numerical analysis of the redistribution of the stress during the drilling of the de-stressing slot has been carried out with the distinct element code 3DEC (Itasca 2003). This simulation includes the effect of the main fractures in the study volume.

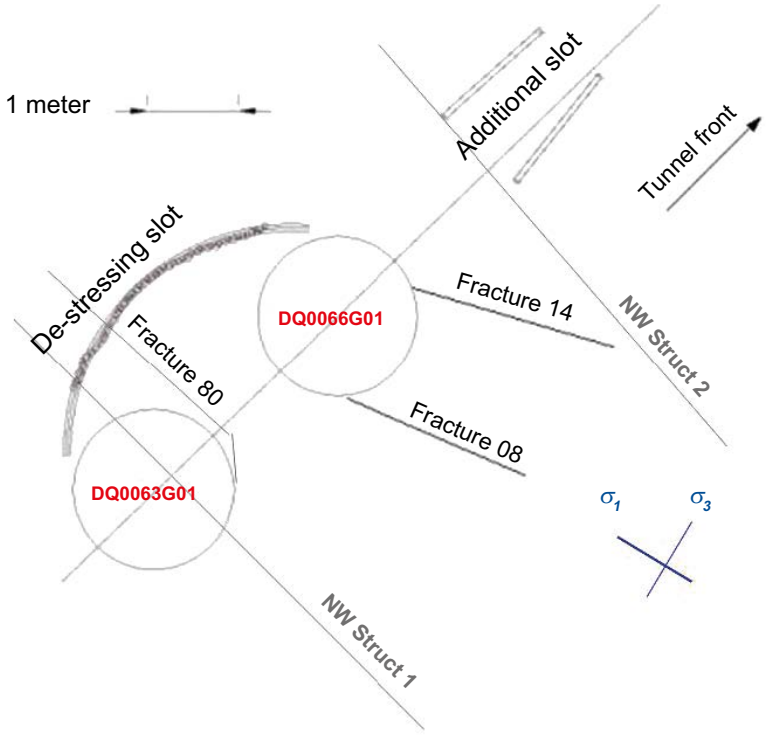

Figure 1-2. *Layout of the HM data acquisition experiment (Mas Ivars 2005). The fractures shown in this figure have been included explicitly in the 3DEC modelling study presented in this report (not to scale).*

2 Objectives of the modelling study

A complete numerical study of the stress evolution during the APSE experiment can be found in Andersson (2004), Fredriksson et al. (2004), Rinne et al. (2004) and Wanne et al. (2004). Since the thermal load phase is already included in these reports, it hasn't been modelled in the present study.

Due to the specific geometry of the APSE experiment, which is non-symmetrical, and the three-dimensional nature of the problem studied in this report, a three-dimensional model is judged appropriate to be able to simulate the complex stress re-distribution during the drilling of the de-stressing slot.

The main objectives of this modelling project are:

- To study and analyze the stress re-distribution during the drilling of the de-stressing slot to better understand the results from the previous field experiments in the APSE site.
- To assess the influence of the larger fractures in the study volume by comparing a continuum simulation with a discontinuum simulation (explicitly representing in the model the larger fractures in the study volume) of the re-distribution of the stresses in the APSE site during the drilling of the de-stressing slot.
- To serve as prediction of the current state of stress for core disking studies at the APSE site. For this reason, a last step was included in this numerical study in which the pillar is removed from the model and the final stress field simulated. The results of this last step are presented in the appendix of this report.

3 Modelling approach

The three-dimensional distinct element code *3DEC* (Itasca 2003) was used to perform the numerical simulations. This code is suited to simulate the behaviour of rock masses containing multiple, intersecting discontinuities.

3.1 Geological overview

A detailed geological description of the TASQ tunnel can be found in Staub et al. (2003, 2004) and Magnor (2004). According to these reports, the geology and rock mechanics properties in the tunnel TASQ area are similar to those found elsewhere in the 450 m level of the Äspö HRL. The only exception to this similarity is a heavily oxidized, brittle-ductile shear zone striking along the TASQ-tunnel and dipping southeast (Figure 3-1). There is no crush zone or open fractures associated to the shear zone, which appears quite old and sealed. However, the strength of the rock in the shear zone is considerably lower than that of fresh Äspö diorite. High stress concentration could induce yielding of the shear zone and its deformation could cause a re-distribution of stresses that would influence the spalling process. Since the final assessment about the influence of the shear zone on the APSE experiment concluded that the presence of this feature would not endanger the outcome of the APSE experiment, this feature was not included in the conceptual model.

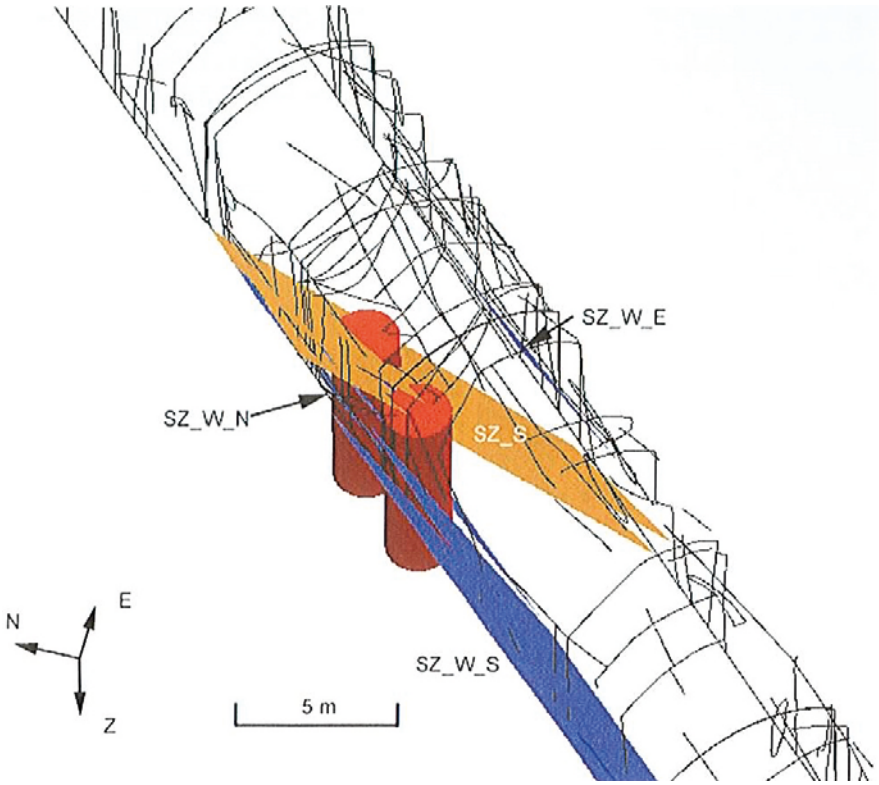

Figure 3-1. *3D visualization of the shear zone. The red cylinders are a visualization of the deposition size holes (Staub et al. 2004).*

3.2 Conceptual model

In order to get more familiar with the rock mass in the APSE volume and to identify the fractures that should be included in the conceptual model, a detailed mapping of the pillar walls and blocks from the APSE experiment was performed. Based on this detailed mapping and on the previous available geological information, the conceptual model of the study volume was created.

3.2.1 Geometry

The geometrical model consisted of the TASQ tunnel, the two individual deposition size holes at the APSE site, the two additional slots excavated before the drilling of the de-stressing slot, the de-stressing slot, and the part of the pillar that was removed. All this elements were embedded in a parallelepiped of rock of 34 m × 50 m in horizontal section and 40 m in height, considered large enough to avoid any mechanical boundary effects. The sides of the parallelepiped were created perpendicular to the principal stress directions. A schematic view of the model containing the tunnel and the deposition holes can be seen in Figure 3-2.

The two additional slots, of one meter depth, were drilled prior to the drilling of the de-stressing slot in order to avoid the cutter for the removal of the pillar to get jammed, and to study the EDZ at the TASQ tunnel.

The mesh, shown in Figure 3-3, consisted of four-node tetrahedral elements which had a minimum side length of 0.2 m in the center of the model, in an area that comprised the deposition holes, the pillar and the de-stressing slot. The mesh becomes gradually coarser with the increase of the distance to the center of the model. The model was discretised in a total number of 853 631 tetrahedral elements and 249 521 nodes.

The fractures included in the model based on the geological information and the mapping performed are listed in Table 3-1. Their location relative to the APSE area is shown in Figure 1-2.

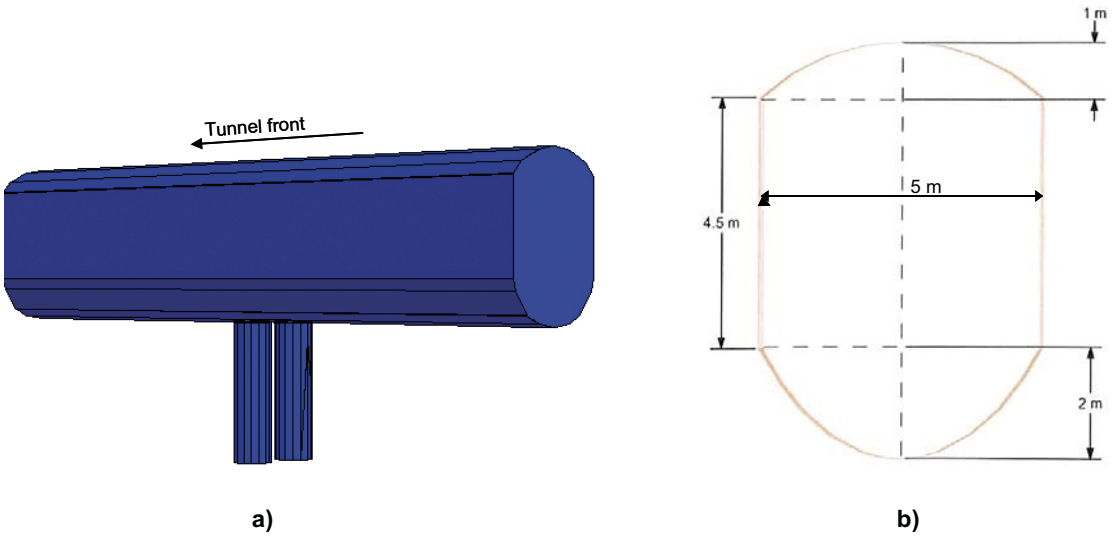

Figure 3-2. *Schematic view showing a) three-dimensional model of the TASQ tunnel and the APSE deposition holes, and b) vertical section of the TASQ tunnel (Staub et al. 2004).*

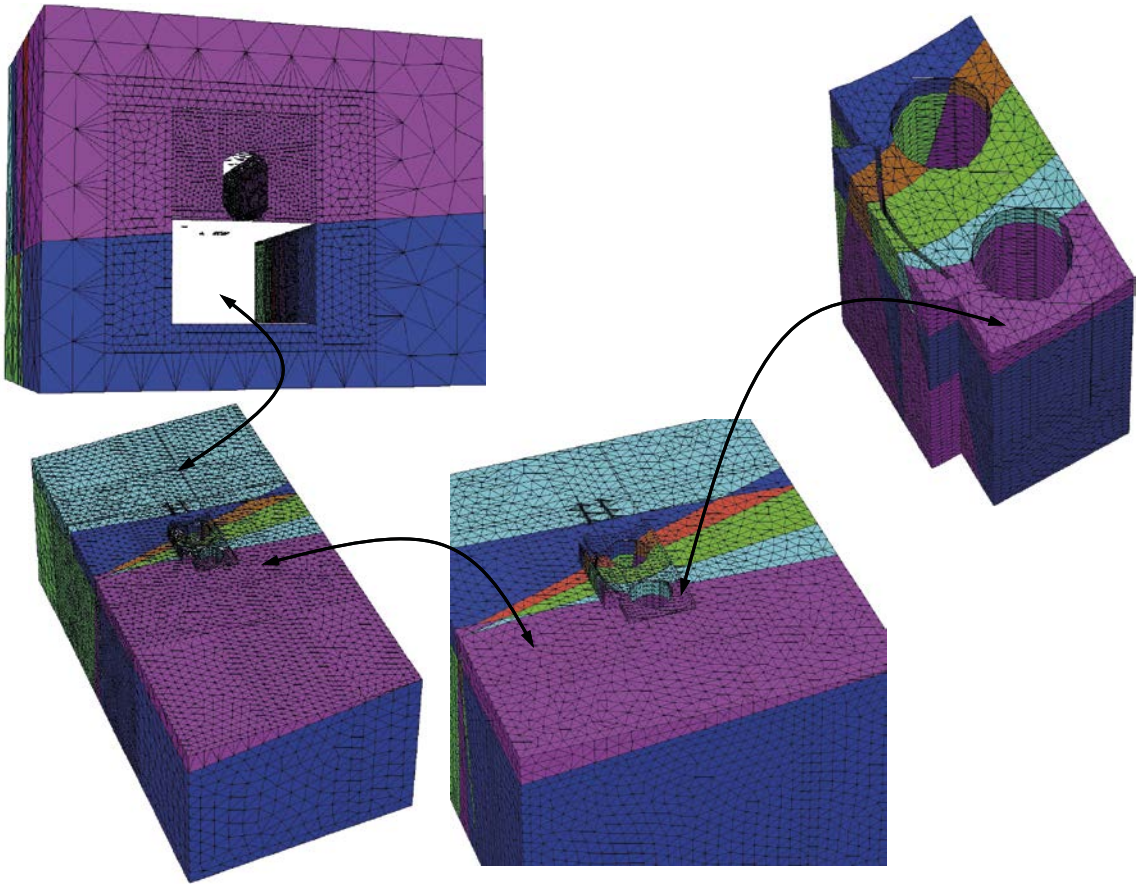

Figure 3-3. *The model mesh.*

Table 3-1. Fractures included in the model.

	Dip (degrees)	Dip direction (degrees)	Comments
Fracture 08	84	74	
Fracture 14	85	250	
Fracture 80	90	83	Initial pre-existing segment of fracture 80 crossing through the de-stressing slot. It is assumed that during the APSE experiment it propagated until intersecting deposition hole DQ0063G01 (see Figure 1-2: red segment of fracture 80).
NW structure 1	81	93	
NW structure 2	81	93	
Sub-horizontal fracture	5	180	Intersecting the centre of the pillar (X = 0; Z = 0) at 0.7 m depth from the tunnel floor.

The model has a continuum rock mass buffer of 4 m thickness in each of the boundaries. This is included to represent the far field rock mass. This means the plane that represents each of these fractures in the model can prolong only until it reaches this rock buffer in any direction. Figure 3-4 shows the model of the tunnel and the deposition holes including the fractures listed in Table 3-1.

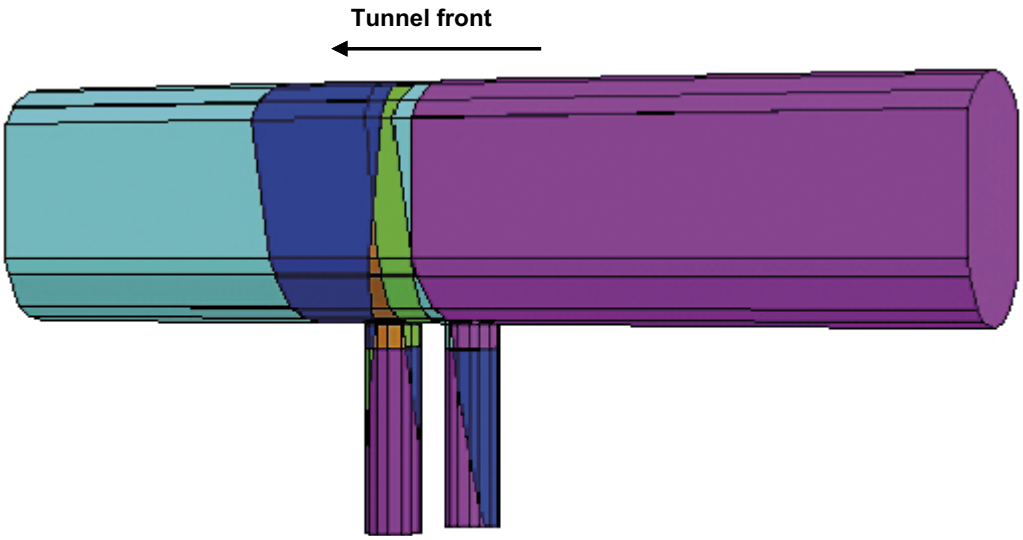

Figure 3-4. *Three-dimensional model of the TASQ tunnel and the APSE deposition holes including the fractures listed in Table 3-1.*

3.2.2 In situ and boundary conditions

The in situ and boundary conditions considered in the model are as follows:

- Hydrostatic water pore pressure (4.5 MPa at the depth level considered) was applied in the discontinuities (fractures).
- The in situ stress applied, shown in Table 3-2, was obtained from results from convergence measurements made during the excavation of the TASQ tunnel (Andersson 2004). The approximate orientation of the major and minor principal stress relative to the APSE tunnel axis is shown in Figure 1-2.

Table 3-2. In situ stress tensor derived by back calculation of the convergence measurements using a Young's modulus of 55 GPa.

	Magnitude (MPa)	Trend/Plunge (degrees)
Sigma 1	30	310/00
Sigma 2	15	090/90
Sigma 3	10	220/00

TASQ tunnel orientation is 046°.

- Roller boundary conditions were applied to the lateral and bottom boundaries, so displacement in the normal direction of these surfaces wasn't allowed.
- In the upper boundary the vertical principal stress (σ_2) was applied as boundary condition.

3.2.3 Rock material properties

A linear elastic constitutive model was adopted for the rock. Two different cases were modeled; the first with rock mass properties and the second with intact rock properties. The material parameters used in each of these cases are shown in Table 3-3.

Table 3-3. Material parameters of the rock (Andersson 2004).

	E (GPa)	*v*	*P* (kg/m^3)
Rock mass	55	0.26	2731
Intact rock	76	0.25	2731

In the first case, the rock mass case, the rock surrounding the explicitly included fractures is considered to contain smaller fractures that change its behavior. When the rock surrounding the explicitly represented fractures is considered intact, the values chosen are derived from the laboratory tests on selected intact rock samples.

The fractures followed a Coulomb slip model in which zero cohesion and tensile strength were assumed. The fracture parameters are shown in Table 3-4.

Table 3-4. Fracture parameters (based on Staub et al. 2003, 2004).

	Kn (GPa/m)	Ks (GPa/m)	Friction angle (degrees)	dilation (degrees)
Fracture 08	61.5	35.5	31	2.5
Fracture 14	61.5	35.5	31	2.5
Fracture 80 (Initial part)*	61.5	35.5	31	2.5
Fracture 80 (New part when active)**	61.5	35.5	40	2.5
NW structure 1	200	100	31	2.5
NW structure 2	200	100	31	2.5
Sub-horizontal fracture	21.9	15.7	30	2.5

* Longer segment of fracture 80 that goes across the de-stressing slot in Figure 1-2.
** Short red segment of fracture 80 that finishes in the deposition hole DQ0063G01 in Figure 1-2.

3.3 Simulation sequence

The simulation sequence followed in this numerical study is as follows:

1. Calculation to initial equilibrium of the parallelepiped of rock mass (all fractures in the model considered non-active).
2. Excavation of the TASQ tunnel. Calculation to equilibrium (all fractures active except for the short red segment of fracture 80 in Figure 1-2).
3. Excavation of the deposition holes. Calculation to equilibrium (the short red segment of fracture 80 in Figure 1-2 is activated as it is assumed to have been created during the APSE experiment. The rest of the fractures are also active).
4. Removal of the part that of the deposition hole DQ0063G01 that fell from the pillar wall due to spalling and calculation to equilibrium (all fractures active).
5. Excavation of both additional slots (Figure 1-2). Calculation to equilibrium (all fractures active).
6. Excavation of the de-stressing slot. Calculation to equilibrium (All fractures active). This part was divided in three stages (Figure 3-5):
   a. Excavation of the central part of the de-stressing slot. Calculation to equilibrium.
   b. Excavation of the lateral right and left middle parts. Calculation to equilibrium.
   c. Excavation of the extreme right and left parts. Calculation to equilibrium.
7. Removal of the pillar. Calculation to equilibrium (all fractures active).

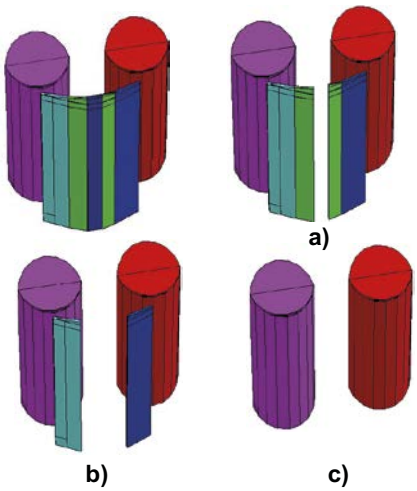

Figure 3-5. *Modelling steps for the excavation of the de-stressing slot in the model, a) central part, b) middle part, and c) extreme right and left parts.*

4 Results

This chapter presents the results for the modelling study described in the previous chapters. As one of the main objectives of this study is to show the effect of the main fractures in the APSE volume on the stress redistribution, we will systematically show the continuum simulated response and the discontinuum simulated response. Figure 4-1 shows the model of the deposition holes, additional slot and de-stressing slot in the continuum and discontinuum cases.

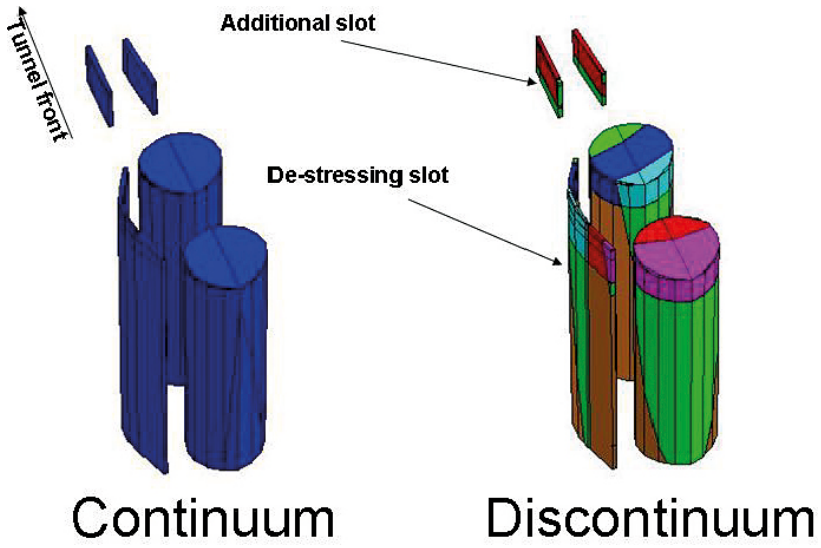

Figure 4-1. *Deposition holes, additional slot and de-stressing slot in the continuum and discontinuum model.*

4.1 Simulated stress response

The following figures present the simulated stress response to the excavation of the TASQ tunnel, the deposition holes, the additional slot and the de-stressing slot. The figures presented in this section correspond to the continuum and discontinuum simulations considering the Young's modulus and Poisson's ratio of the rock mass as in Table 3-3.

As 3DEC is a three-dimensional discontinuum code, it allows stresses to change in a discontinuous manner, creating non-smooth contours. A proper way to show stresses in a discontinuous rock mass is by using principal stress vector plots coloured by magnitude. It must be noted however, that in vector plots (principal stress, traction, velocity, displacement, etc) the length of a vector is affected by the perspective and orientation of observation. This implies that, in cross-section plots, the displayed vectors are projections onto the view plane and, consequently, their length is not indicative of their absolute magnitude. For this reason, the vectors are coloured by magnitude. It should be noticed that the maximum compressive stress magnitude shown under the legend menu is only a very local value and it can be caused by stress concentration in a very small corner of the model due to the complex mesh geometry caused by the presence of many fictitious joints used to define the volumes of the different excavation stages. For this reason, quantitative evaluation of the results should be based on the ranges on the legend. It is important to notice that, in 3DEC, a negative value of stress means compressive stress, and a positive value means tensile stress.

The first set of figures (Figure 4-2 to Figure 4-6) shows the change of the principal stress (colored by magnitude of σ1) projected on a vertical cross section perpendicular to the longitudinal axis of the tunnel in the center of the pillar, from the moment when the TASQ tunnel is excavated (Figure 4-2) until the drilling of the de-stressing slot is complete (Figure 4-6). Both the continuum and the discontinuum model results are included.

The second set of figures (Figure 4-7 to Figure 4-10) shows the change of the principal stress (colored by magnitude of σ_1) projected on a vertical cross-section along the axis of the TASQ tunnel, from the moment when the deposition holes are excavated (Figure 4-7) to the end of the drilling of the de-stressing slot (Figure 4-10). The continuum and discontinuum model results are included.

The third set of figures (Figure 4-11 to Figure 4-14) shows the evolution of the principal stress (colored by magnitude of σ_1) projected on a horizontal cross-section at 1.5 m depth from the floor of the TASQ tunnel, from the moment when the deposition holes are excavated (Figure 4-11) until the drilling of the de-stressing slot is complete (Figure 4-14). Both continuum and discontinuum model results are shown in these figures.

Finally, Figure 4-15 and Figure 4-16 show the principal stress (colored by magnitude of σ_1 and σ_3 respectively) projected on a horizontal cross-section at 1.5 m depth from the floor of the TASQ tunnel before and after the de-stressing slot has been excavated. These figures are included in the report to facilitate the comparison between the continuum and discontinuum model results.

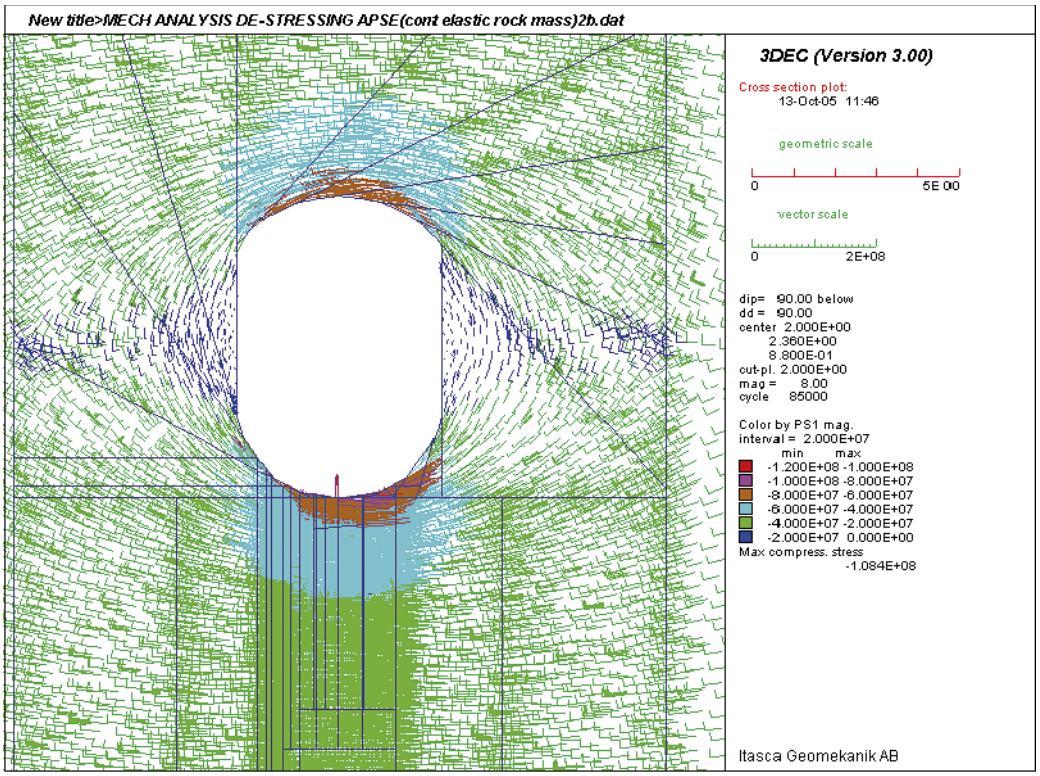

a) Continuum

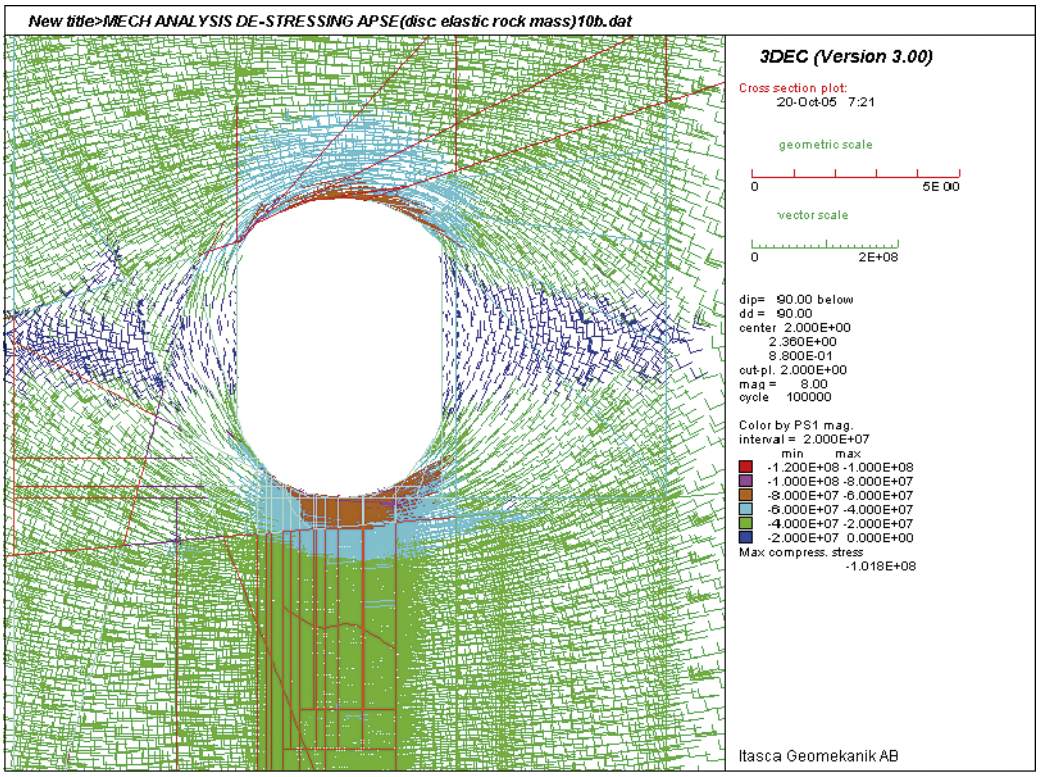

b) Discontinuum

Figure 4-2. *Vertical cross section showing the projected principal stress on the center of the pillar before the deposition holes are excavated (Colors by magnitude of σ1).*

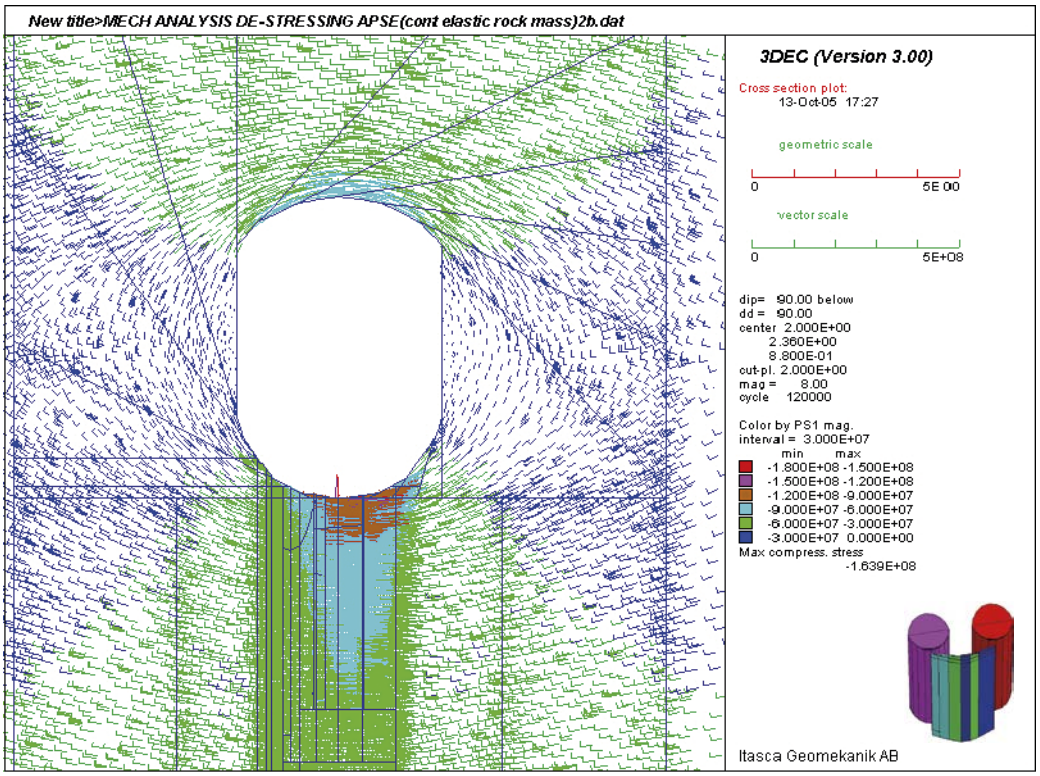

a) Continuum

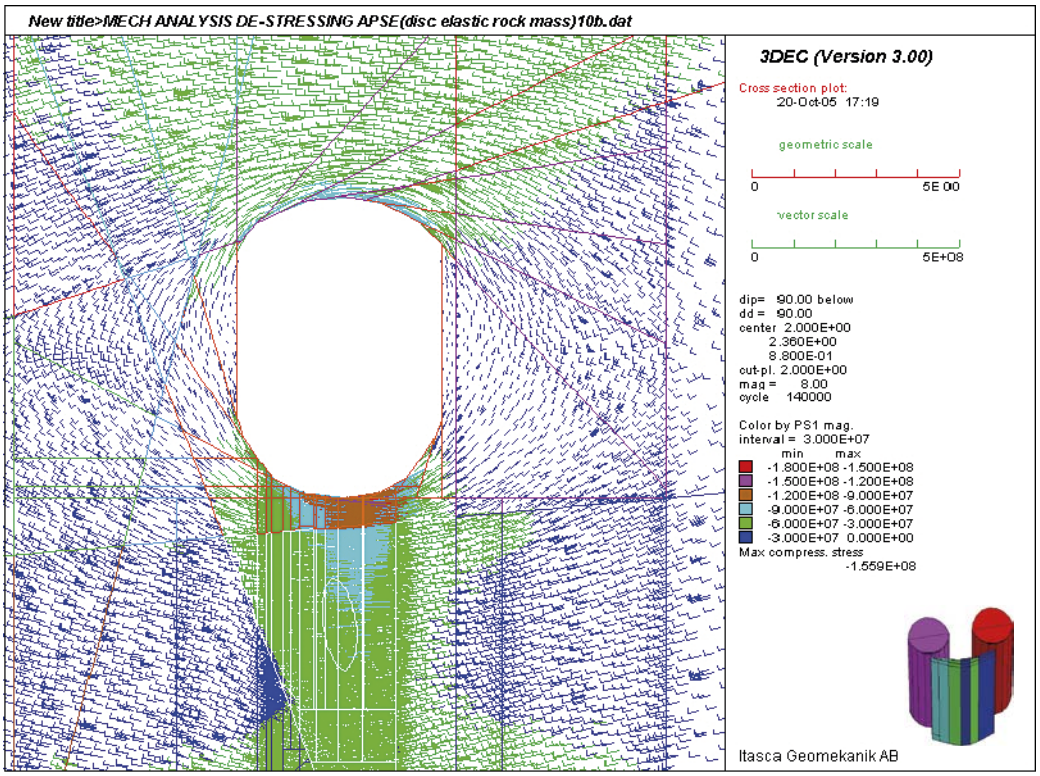

b) Discontinuum

Figure 4-3. *Vertical cross section showing the projected principal stress on the center of the pillar after the deposition holes have been excavated (Colors by magnitude of σ1).*

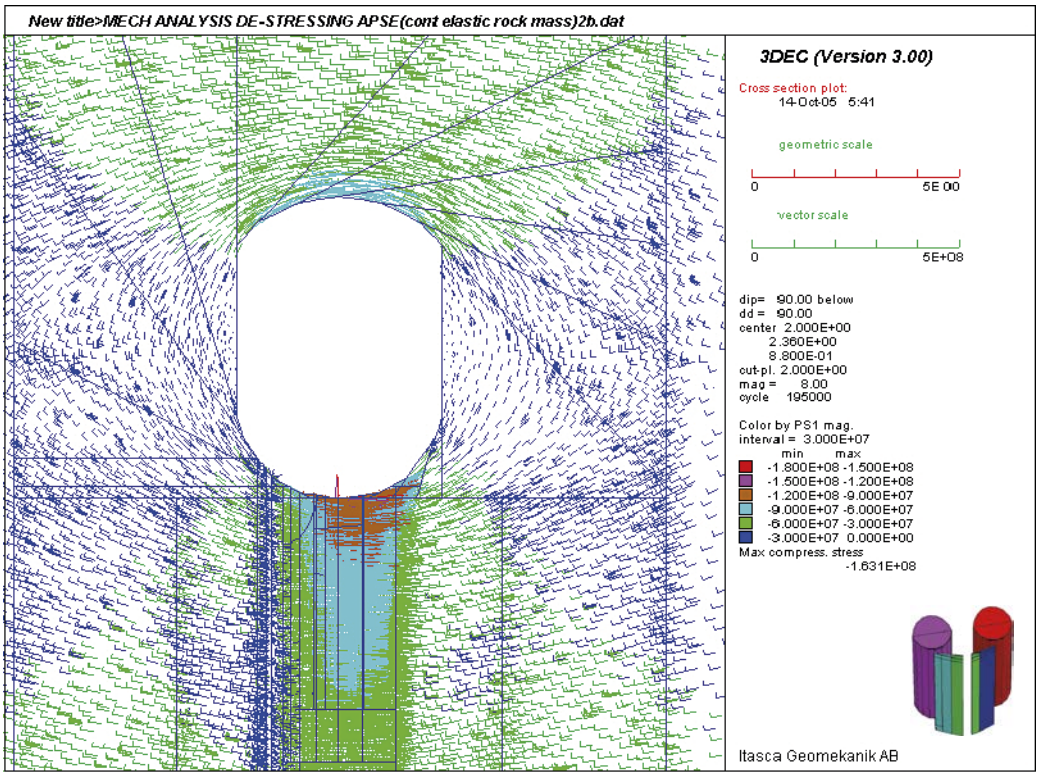

a) Continuum

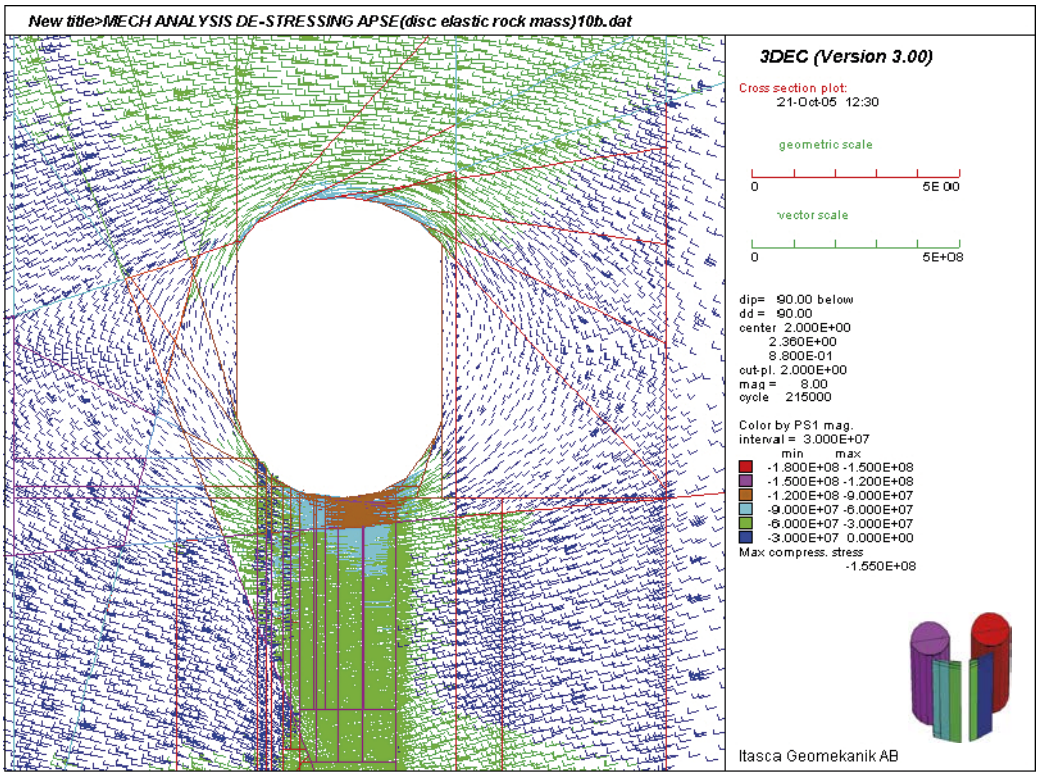

b) Discontinuum

Figure 4-4. *Vertical cross section showing the projected principal stress on the center of the pillar after the central part of the de-stressing slot has been excavated (Colors by magnitude of σ1).*

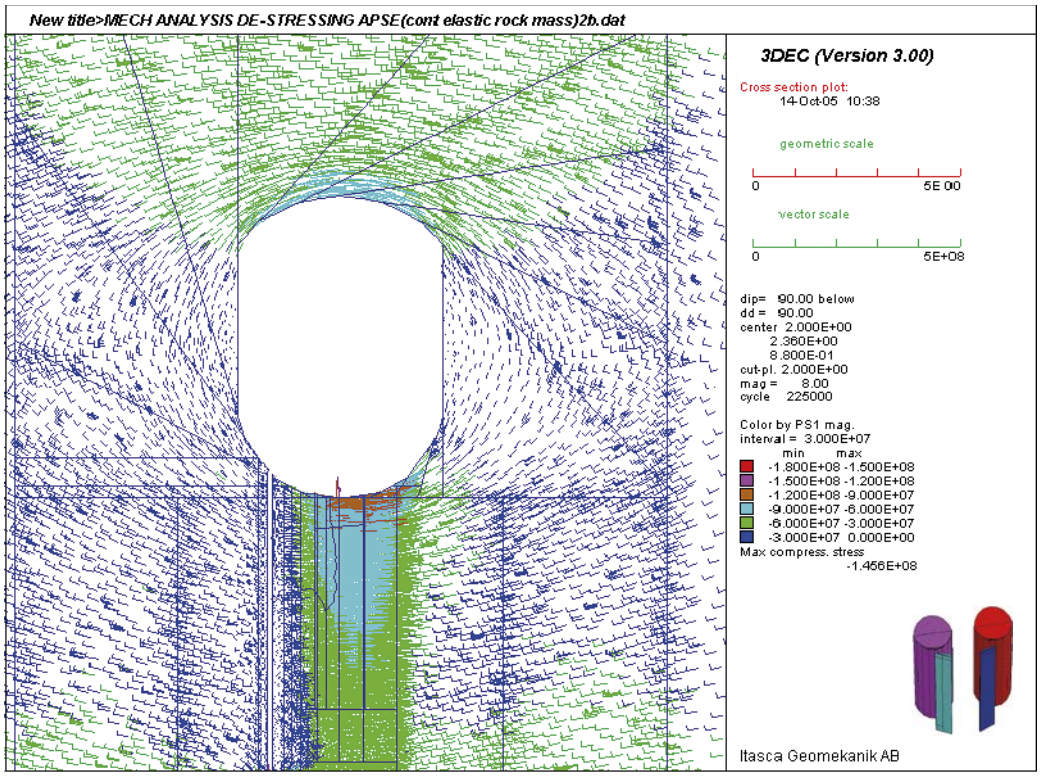

a) Continuum

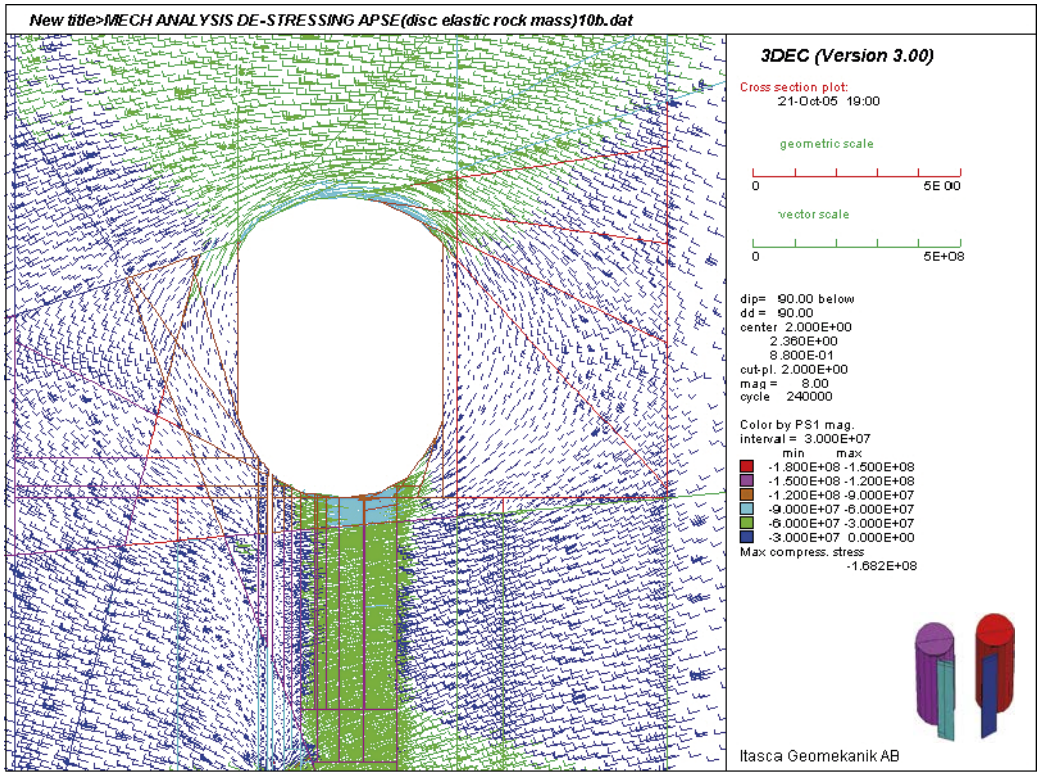

b) Discontinuum

Figure 4-5. *Vertical cross section showing the projected principal stress on the center of the pillar after the middle part of the de-stressing slot has been excavated (Colors by magnitude of σ1).*

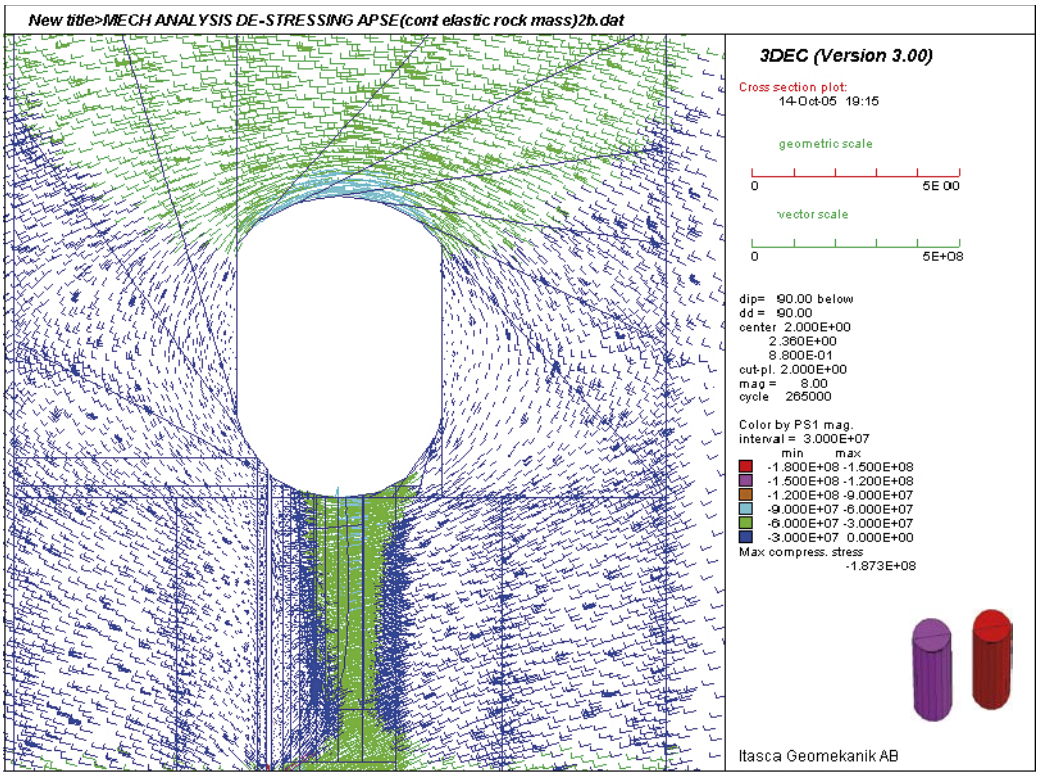

a) Continuum

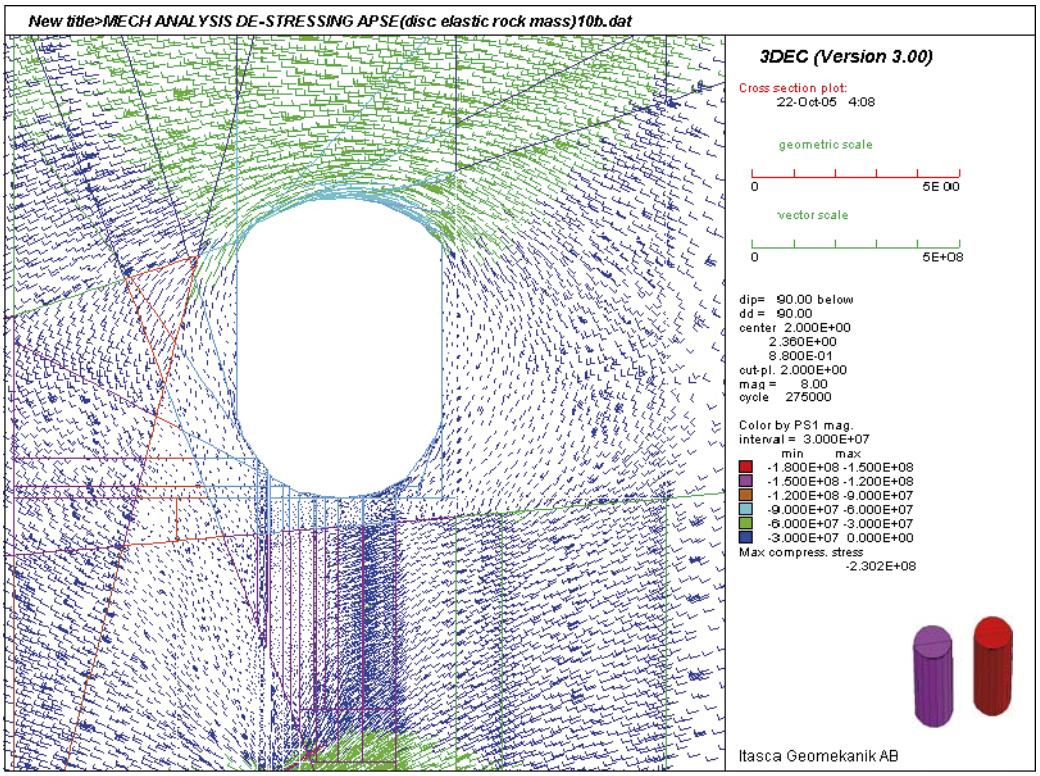

b) Discontinuum

Figure 4-6. *Vertical cross section showing the projected principal stress on the center of the pillar after the whole de-stressing slot has been excavated (Colors by magnitude of σ1).*

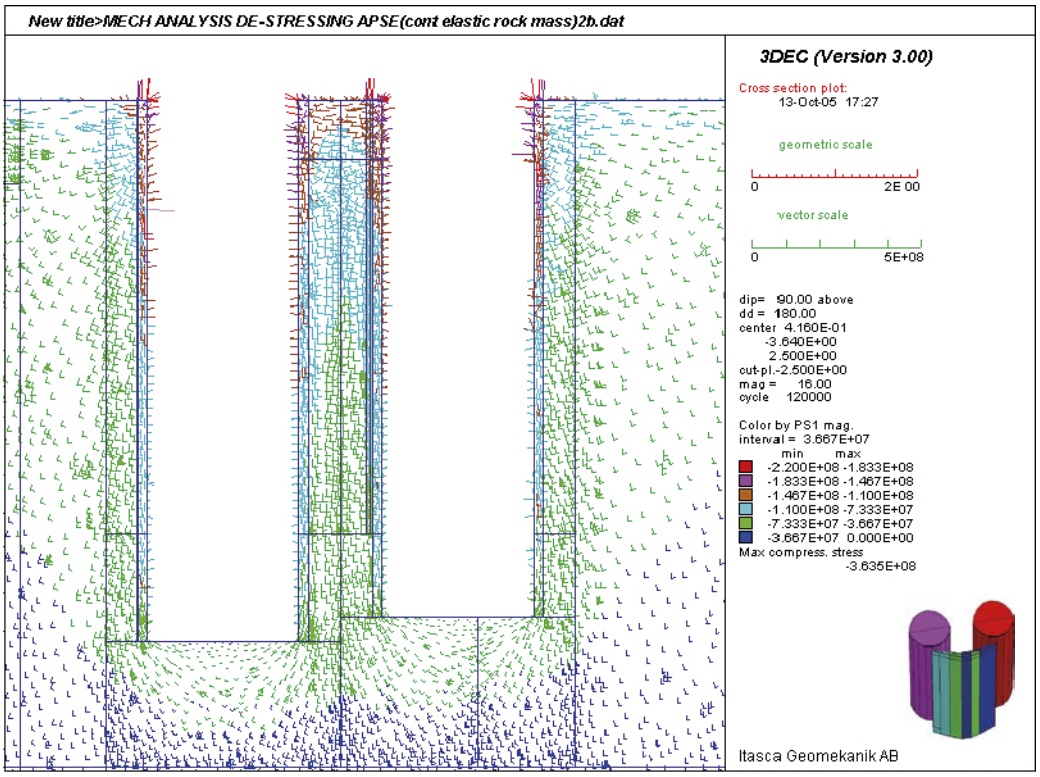

a) Continuum

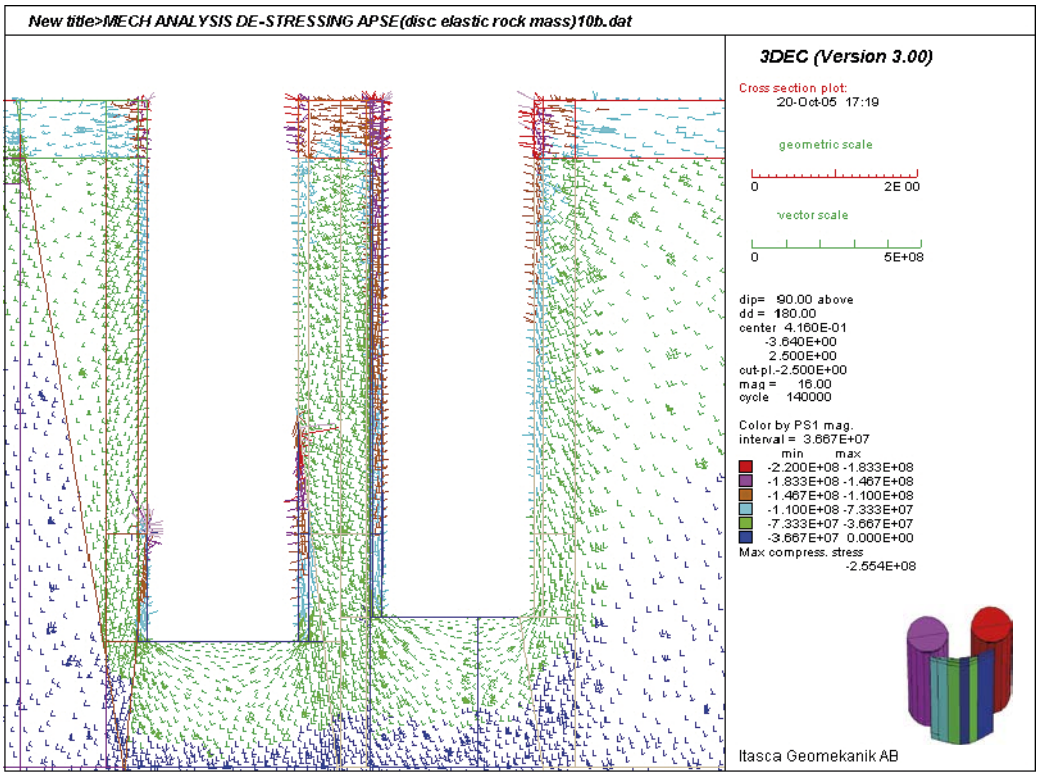

b) Discontinuum

Figure 4-7. *Vertical cross-section showing the projected principal stress along the axis of the tunnel after the deposition holes have been excavated (Colors by magnitude of σ1).*

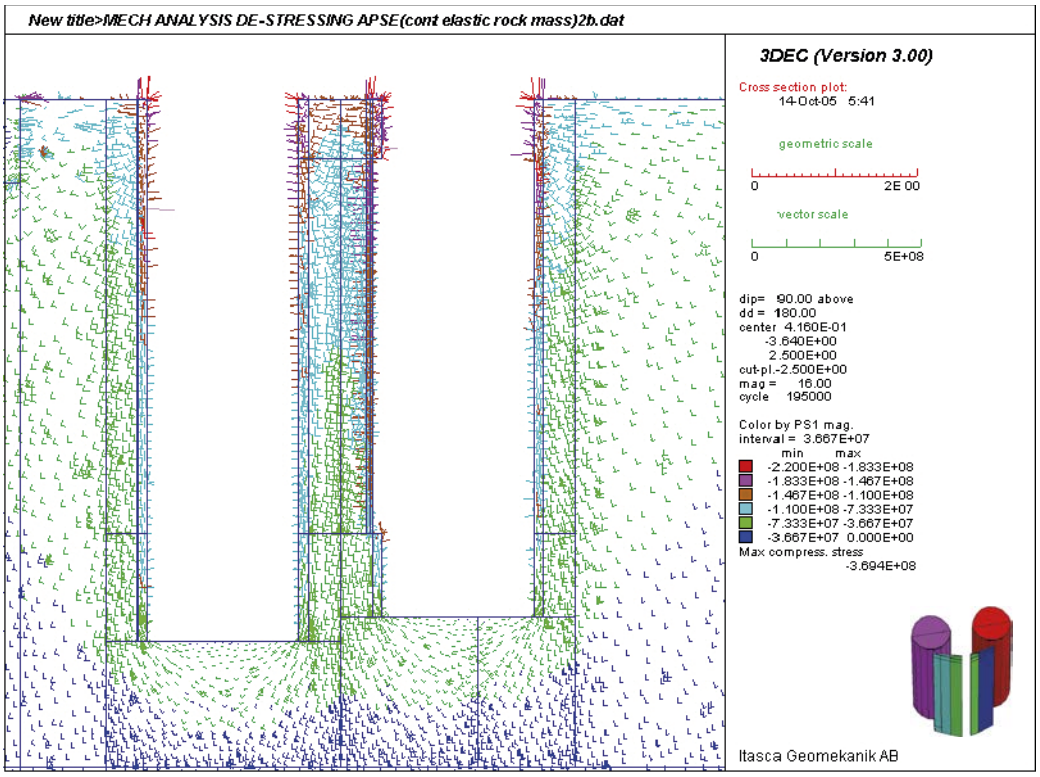

a) Continuum

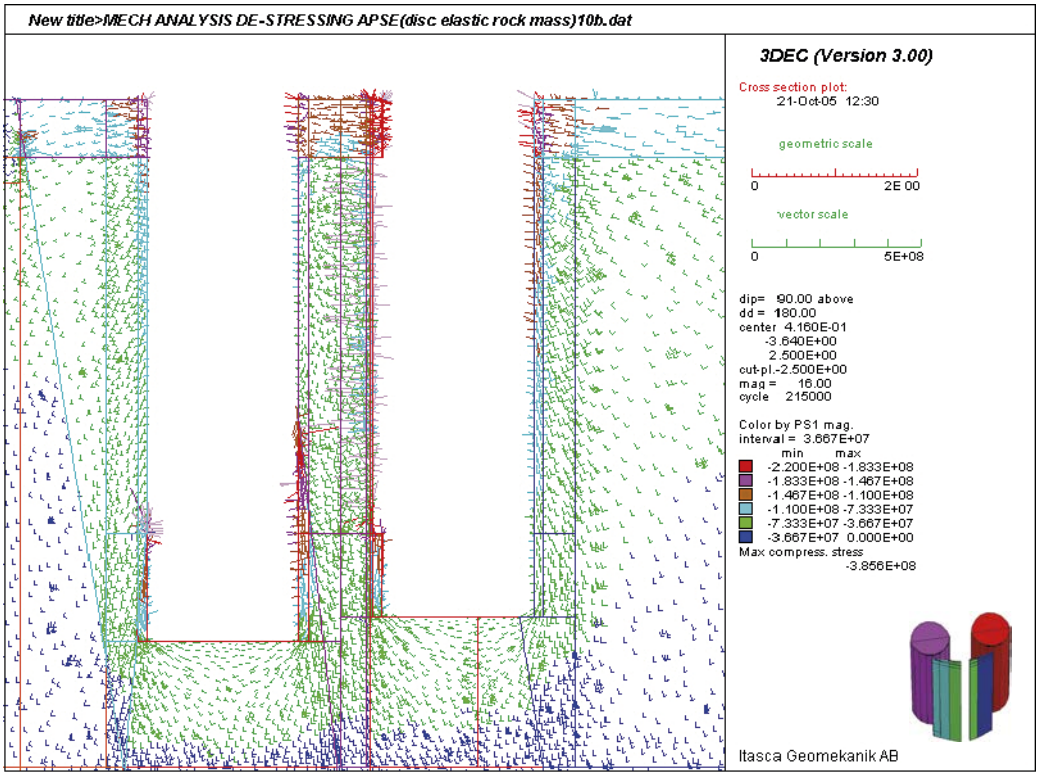

b) Discontinuum

Figure 4-8. *Vertical cross-section showing the projected principal stress along the axis of the tunnel after the central part of the de-stressing slot has been excavated (Colors by magnitude of σ1).*

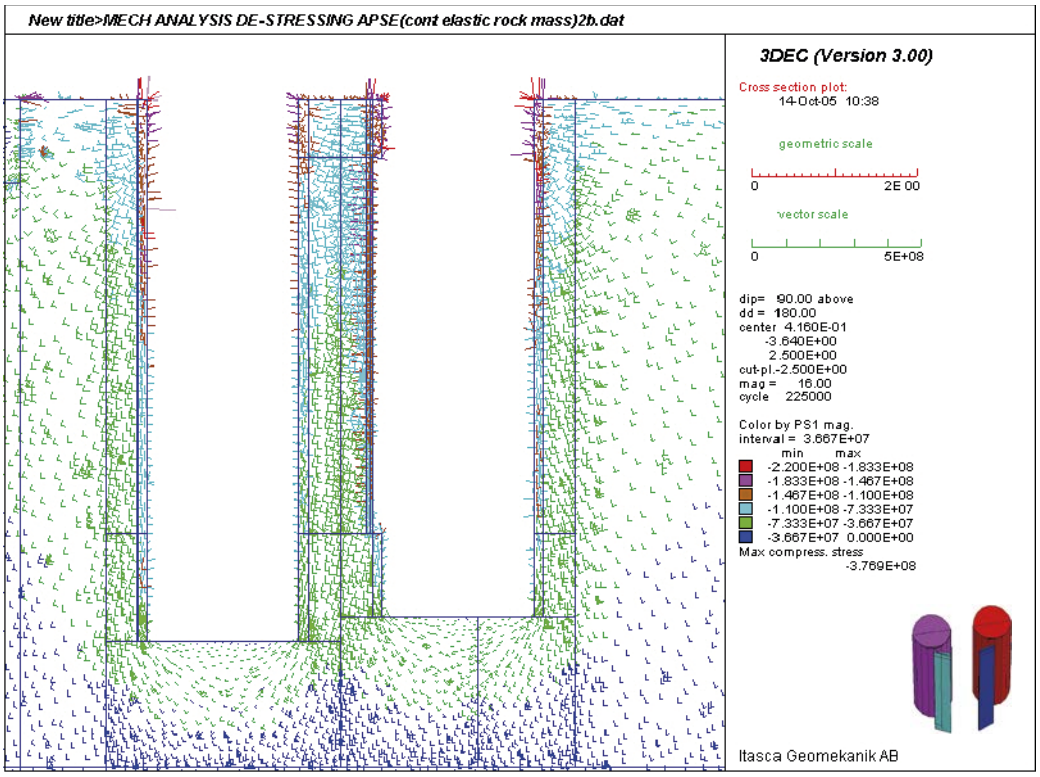

a) Continuum

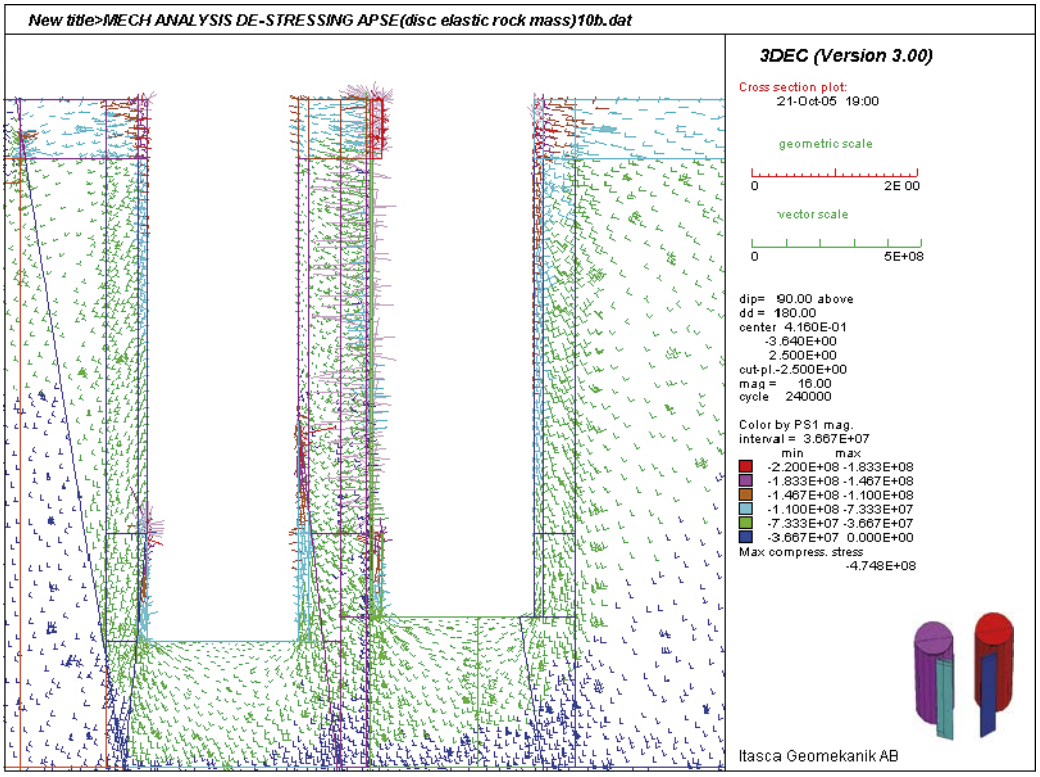

b) Discontinuum

Figure 4-9. *Vertical cross-section showing the projected principal stress along the axis of the tunnel after the middle part of the de-stressing slot has been excavated (Colors by magnitude of σ1).*

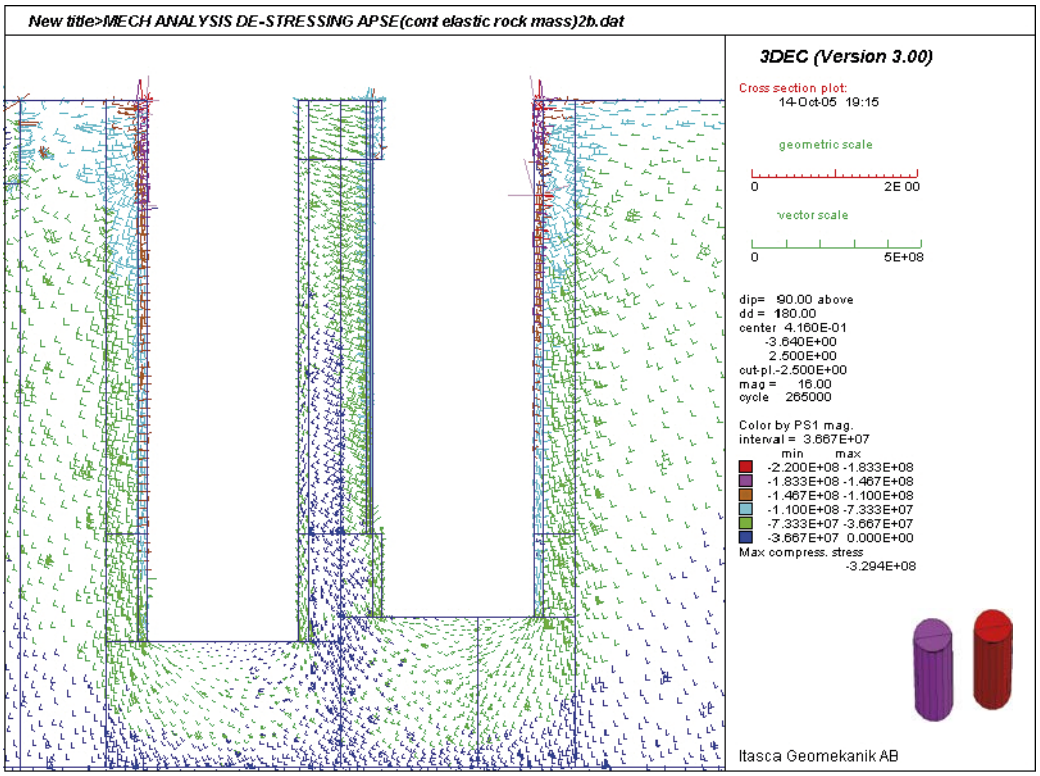

a) Continuum

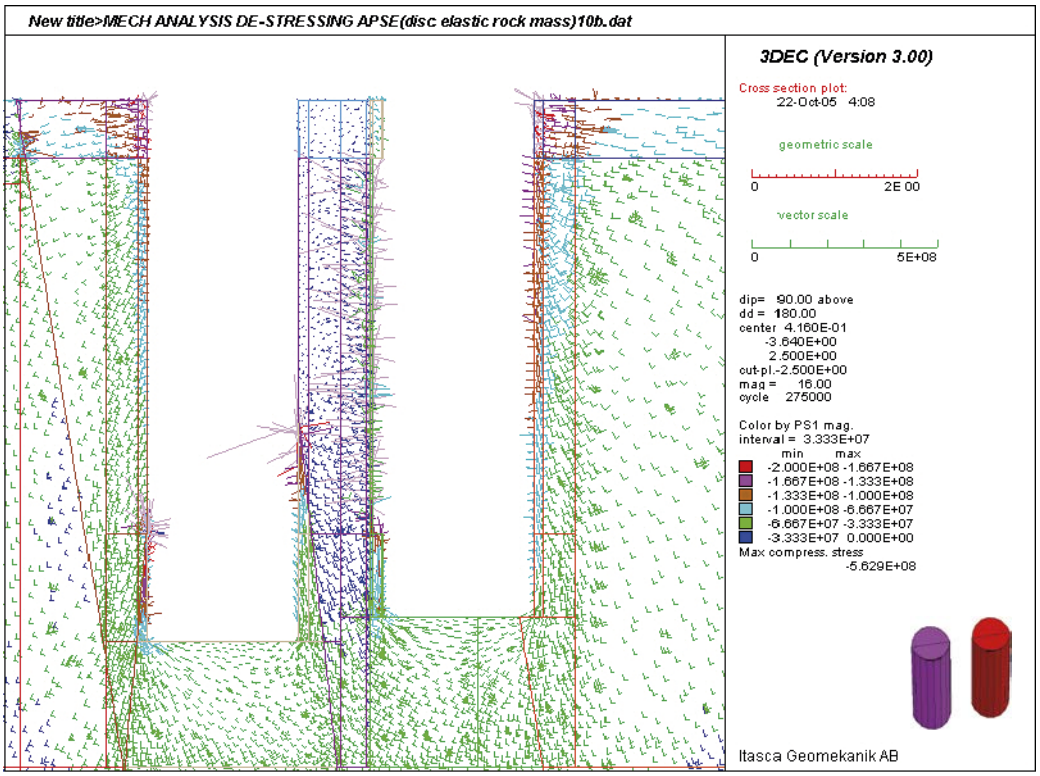

b) Discontinuum

Figure 4-10. *Vertical cross-section showing the projected principal stress along the axis of the tunnel after the whole de-stressing slot has been excavated (Colors by magnitude of σ1).*

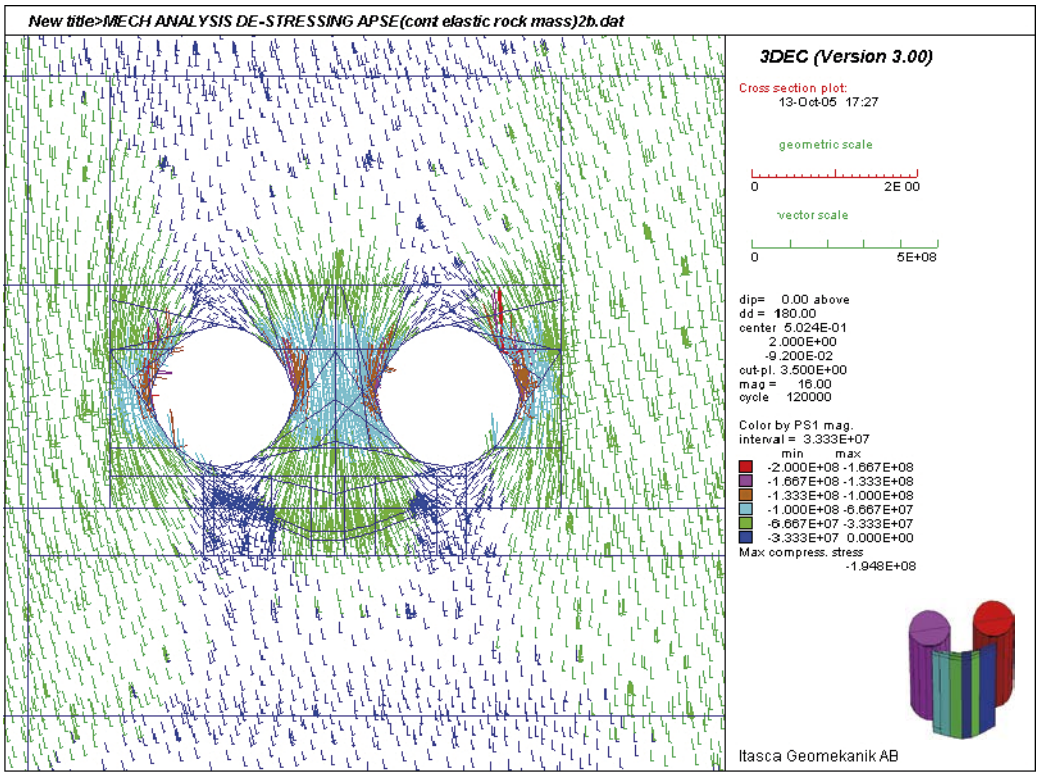

a) Continuum

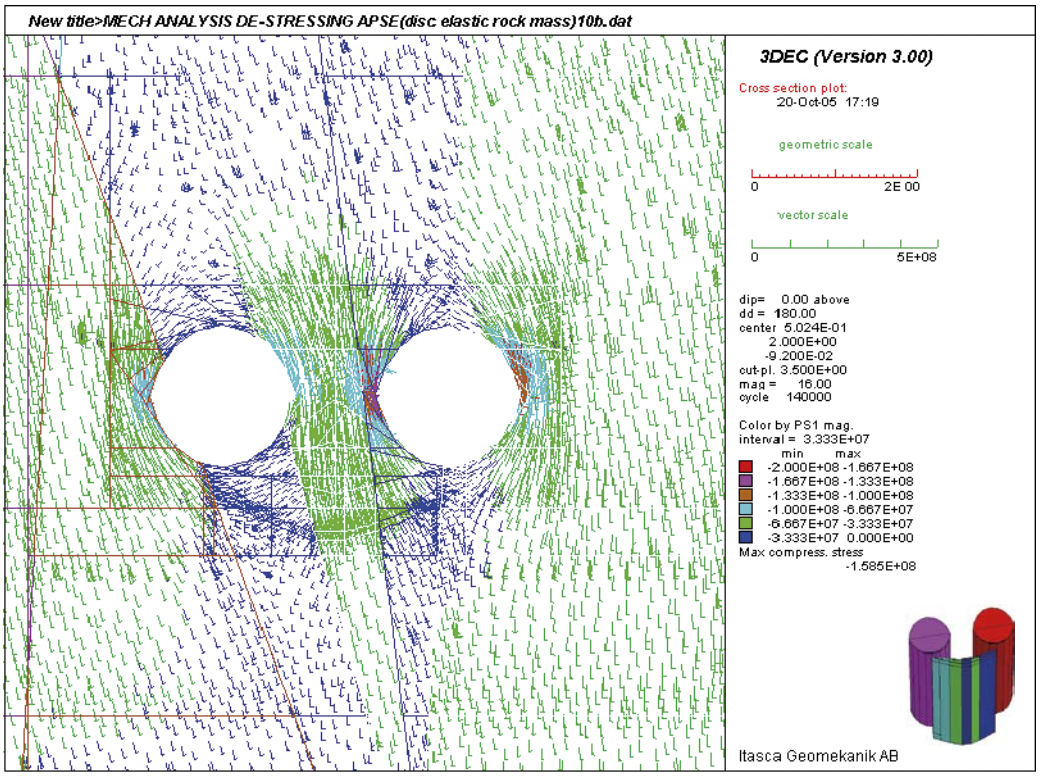

b) Discontinuum

Figure 4-11. *Horizontal cross-section showing the projected principal stress at 1.5 m depth from the floor of the APSE tunnel after the deposition holes have been excavated (Colors by magnitude of σ1).*

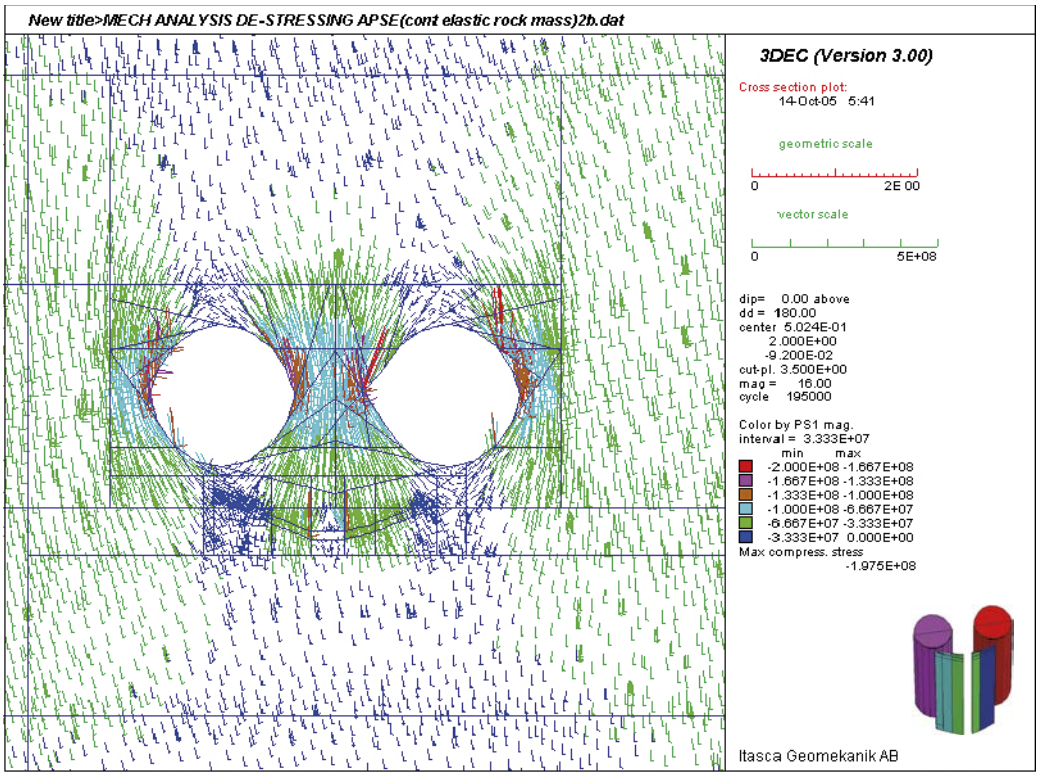

a) Continuum

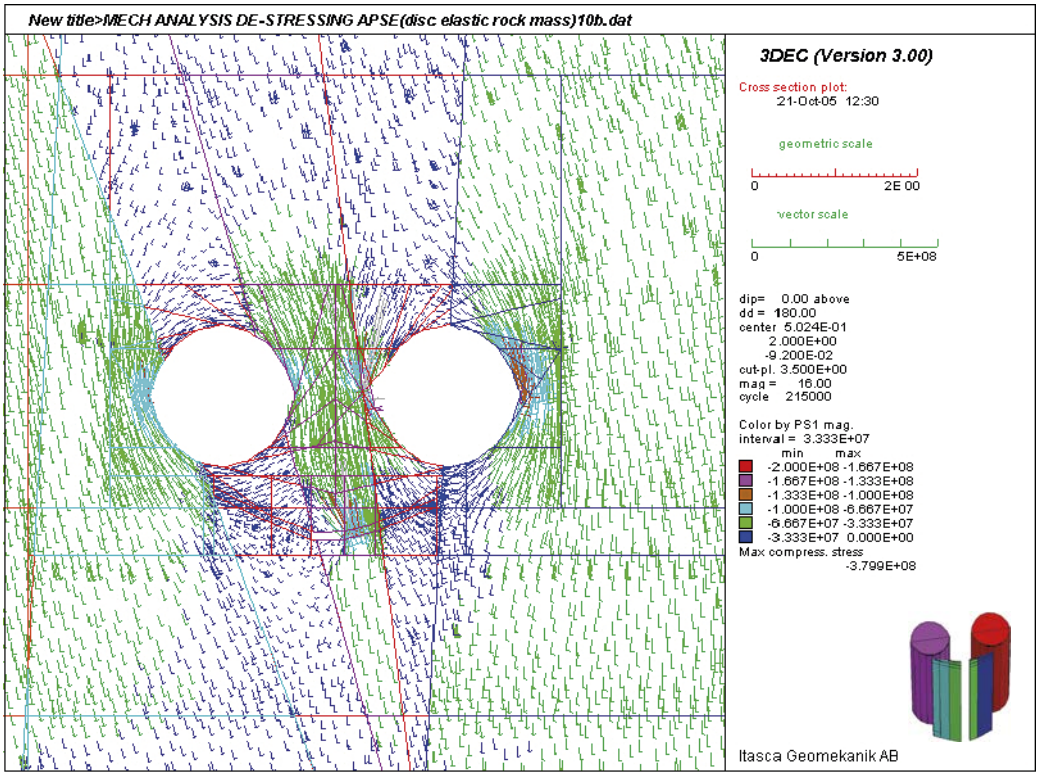

b) Discontinuum

Figure 4-12. *Horizontal cross-section showing the projected principal stress at 1.5 m depth from the floor of the APSE tunnel after the central part of the de-stressing slot has been excavated (Colors by magnitude of σ1).*

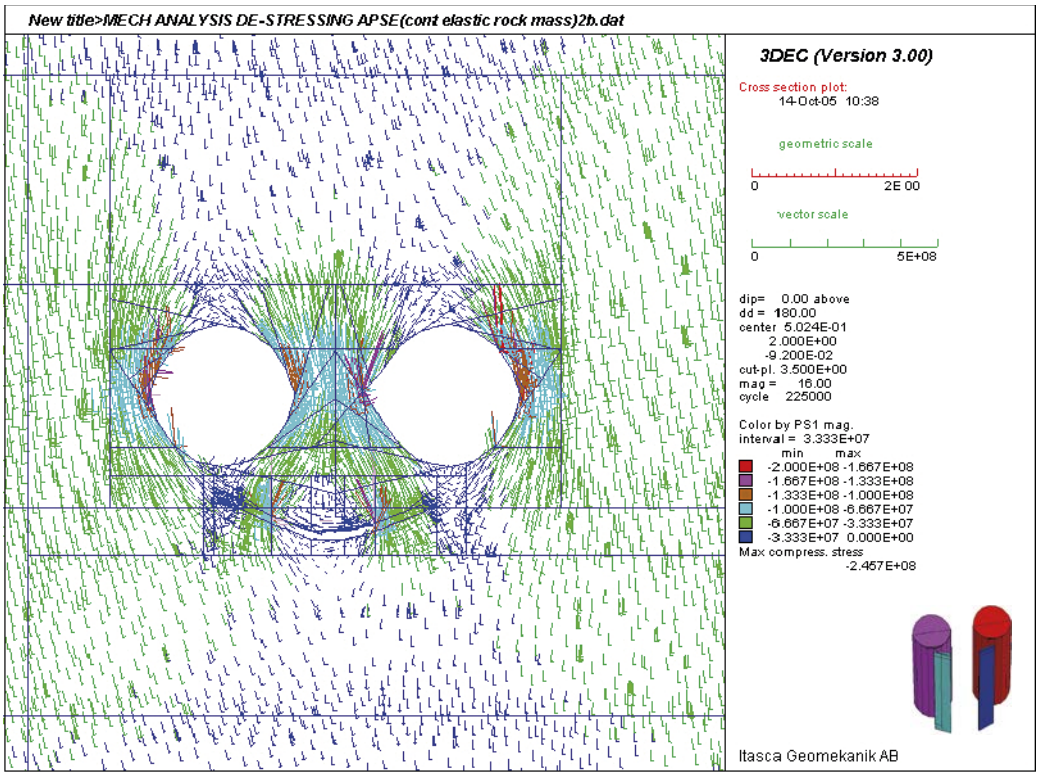

a) Continuum

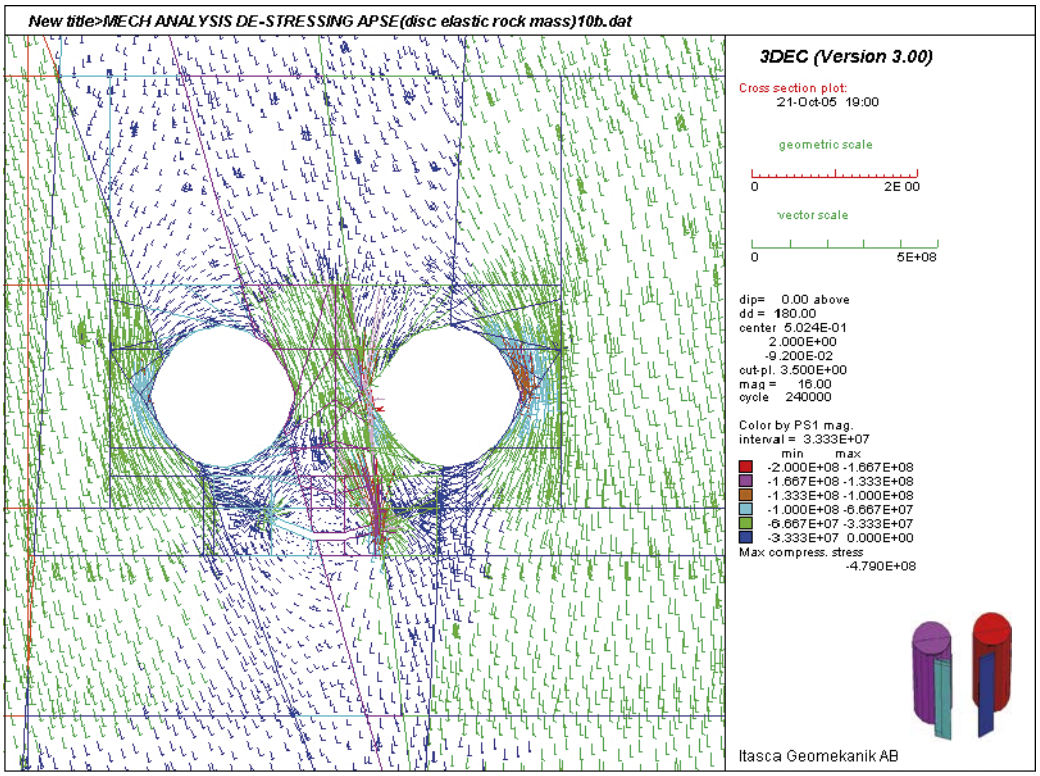

b) Discontinuum

Figure 4-13. *Horizontal cross-section showing the projected principal stress at 1.5 m depth from the floor of the APSE tunnel after the middle part of the de-stressing slot has been excavated (Colors by magnitude of σ1).*

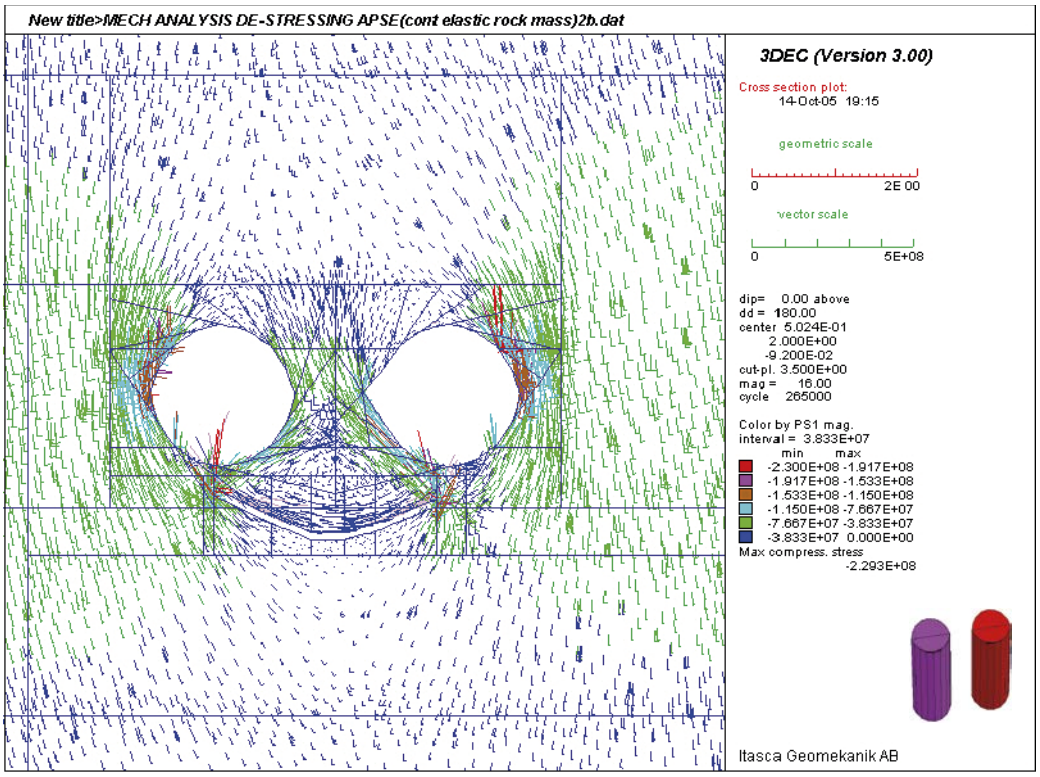

a) Continuum

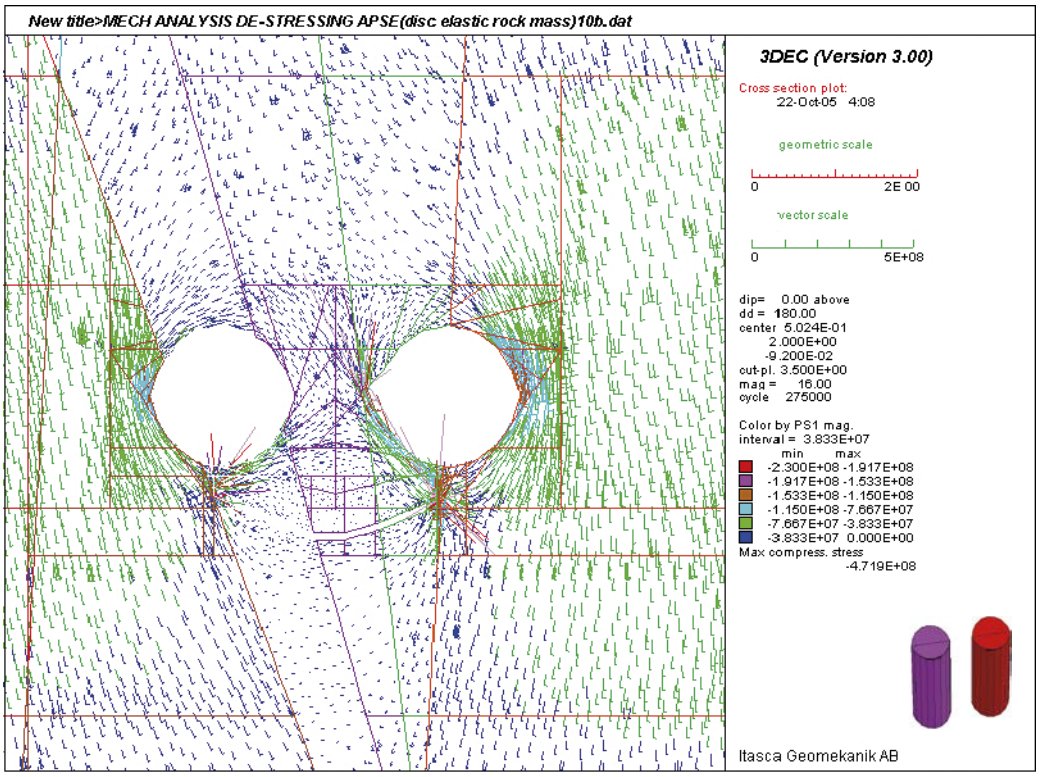

b) Discontinuum

Figure 4-14. *Horizontal cross-section showing the projected principal stress at 1.5 m depth from the floor of the APSE tunnel after the whole de-stressing slot has been excavated (Colors by magnitude of σ1).*

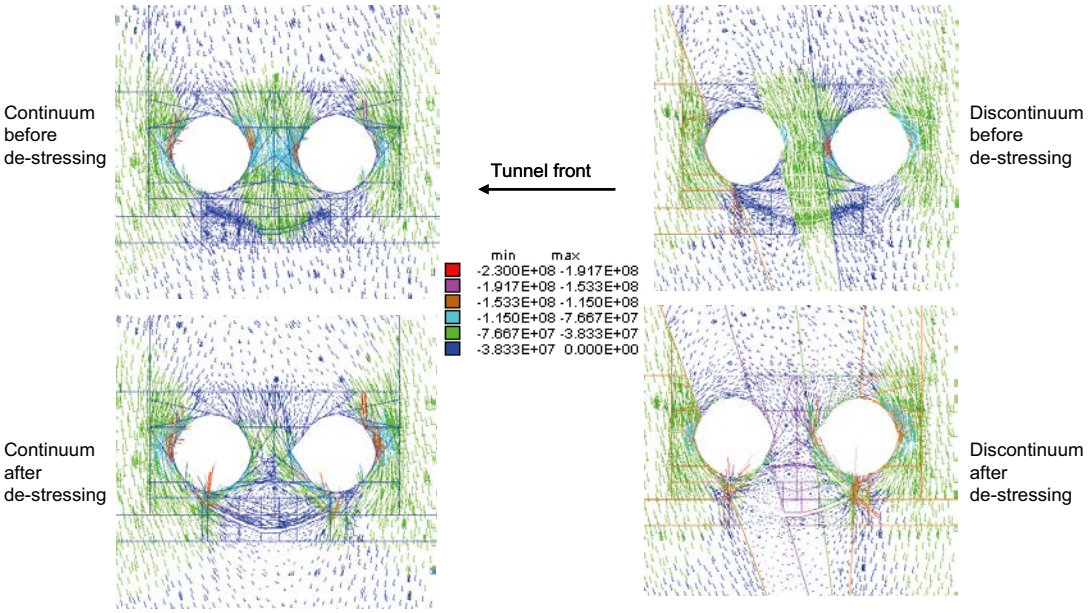

Figure 4-15. *Horizontal cross-section showing the projected principal stress at 1.5 m depth from the floor of the APSE tunnel before and after the de-stressing slot has been excavated (Colors by magnitude of σ1).*

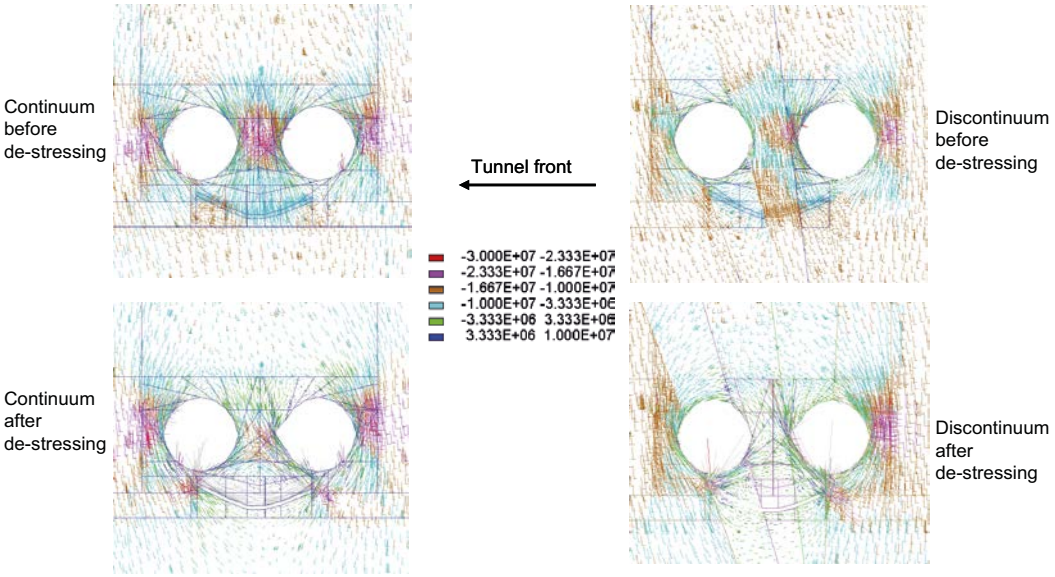

Figure 4-16. *Horizontal cross-section showing the projected principal stress at 1.5 m depth from the floor of the APSE tunnel before and after the de-stressing slot has been excavated (Colors by magnitude of σ3).*

4.2 Simulated displacements

The two figures included in this section show the projected displacement vector field on a horizontal cross-section at 1.5 m depth from the floor of the TASQ tunnel just after the deposition holes have been excavated (Figure 4-17) and after the de-stressing slot has been drilled (Figure 4-18).

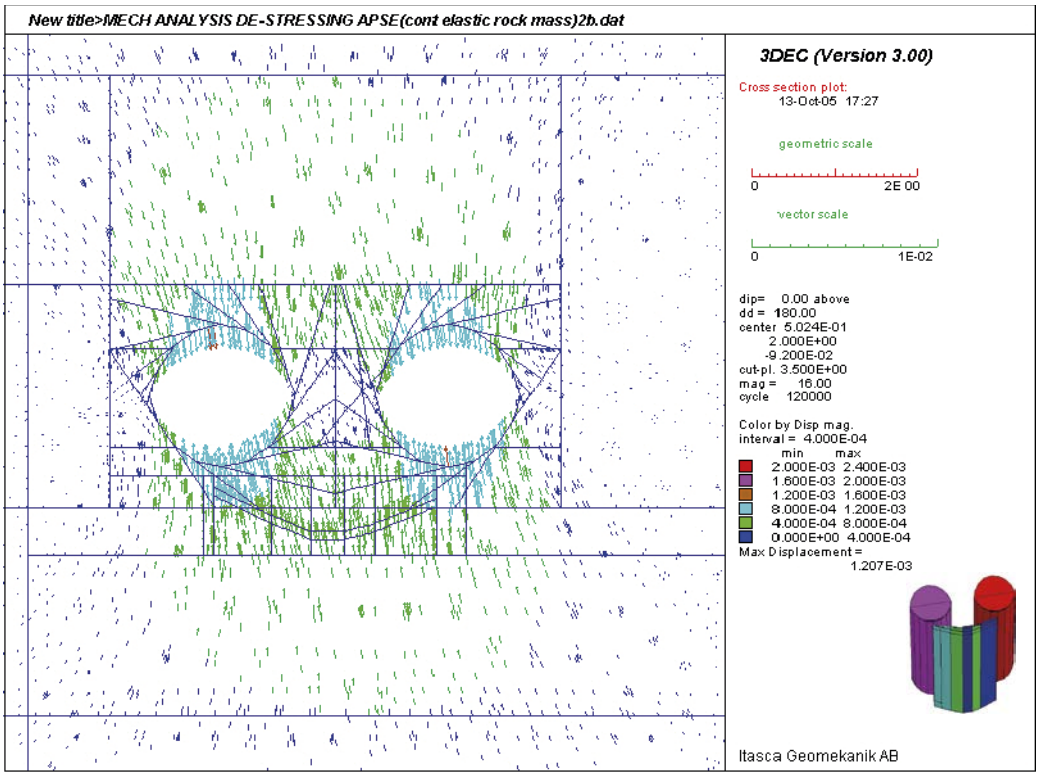

a) Continuum

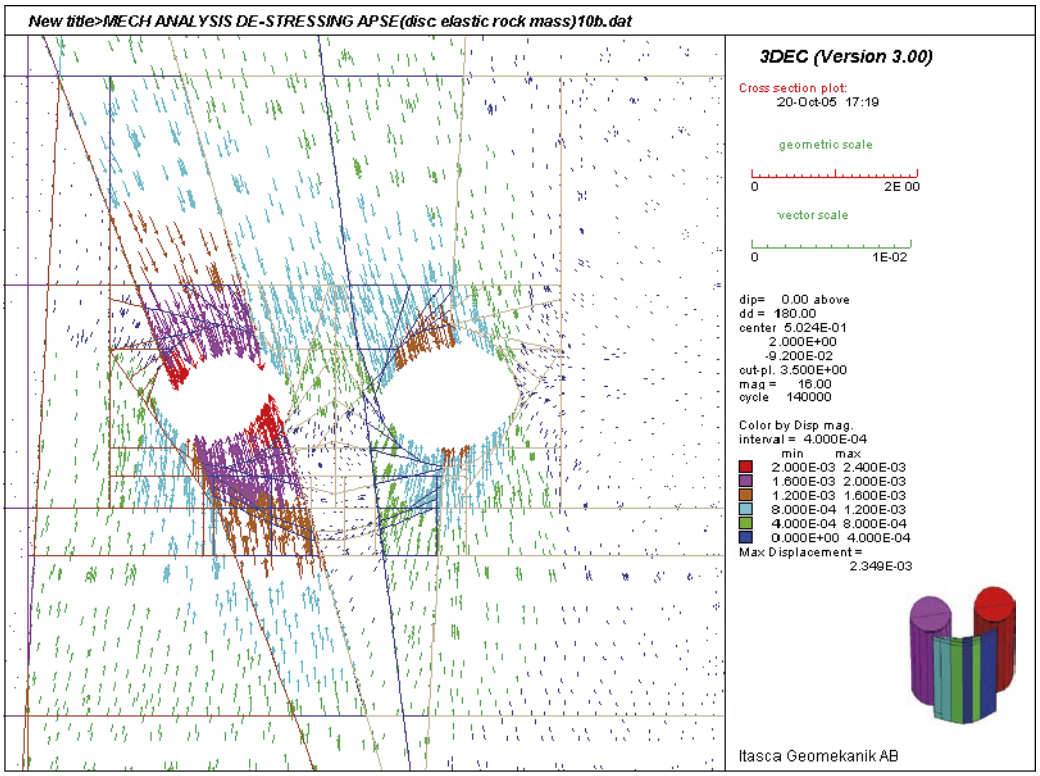

b) Discontinuum

Figure 4-17. *Horizontal cross-section showing the projected displacement vector field at 1.5 m depth from the floor of the APSE tunnel after the deposition holes have been excavated (Colors by displacement magnitude).*

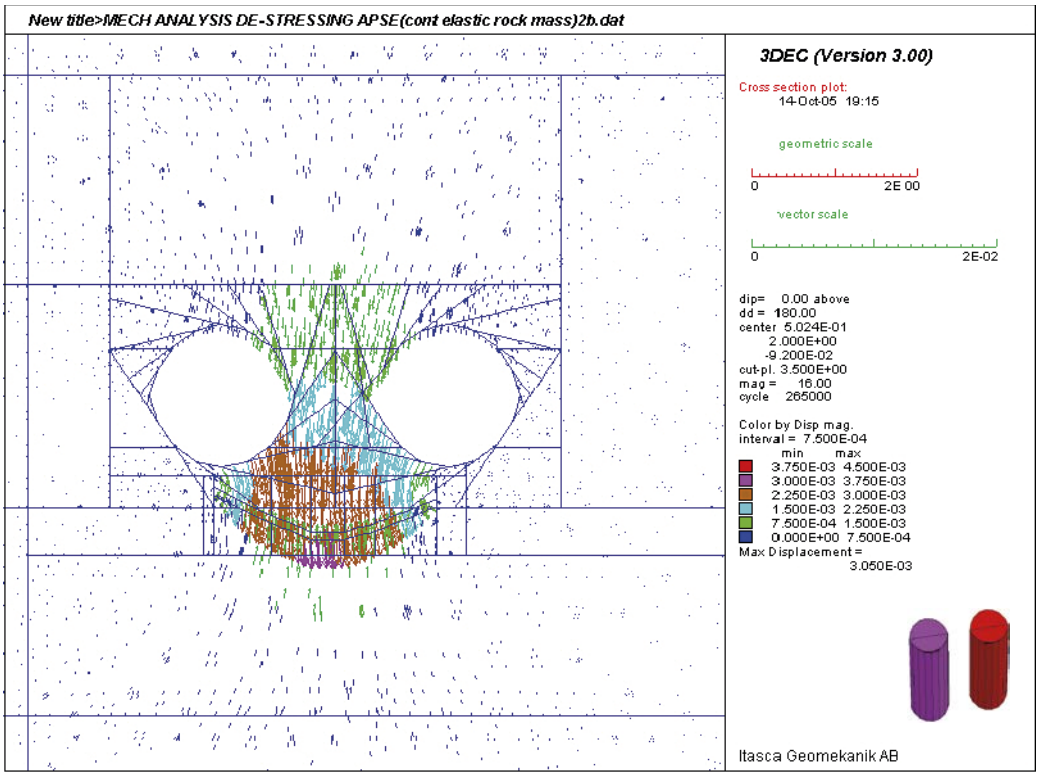

a) Continuum

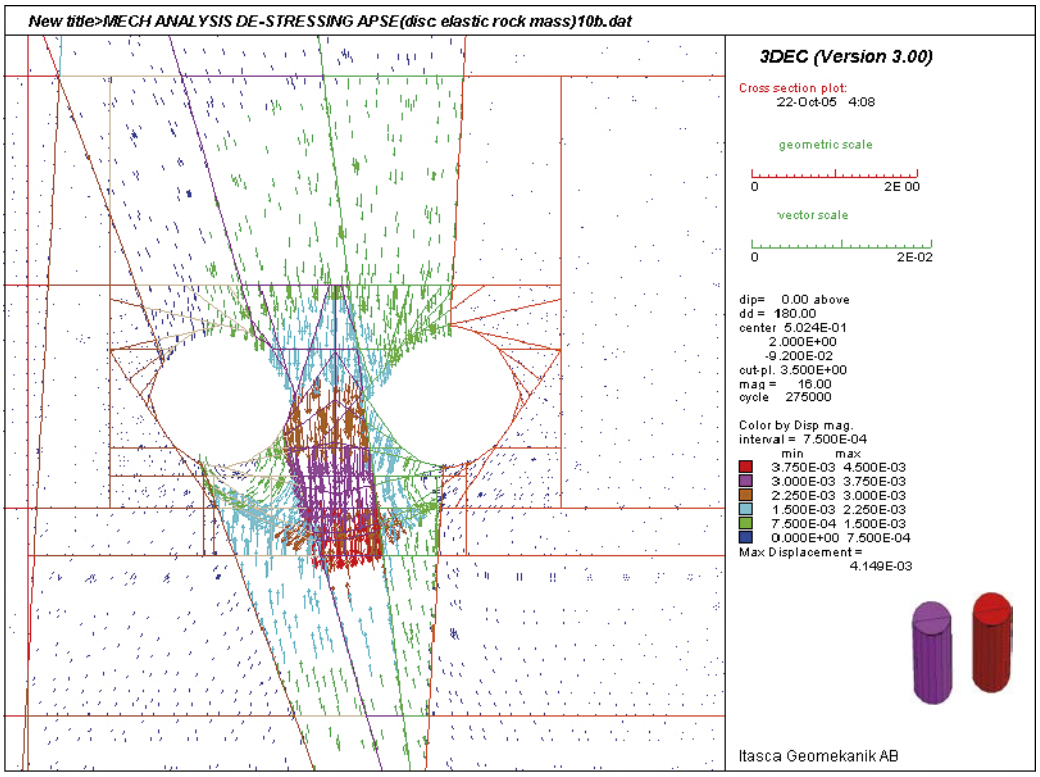

b) Discontinuum

Figure 4-18. *Horizontal cross-section showing the projected displacement vector field at 1.5 m depth from the floor of the APSE tunnel after the whole de-stressing slot has been excavated (Colors by displacement magnitude).*

4.3 Simulated stress response with the Young's modulus of the intact rock

The same continuum and discontinuum models presented in Section 4.1 were run with a Young's modulus and a Poisson's ratio representing the intact rock (Table 3-3). Figure 4-19 shows a comparison of the simulated principal stress magnitude change (σ_1 and σ_3) at the centre of the pillar (at 0.5 m and 2.5 m depth) between the rock mass case (RM) and the intact rock case (IR), during the drilling of the de-stressing slot for continuum and discontinuum simulations. Figure 4-20 shows the difference between the continuum case and discontinuum case simulated principal stress magnitude change (σ_1 and σ_3) at the centre of the pillar (at 0.5 m and 2.5 m depth) during de-stressing for the rock mass case and the intact rock case.

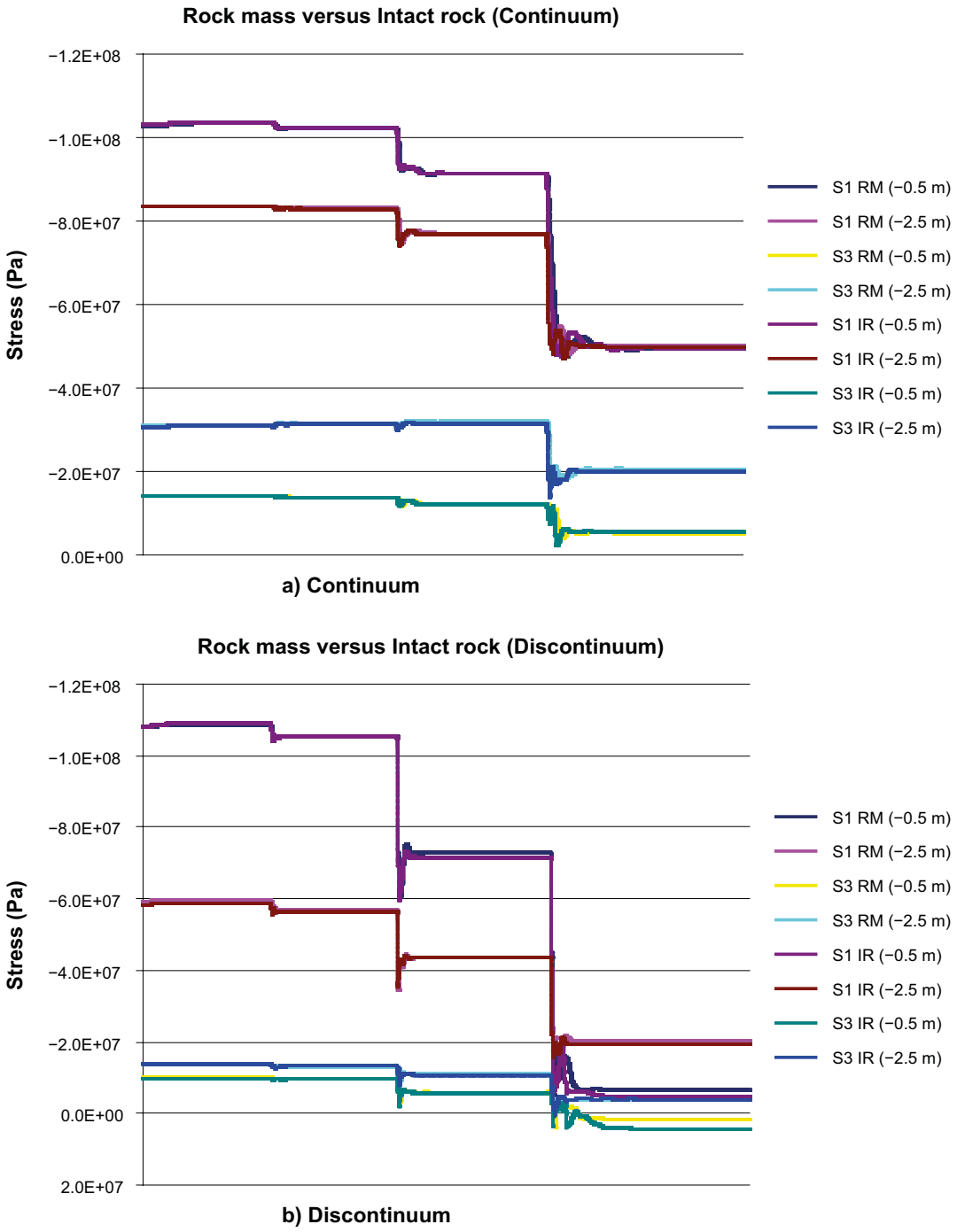

Figure 4-19. *Rock mass case (RM) versus intact rock case (IR) simulated principal stress change (σ1 and σ3) at the centre of the pillar (at 0.5 m and 2.5 m depth) during de-stressing for continuum and discontinuum simulations.*

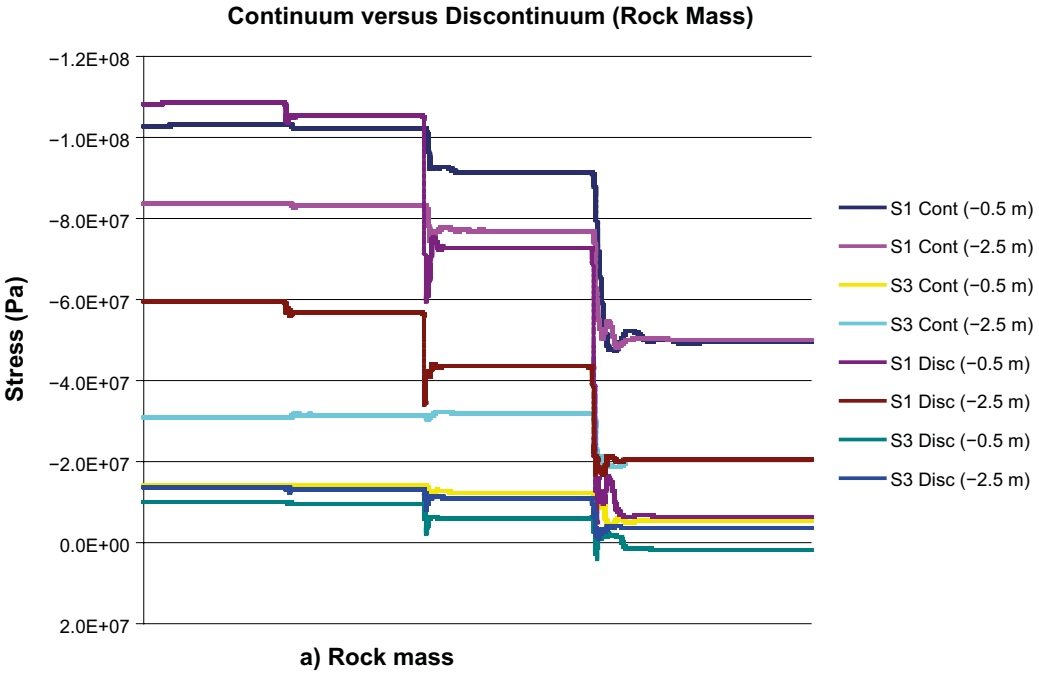

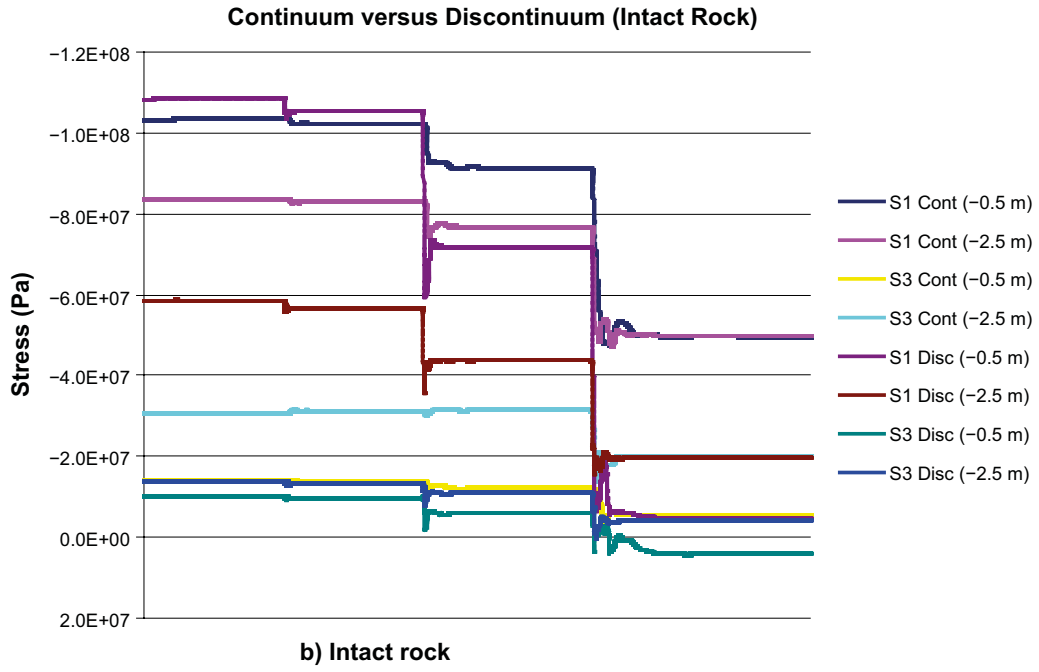

Figure 4-20. *Continuum case versus discontinuum case simulated principal stress change (σ1 and σ3) at the centre of the pillar (at 0.5 m and 2.5 m depth) during de-stressing for rock mass case and intact rock case.*

4.4 Simulated fracture stress and displacement

The simulated normal and shear displacements and normal and shear stress change during the de-stressing of the pillar at the APSE site was monitored at 0.5 and 2.5 m depth in fractures 08 and 14 (Figure 1-2). The results are shown in the following Figure 4-21 and Figure 4-22, for both the rock mass simulation case and the intact rock simulation case.

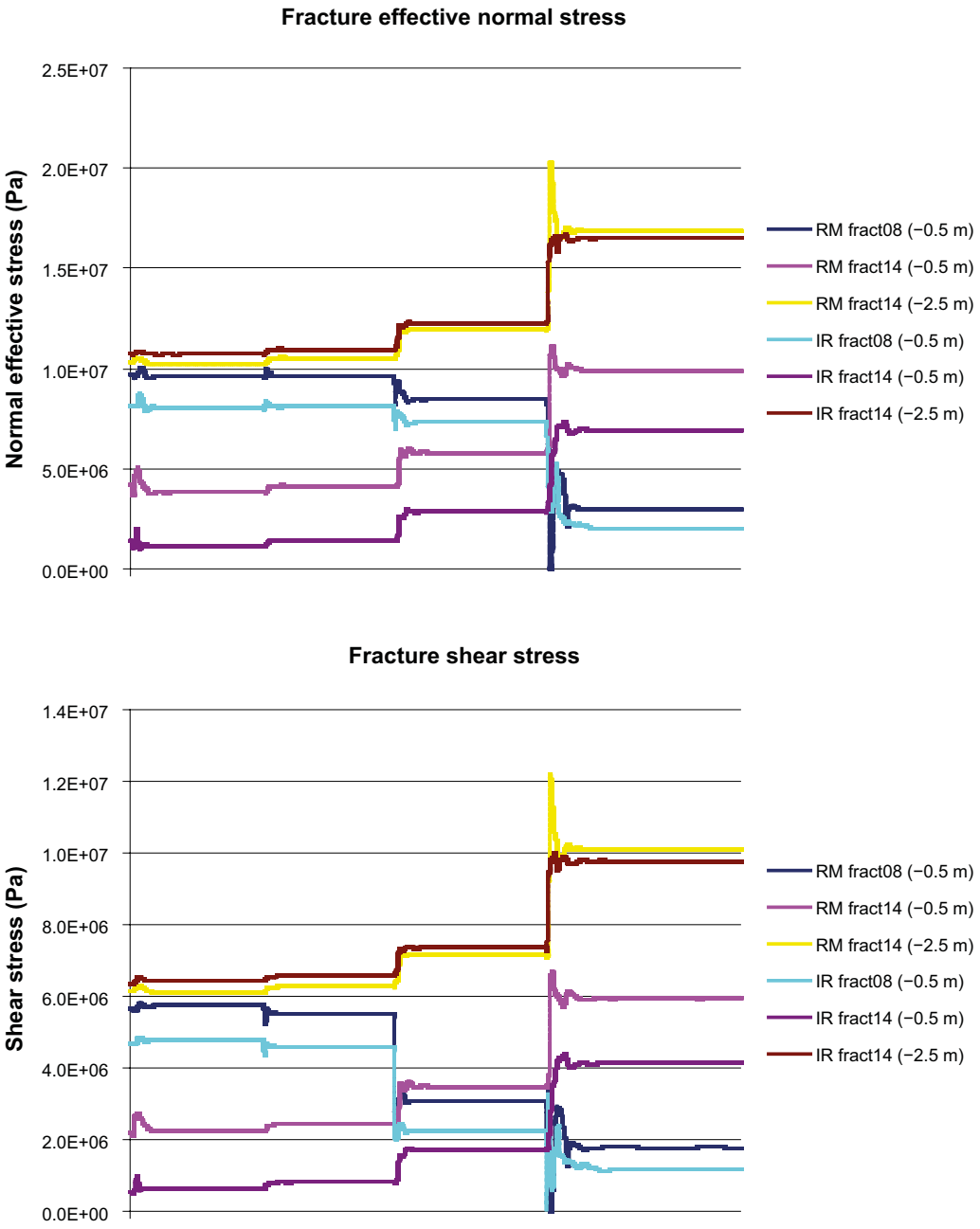

Figure 4-21. *Simulated effective normal stress and shear stress on fractures 14 and 08 at 0.5 m and 2.5 m depth during the de-stressing of the APSE pillar for rock mass (RM) and intact rock (IR) simulation cases.*

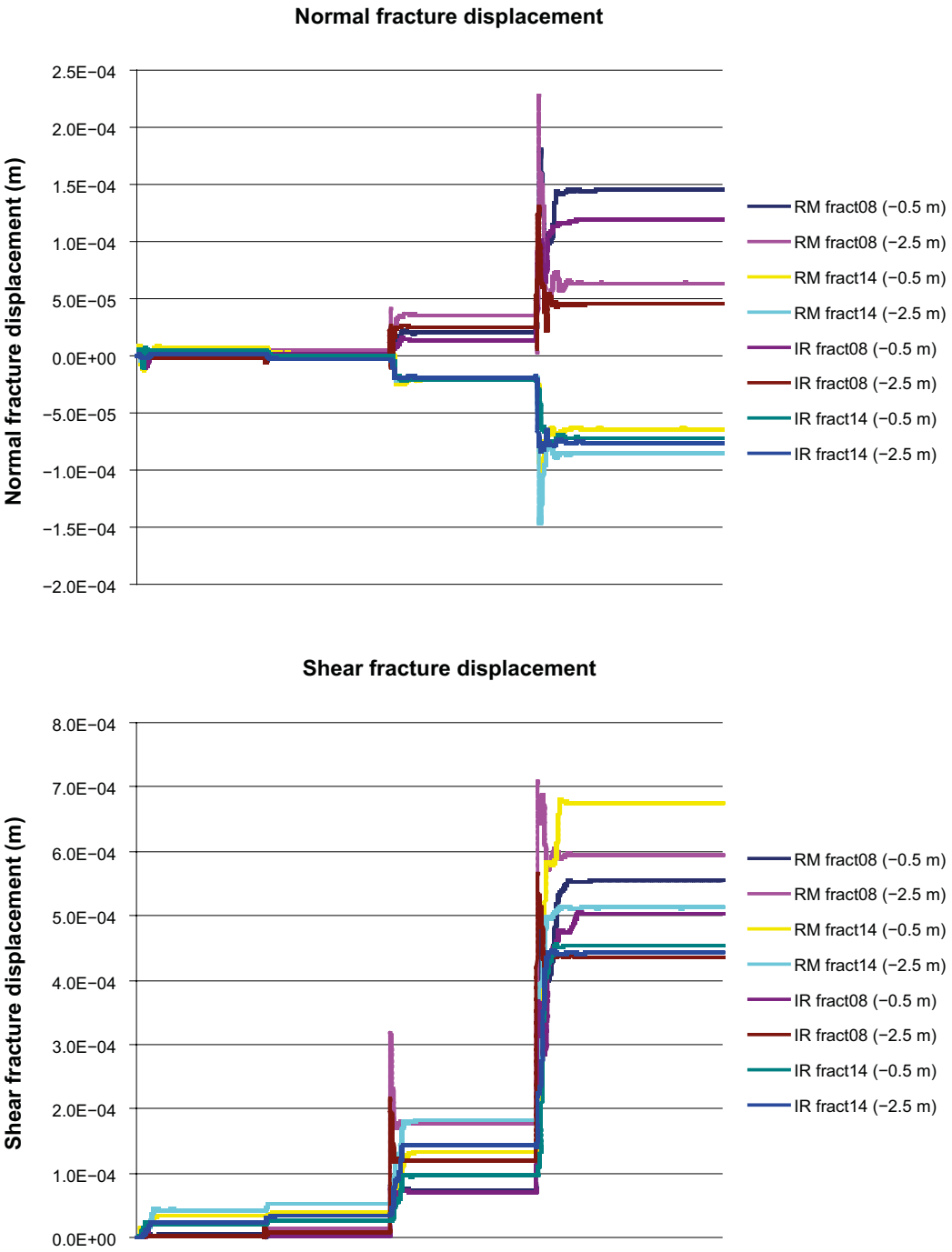

Figure 4-22. *Normal and shear displacement on fractures 14 and 08 at 0.5 m and 2.5 m depth during the de-stressing of the APSE pillar for rock mass (RM) and intact rock (IR) simulation cases.*

For comparison we add Figure 4-23 and Figure 4-24 which show the field monitored normal and shear displacement at different depths in fractures 14 and 08 during the de-stressing of the APSE pillar (Mas Ivars 2005).

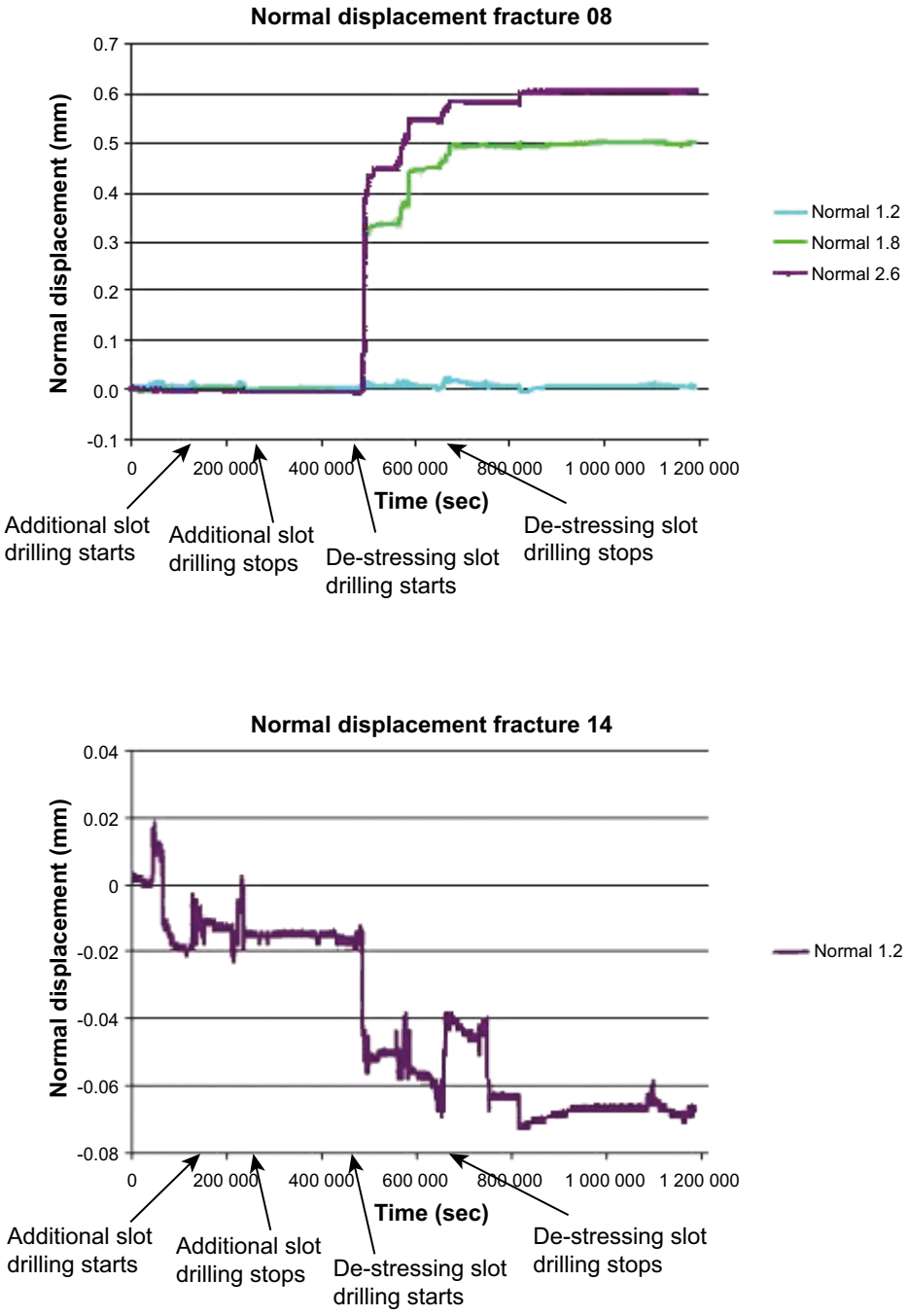

Figure 4-23. *Monitored normal displacement at different depths in fractures 08 and 14 during the de-stressing of the APSE pillar (Mas Ivars 2005).*

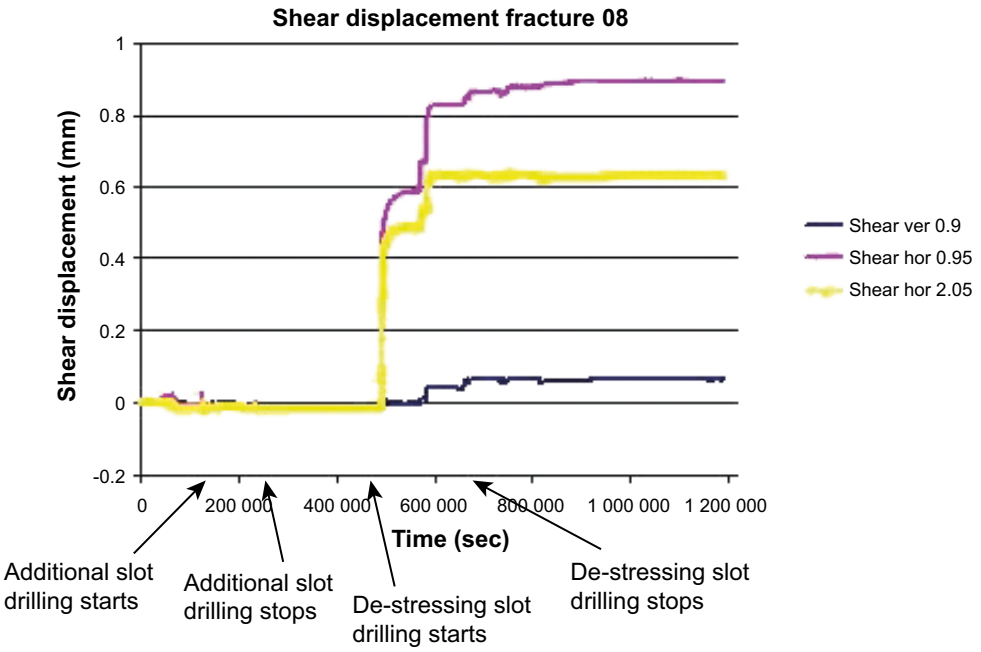

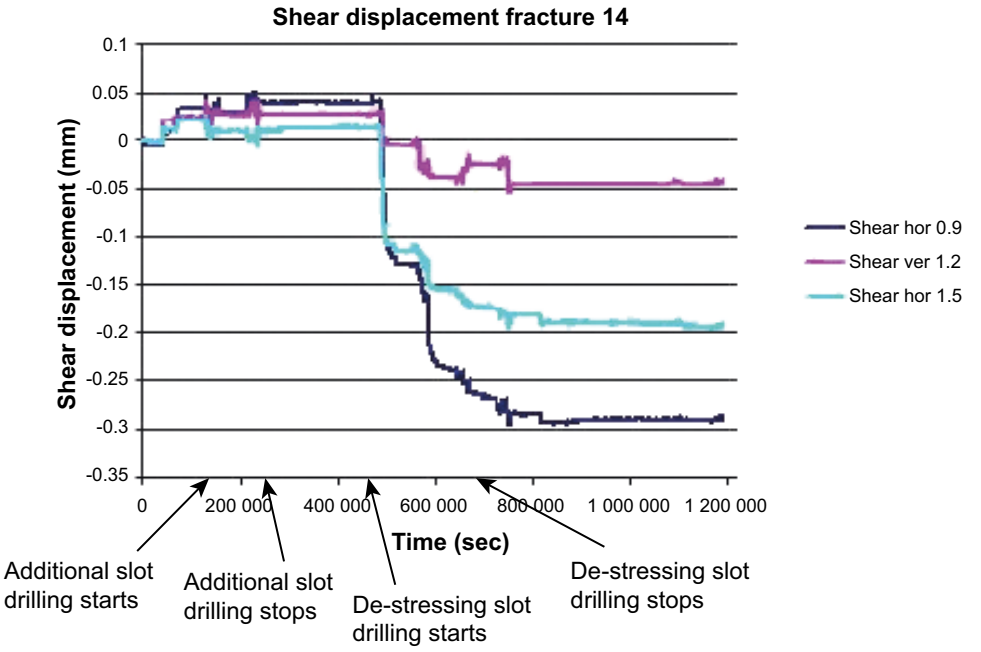

Figure 4-24. *Monitored shear displacement at different depths in fractures 08 and 14 during the de-stressing of the APSE pillar (Mas Ivars 2005).*

4.5 Laboratory test results from fracture samples from the APSE area

Although data on average fracture mechanical properties was already available from previous reports (Staub et al. 2003, 2004), a number of sub-vertical fracture samples were selected from the available cores from exploratory boreholes at the APSE area. Normal load tests and shear tests were performed on these fracture samples. The identification marks, upper sampling depth and borehole number of the samples are shown in Table 4-1.

Table 4-1. Specimen identification, upper sampling depth and borehole number.

Identification	Borehole	Sampling depth (m)
1	KQ0065G03	452.32
3	KQ0064G06	451.70
4a	KQ0064G06	451.84
4b	KQ0064G06	451.84
5	KQ0065G02	448.06
6a	KQ0065G02	449.15
6b	KQ0065G02	449.15

The laboratory test results are reported in Jacobsson and Flansbjer (2005). Table 4-2 shows the mechanical properties of the fractures evaluated from the laboratory tests following the methodology described in Lanaro et al. (2006).

Table 4-2. Mechanical properties of sub-vertical fracture samples from the APSE area evaluated from laboratory tests.

Sample	1	3	4a	4b	5	6a	6b	Mean
Peak Cohesion (MPa)	1.36	0.86	*	1.02	0.73	0.95	0.94	0.98
Residual cohesion (MPa)	0.21	0.66	*	0.49	0.24	0.23	0.31	0.36
Peak friction angle (degrees)	35.99	41.47	*	38.95	38.55	35.85	36.40	37.87
Residual friction angle (degrees)	34.23	36.82	*	35.78	37.94	35.25	35.43	35.91
Normal stiffness (GPa/m)	1055.55	431.81	500.00	772.35	141.59	242.96	510.75	522.14
Shear stiffness (GPa/m)	19.00	14.00	*	25.00	15.00	21.00	18.00	18.67
Dilation angle at 0.5 MPa (degrees)	15.81	13.85	*	15.85	11.72	14.03	13.67	14.16
Dilation angle at 5 MPa (degrees)	5.71	6.50	*	7.06	4.00	3.09	3.43	4.97

* Failure in the epoxy during the shear test.

The results presented in Table 4-2 were obtained after the numerical work presented in this report had been finalized and therefore they were not used as input in these models. The samples selected had a joint area ranging from 23.6 cm2 to 27.4 cm^2 so the values reported in Table 4-2 would have to be adjusted due to the scale effect before using them as input for a model of the scale represented in our study. The values used for the analysis performed in this study (see Table 3-4) will not differ significantly from the ones presented in Table 4-2 once the scale effect is accounted for. The new values of the fracture mechanical properties in Table 4-2 should be considered in future analyses.

5 Discussion and conclusions

Due to the fact that there were no stress measurements during the de-stressing of the APSE pillar, a three-dimensional mechanical numerical analysis of the redistribution of the stress during the drilling of the de-stressing slot has been conducted with the distinct element code 3DEC (Itasca 2003). This simulation exercise included explicitly the main fractures in the study volume, selected from the detailed mapping of the pillar walls and the APSE area. It must be taken into account that the results reported are dependent on the assumptions made and the simplified fracture geometry and geology of the conceptual model.

Measurements at boreholes located at the 450 m depth level in the Äspö HRL indicate that the water pore pressure is in the range 2 MPa – 4 MPa. This implies that the fracture water pore pressure considered in the model might be slightly overestimated. As a consequence of this overestimation, the effective normal stress acting on the fractures can be slightly lower and this can cause an overestimation of the fracture slip in our model.

The main conclusions that can be drawn from this numerical study are the following:

- At an early stage in the simulation, when the TASQ tunnel is excavated, the difference between the continuum and the discontinuum approach is negligible (Figure 4-2). However, as the excavation of the deposition holes and the additional slots and the drilling of the de-stressing slot progresses, the difference between the continuum and the discontinuum simulation of the stress redistribution around the TASQ tunnel in the APSE area increases (Figure 4-3 to Figure 4-6). After the de-stressing slot has been drilled, the pillar is completely de-stressed in the discontinuum case but not in the continuum case (Figure 4-6).
- A similar conclusion can be reached looking at Figure 4-7 to Figure 4-10. Even from the moment in which both deposition holes have just been excavated (Figure 4-7), the stress in the pillar in the continuum case is different than in the discontinuum case. This difference increases as the drilling of the de-stressing slot progresses. Finally, it can be appreciated in Figure 4-10 that the stress in the pillar is larger in the continuum model than in the discontinuum model after the de-stressing slot has been fully drilled.
- Again, a similar conclusion can be drawn looking at Figure 4-11 to Figure 4-14. The stress redistribution caused by the drilling of the de-stressing slot is very much affected by the explicit consideration of fracture 08 and fracture 14 in the model (Figure 1-2). As can be seen in this set of figures the stress field is symmetric before, during and after the whole de-stressing period for the continuum model, as it was expected. On the other hand, there is a clear asymmetry on the stress field in every step of the simulation in the discontinuum case. In this case, the maximum stress in the near field surrounding the deposition hole DQ0066G01 is much lower, in every step, than that around the deposition hole DQ0063G01. This asymmetry is caused by the stress release effect induced by movement along fracture 08 and 14. A similar conclusion has been reported in Fälth et al. (2005). In this case, the induced thermal stresses in the pillar during the heating phase of the APSE experiment (Andersson 2004, Fredriksson et al. 2004, Rinne et al. 2004, Wanne et al. 2004) were simulated considering the cooling effect of the water conductive fracture 08. The presence of the water bearing fracture caused the simulated induced thermal stress to be asymmetric (lower in the surroundings of deposition hole DQ0066G01 than around DQ0063G01).
- The simulated displacements are also symmetric in the continuum case and asymmetric in the discontinuum case (Figure 4-17 and Figure 4-18). In the discontinuum case the displacement field is dominated in both magnitude and direction by the presence of the fractures. The maximum displacement is larger in the discontinuum case than in the continuum case, as expected.
- Figure 4-19 shows the change in σ_1 and σ_3 at the center of the pillar as the drilling of the de-stressing slot progresses. This figure illustrates well the difference between the continuum and the discontinuum case. The final principal stress magnitudes at the monitored points are more than 50 % lower in the discontinuum case than in the continuum case. It can also be concluded that the difference between considering the rock mass Young's modulus and Poisson's ratio or the intact rock Young's modulus and Poisson's ratio is negligible concerning the change in stress during the de-stressing of the pillar (see also Figure 4-20).

- Figure 4-21 shows the simulated evolution of the normal effective stress and shear stress on fracture 08 and 14 during the drilling of the de-stressing slot. From a purely mechanical point of view the consideration of rock mass or intact rock Young's modulus and Poisson's ratio is negligible. The normal and shear stress increase along fracture 14 and decrease along fracture 08 during the de-stressing of the pillar.
- The simulated normal and shear displacement on fracture 08 and 14 are shown in Figure 4-22. As expected, fracture 08 is opening due to the decrease in normal stress and fracture 14 is closing due to the increase in normal stress. This compares well with the behaviour observed in the field measurements performed during the de-stressing of the APSE pillar, shown in Figure 4-23. The measured and simulated closure on fracture 14 match satisfactorily. This could be an indication that the fracture normal stiffness for fracture 14 and the in situ stress field used in the simulations are correct. However, the measured displacement (opening) of fracture 08 is from 3 to 4 times larger than the simulated one, although this is difficult to assess as the measured displacement varies strongly with depth. This should be considered carefully in future studies in order to improve the agreement between the model and the measurements. One possible reason is perhaps that the fracture dilation angle used in the model for fracture 08 is too low. Furthermore, while the simulated shear displacement on fracture 14 is double as much as the measured one shown in Figure 4-24, the simulated shear displacement along fracture 08 compares well with the measured one.

Summarizing, the results presented in this report support the fact that fracture orientation and location with respect to in situ stress field and pre-existing excavations can play a significant role in the redistribution of stresses due to new excavations (de-stressing slot).

References

SKB's (Svensk Kärnbränslehantering AB) publications can be found at www.skb.com/publications.

Andersson J C, 2004. Äspö Pillar Stability Experiment. Summary of preparatory work and predictive modelling. SKB R-03-02, Svensk Kärnbränslehantering AB.

Fredriksson A, Staub I, Outers N, 2004. Äspö Pillar Stability Experiment. Final 2D coupled thermo-mechanical modelling. SKB R-04-02, Svensk Kärnbränslehantering AB.

Fälth B, Kristensson O, Hökmark H, 2005. Äspö Hard Rock Laboratory. Äspö Pillar Stability Experiment. Thermo-mechanical 3D back analyze of the heating phase. SKB IPR-05-19, Svensk Kärnbränslehantering AB.

Itasca, 2003. 3DEC – 3 Dimensional Distinct Element Code, User's Manual. Minneapolis, MN: Itasca Consulting Group, Inc.

Jacobsson L, Flansbjer M, 2005. Äspö Hard Rock Laboratory. Äspö Pillar Stability Experiment. Samples from TASQ tunnel at Äspö HRL. Normal loading and shear tests on joints. SKB IPR-05-23, Svensk Kärnbränslehantering AB.

Lanaro F, Öhman J, Fredriksson A, 2006. Rock mechanics modeling of rock mass properties – Summary of primary data. Preliminary site description. Laxemar subarea – version 1.2. SKB R-06-15, Svensk Kärnbränslehantering AB.

Magnor B, 2004. Äspö Hard Rock Laboratory. Äspö Pillar Stability Experiment. Geological mapping of tunnel TASQ. SKB IPR-04-03, Svensk Kärnbränslehantering AB.

Mas Ivars D, 2005. Äspö Hard Rock Laboratory. Äspö Pillar Stability Experiment. Hydromechanical data acquisition experiment at the APSE site. SKB IPR-05-21, Svensk Kärnbränslehantering AB.

Rinne M, Shen B, Lee H-S, 2004. Äspö Pillar Stability Experiment. Modelling of fracture development of APSE by FRACOD. SKB R-04-04, Svensk Kärnbränslehantering AB.

Staub I, Andersson J C, Magnor B, 2004. Äspö Pillar Stability Experiment. Geology and mechanical properties of the rock in TASQ. SKB R-04-01, Svensk Kärnbränslehantering AB.

Staub I, Janson T, Fredriksson A, 2003. Äspö Hard Rock Laboratory. Äspö Pillar Stability Experiment. Geology and properties of the rock mass around the experiment volume. SKB IPR-03-02, Svensk Kärnbränslehantering AB.

Wanne T, Johansson E, Potyondy D, 2004. Äspö Pillar Stability Experiment. Final coupled 3d thermo-mechanical modelling. Preliminary particle-mechanical modelling. SKB R-04-03, Svensk Kärnbränslehantering AB.

Appendix

Modelling of the stress redistribution due to the removal of the pillar

Once the de-stressing slot had been drilled it was possible to cut and remove the pillar in between the two deposition size holes. As feedback for core disking studies in the APSE tunnel area and for completing the stress analysis presented in this report, the pillar was removed from the 3DEC model and the system was run to equilibrium again. The resulting state of stress is shown in the following figures. The figures refer to the discontinuum case with Young's modulus and Poisson's ratio of the rock mass (Table 3-3). As the interest was focused on the stresses at the outer part of the deposition size holes, the stress ranges for the plots were selected accordingly.

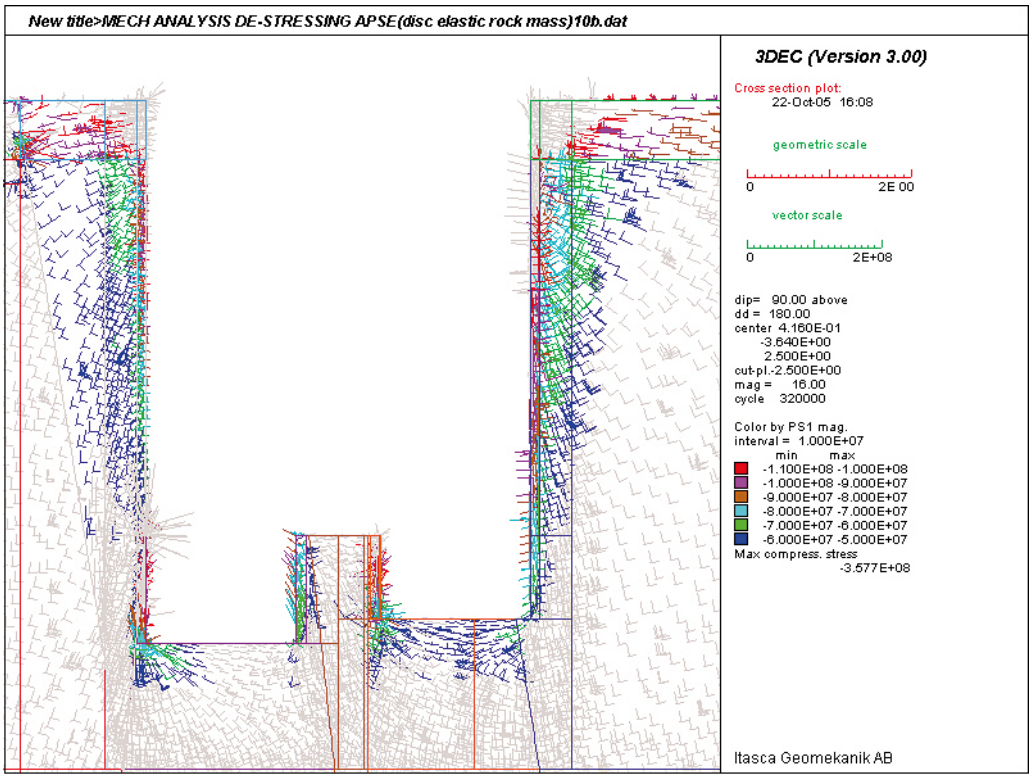

Figure A-1. *Vertical cross-section showing the projected principal stress along the axis of the tunnel after the central pillar has been removed (Colors by magnitude of σ1).*

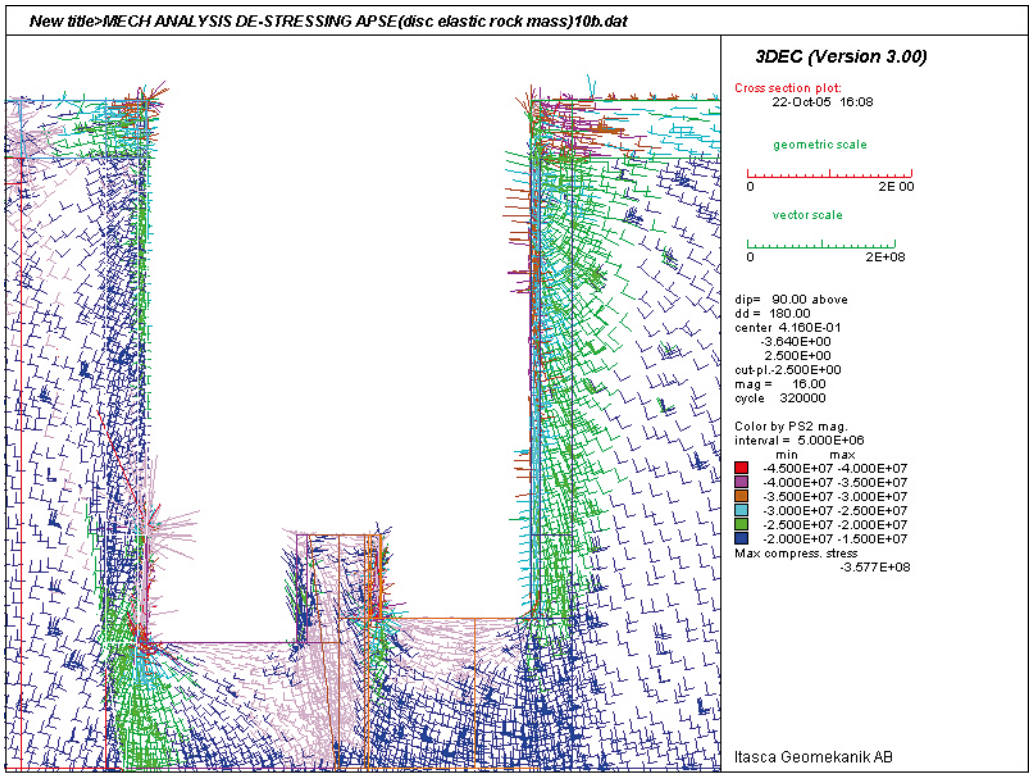

Figure A-2. *Vertical cross-section showing the projected principal stress along the axis of the tunnel after the central pillar has been removed (Colors by magnitude of σ2).*

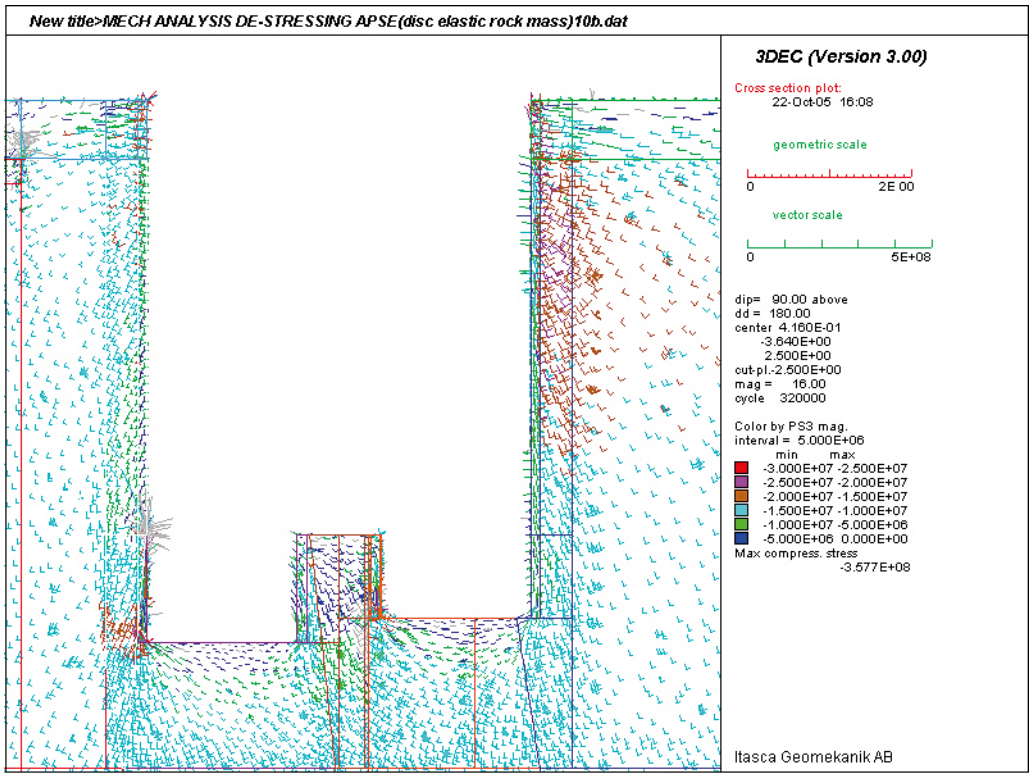

Figure A-3. *Vertical cross-section showing the projected principal stress along the axis of the tunnel after the central pillar has been removed (Colors by magnitude of σ3).*

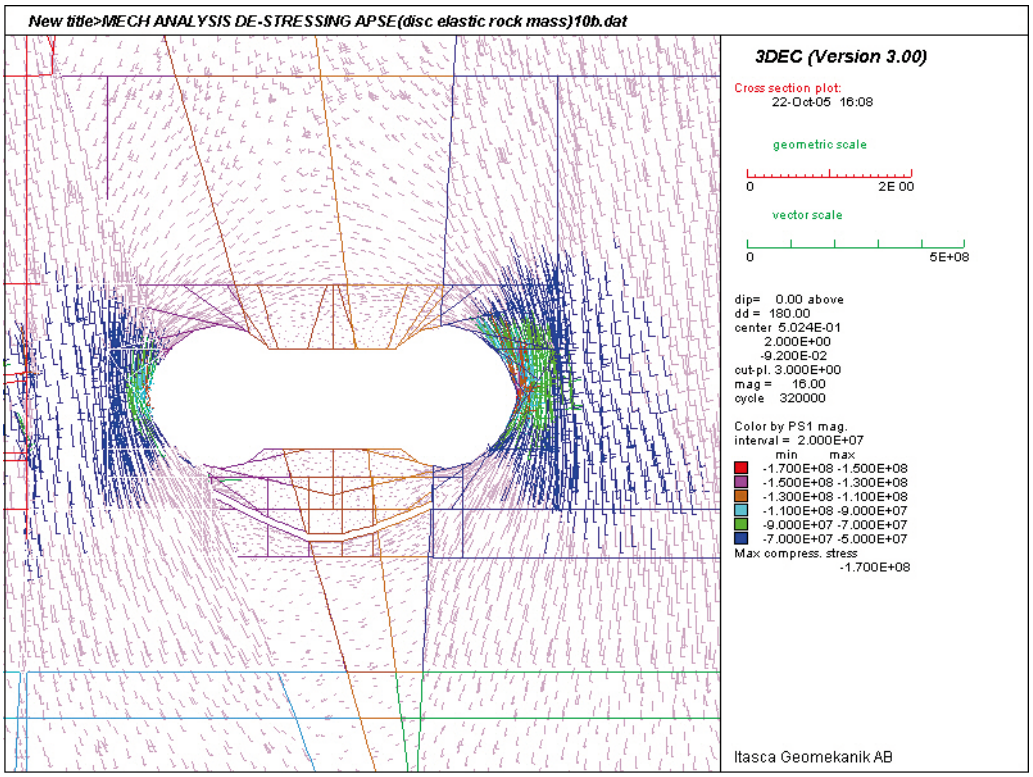

Figure A-4. *Horizontal cross-section showing the projected principal stress at 1 m depth from the floor of the APSE tunnel after the central pillar has been removed (Colors by magnitude of σ1).*

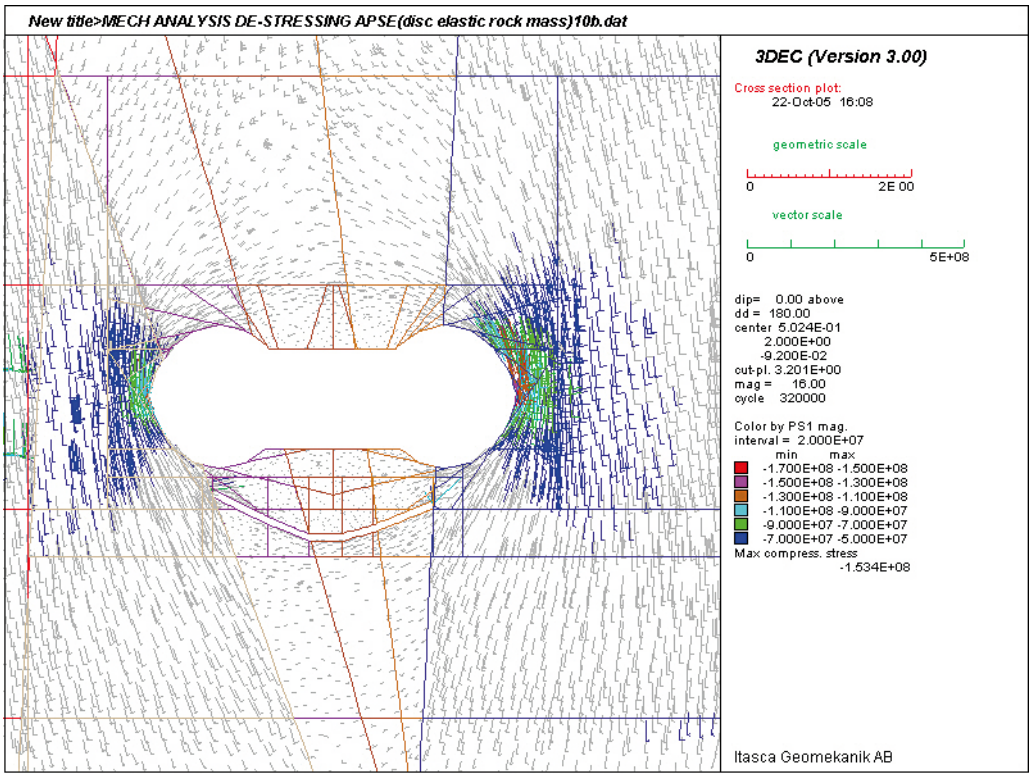

Figure A-5. *Horizontal cross-section showing the projected principal stress at 1.2 m depth from the floor of the APSE tunnel after the central pillar has been removed (Colors by magnitude of σ1).*

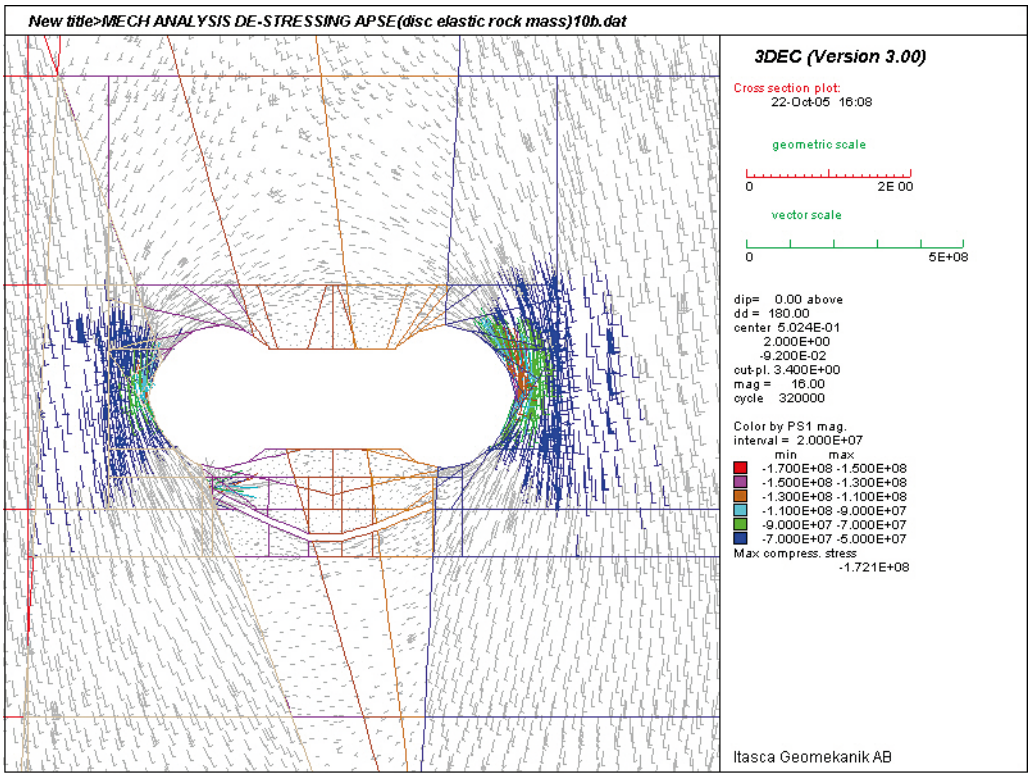

Figure A-6. *Horizontal cross-section showing the projected principal stress at 1.4 m depth from the floor of the APSE tunnel after the central pillar has been removed (Colors by magnitude of σ1).*

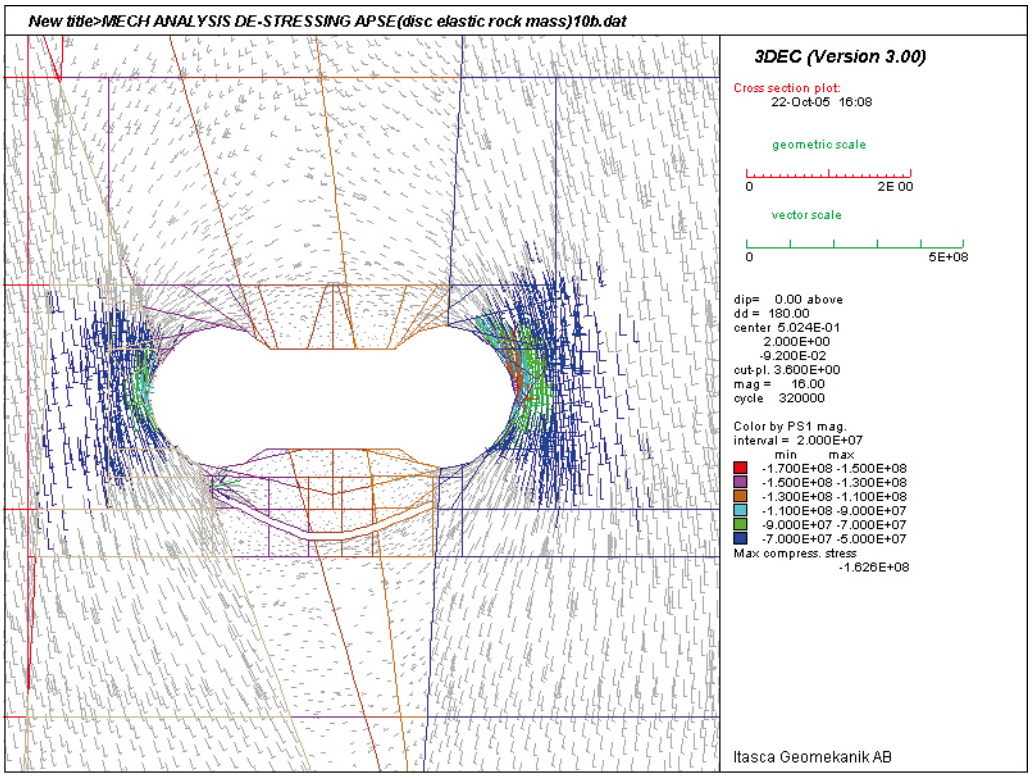

Figure A-7. *Horizontal cross-section showing the projected principal stress at 1.6 m depth from the floor of the APSE tunnel after the central pillar has been removed (Colors by magnitude of σ1).*

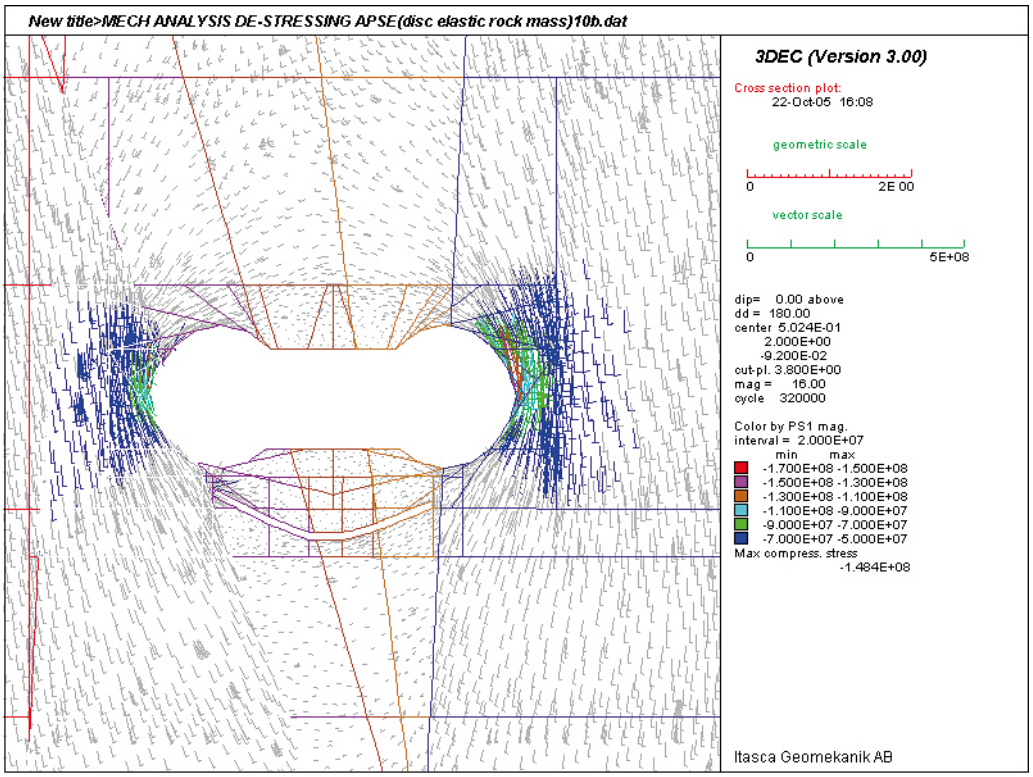

Figure A-8. *Horizontal cross-section showing the projected principal stress at 1.8 m depth from the floor of the APSE tunnel after the central pillar has been removed (Colors by magnitude of σ1).*

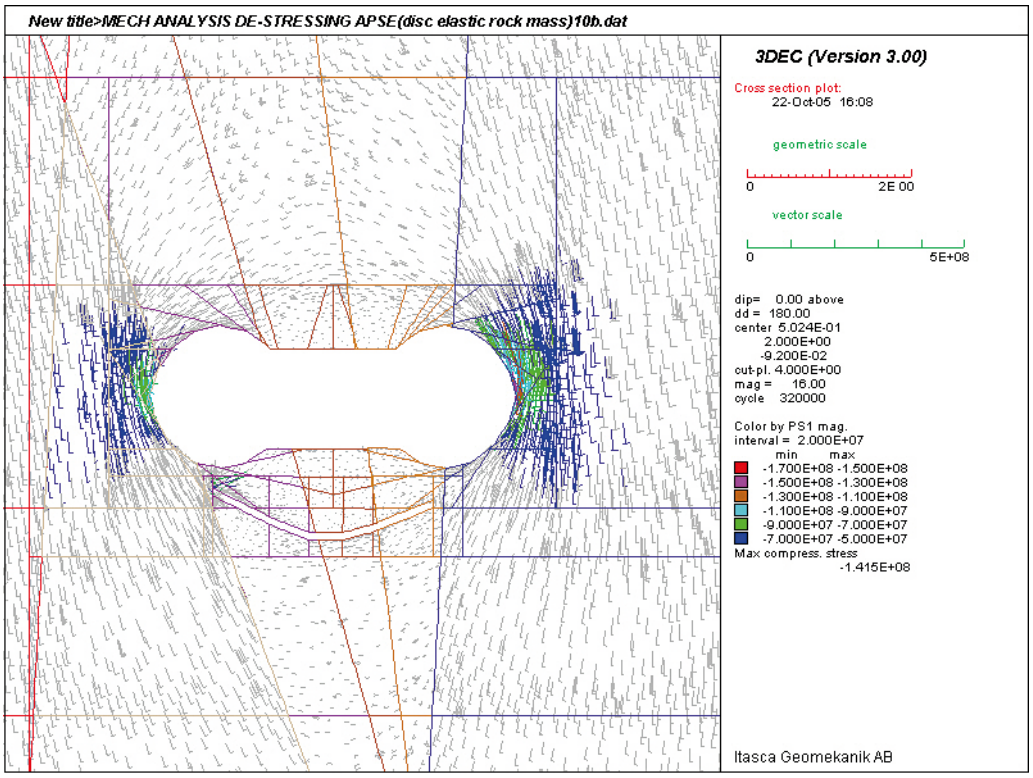

Figure A-9. *Horizontal cross-section showing the projected principal stress at 2 m depth from the floor of the APSE tunnel after the central pillar has been removed (Colors by magnitude of σ1).*

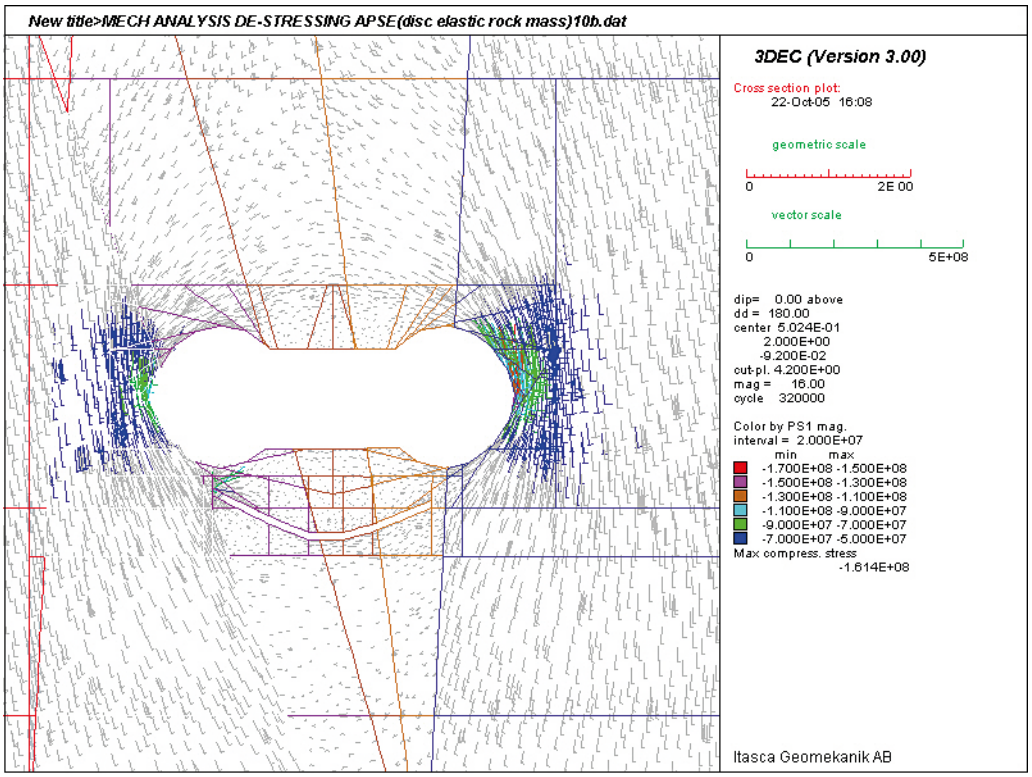

Figure A-10. *Horizontal cross-section showing the projected principal stress at 2.2 m depth from the floor of the APSE tunnel after the central pillar has been removed (Colors by magnitude of σ1).*

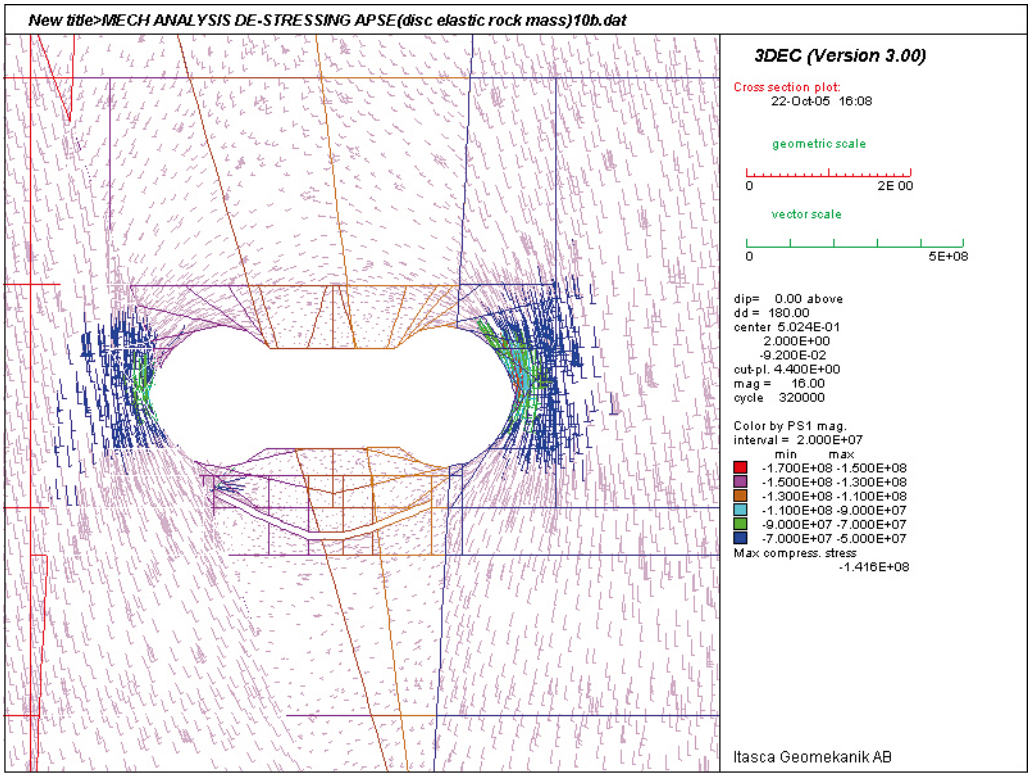

Figure A-11. *Horizontal cross-section showing the projected principal stress at 2.4 m depth from the floor of the APSE tunnel after the central pillar has been removed (Colors by magnitude of σ1).*

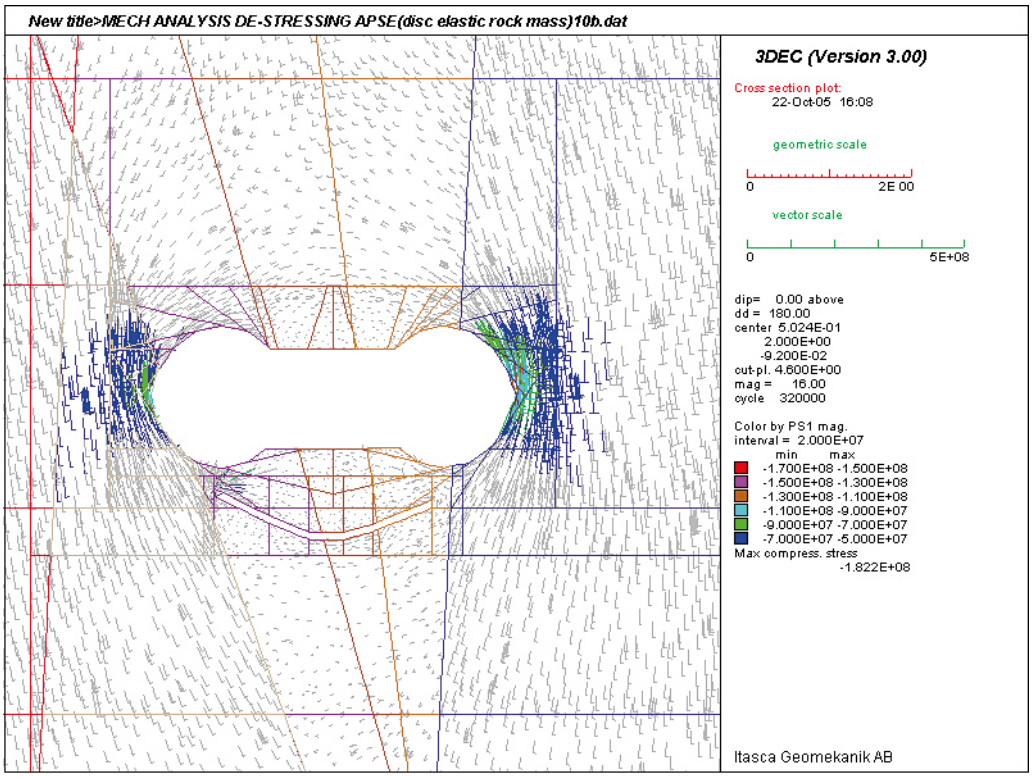

Figure A-12. *Horizontal cross-section showing the projected principal stress at 2.6 m depth from the floor of the APSE tunnel after the central pillar has been removed (Colors by magnitude of σ1).*

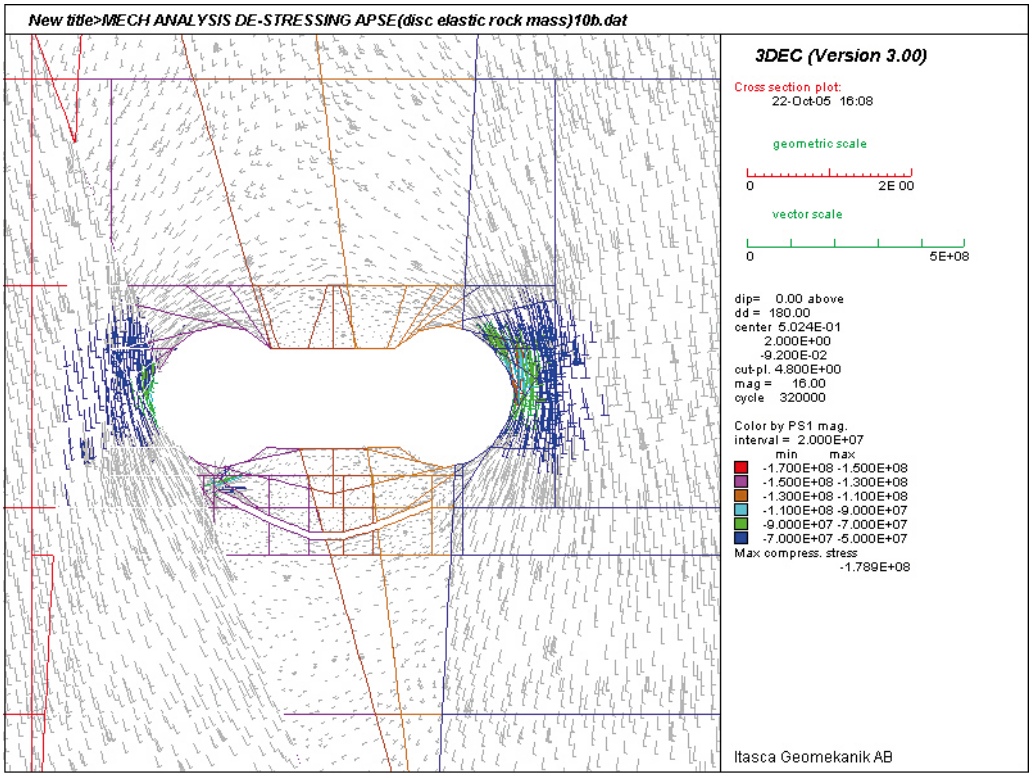

Figure A-13. *Horizontal cross-section showing the projected principal stress at 2.8 m depth from the floor of the APSE tunnel after the central pillar has been removed (Colors by magnitude of σ1).*

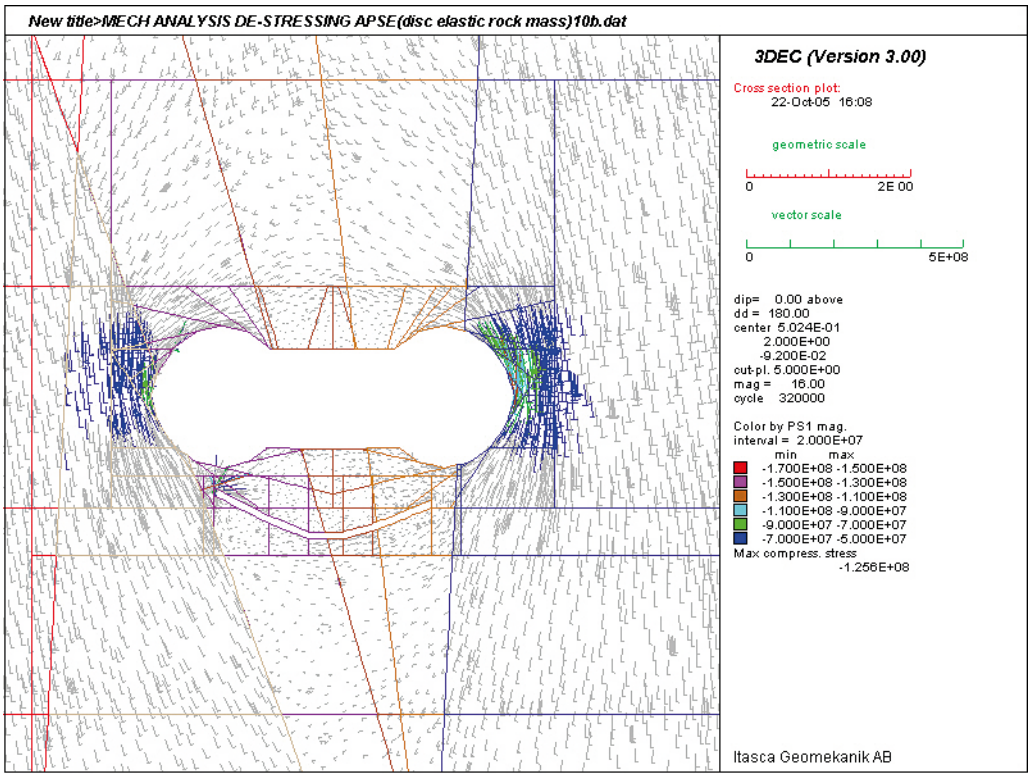

Figure A-14. *Horizontal cross-section showing the projected principal stress at 3 m depth from the floor of the APSE tunnel after the central pillar has been removed (Colors by magnitude of σ1).*

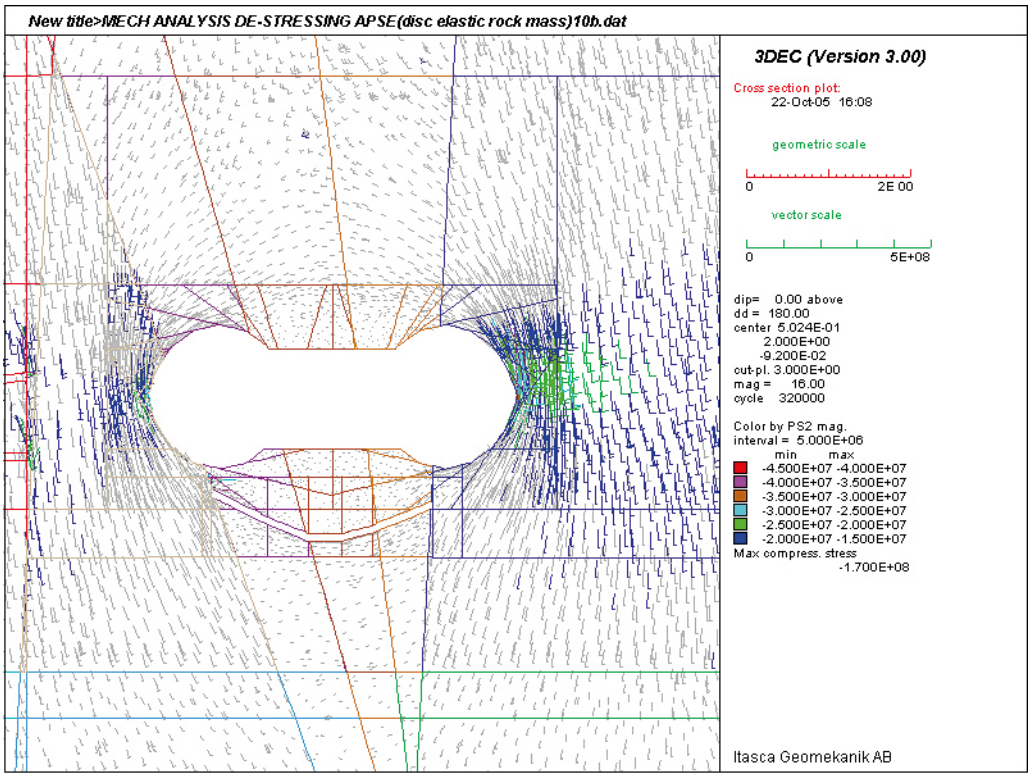

Figure A-15. *Horizontal cross-section showing the projected principal stress at 1 m depth from the floor of the APSE tunnel after the central pillar has been removed (Colors by magnitude of σ2).*

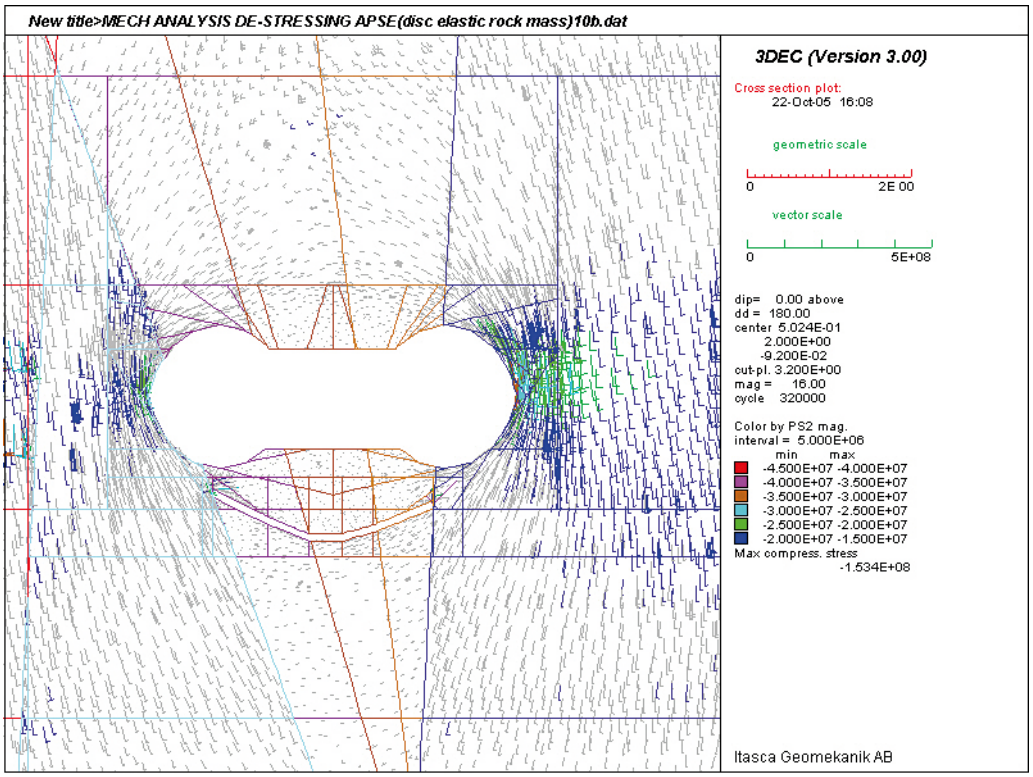

Figure A-16. *Horizontal cross-section showing the projected principal stress at 1.2 m depth from the floor of the APSE tunnel after the central pillar has been removed (Colors by magnitude of σ2).*

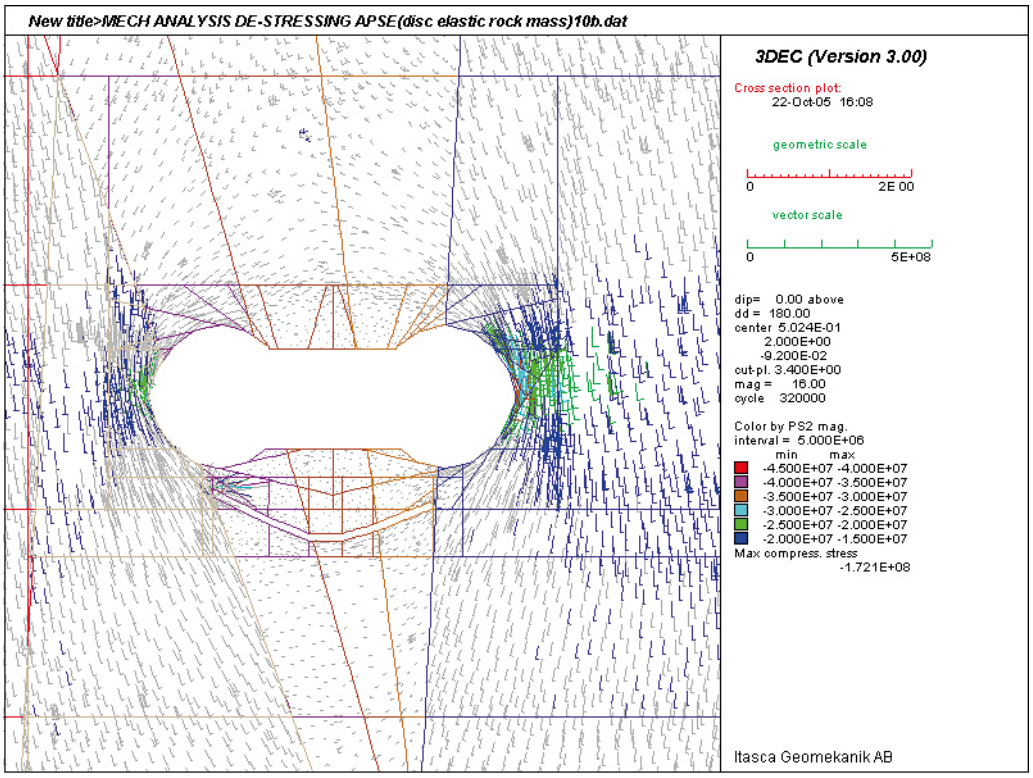

Figure A-17. *Horizontal cross-section showing the projected principal stress at 1.4 m depth from the floor of the APSE tunnel after the central pillar has been removed (Colors by magnitude of σ2).*

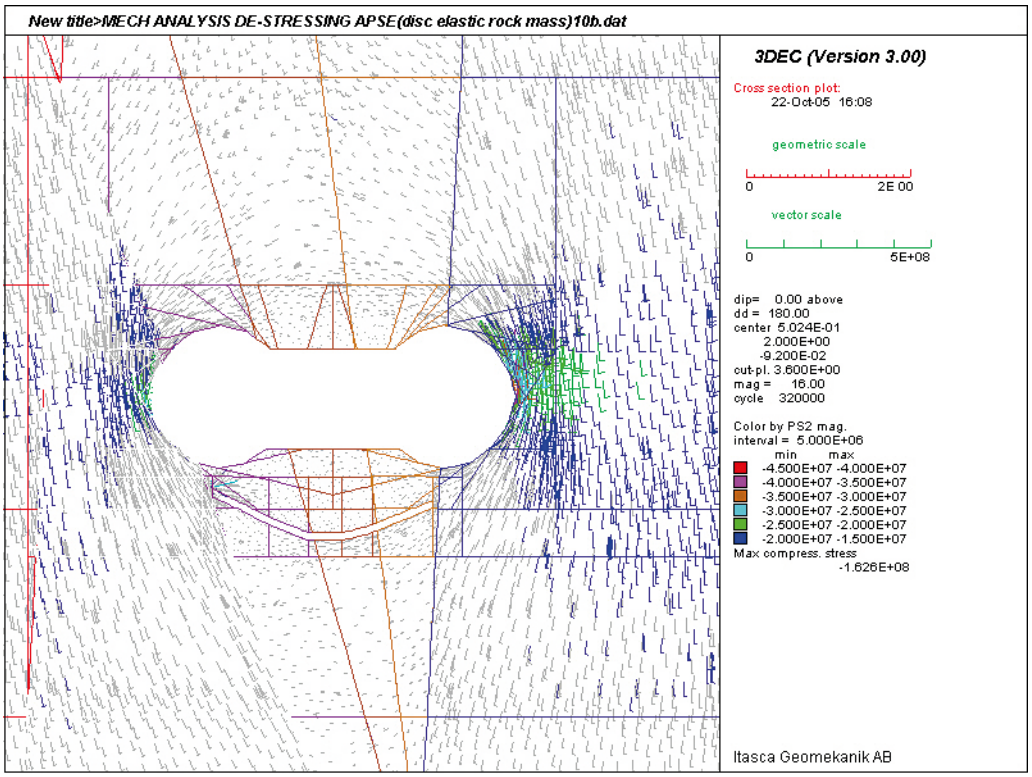

Figure A-18. *Horizontal cross-section showing the projected principal stress at 1.6 m depth from the floor of the APSE tunnel after the central pillar has been removed (Colors by magnitude of σ2).*

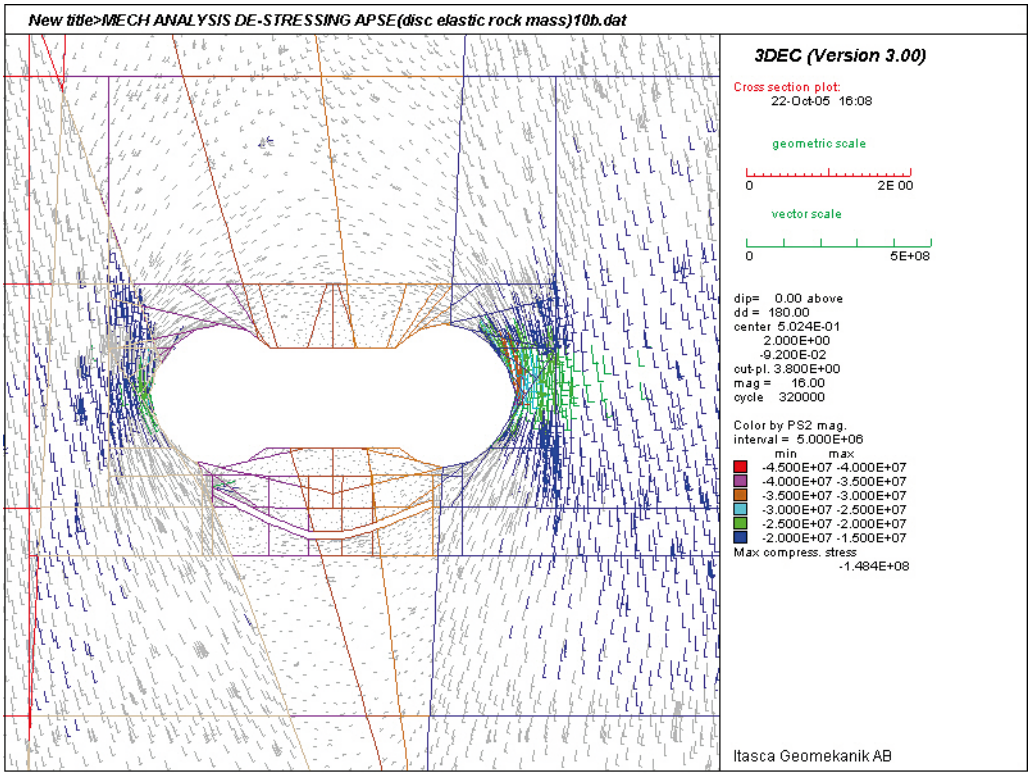

Figure A-19. *Horizontal cross-section showing the projected principal stress at 1.8 m depth from the floor of the APSE tunnel after the central pillar has been removed (Colors by magnitude of σ2).*

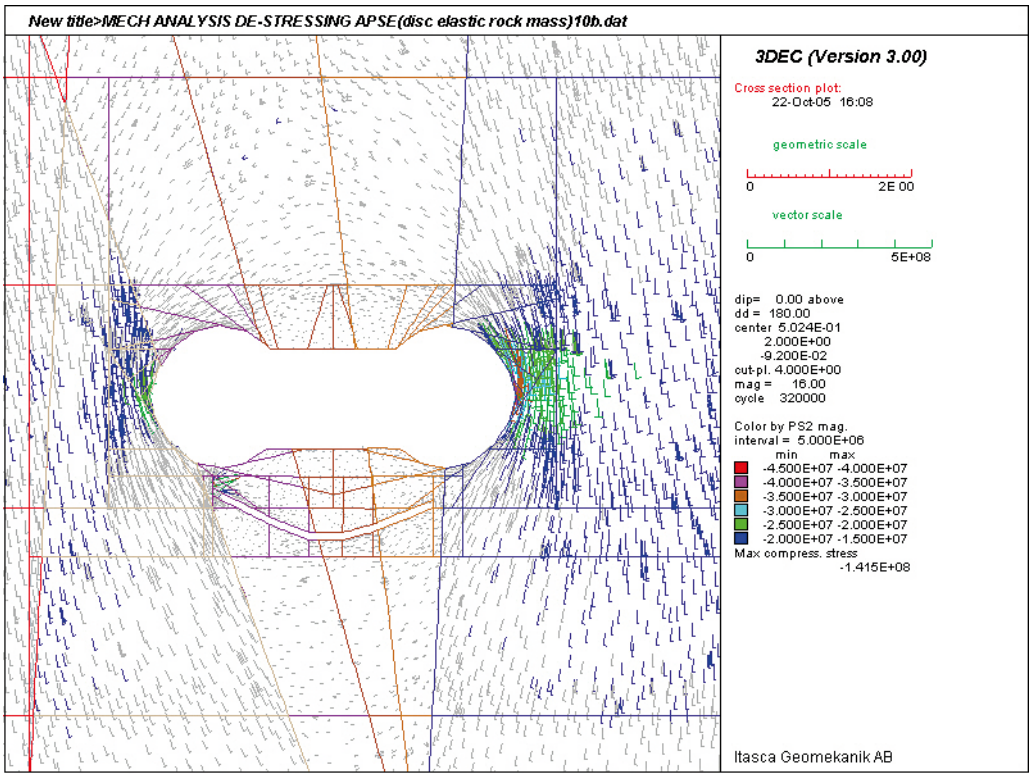

Figure A-20. *Horizontal cross-section showing the projected principal stress at 2 m depth from the floor of the APSE tunnel after the central pillar has been removed (Colors by magnitude of σ2).*

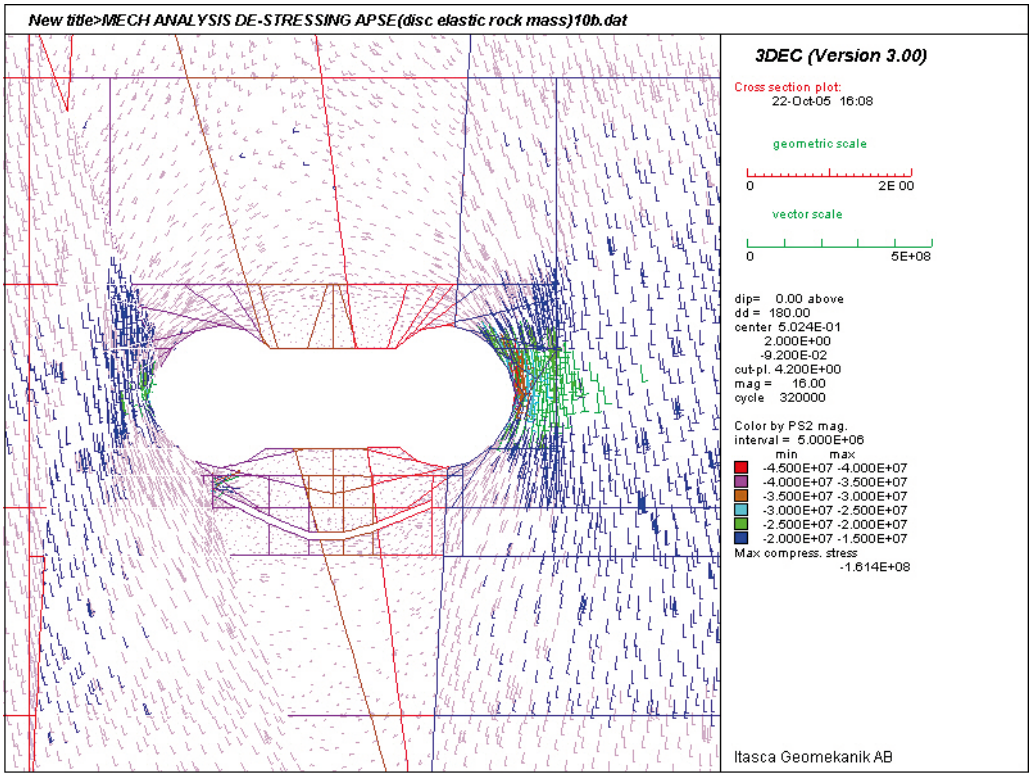

Figure A-21. *Horizontal cross-section showing the projected principal stress at 2.2 m depth from the floor of the APSE tunnel after the central pillar has been removed (Colors by magnitude of σ2).*

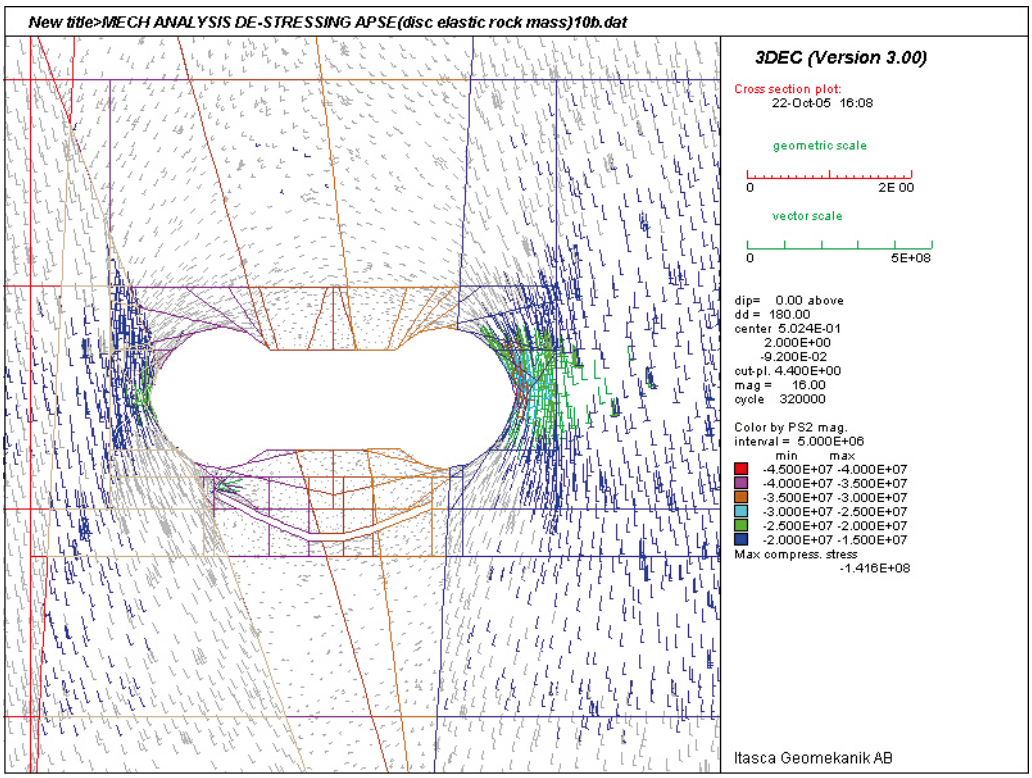

Figure A-22. *Horizontal cross-section showing the projected principal stress at 2.4 m depth from the floor of the APSE tunnel after the central pillar has been removed (Colors by magnitude of σ2).*

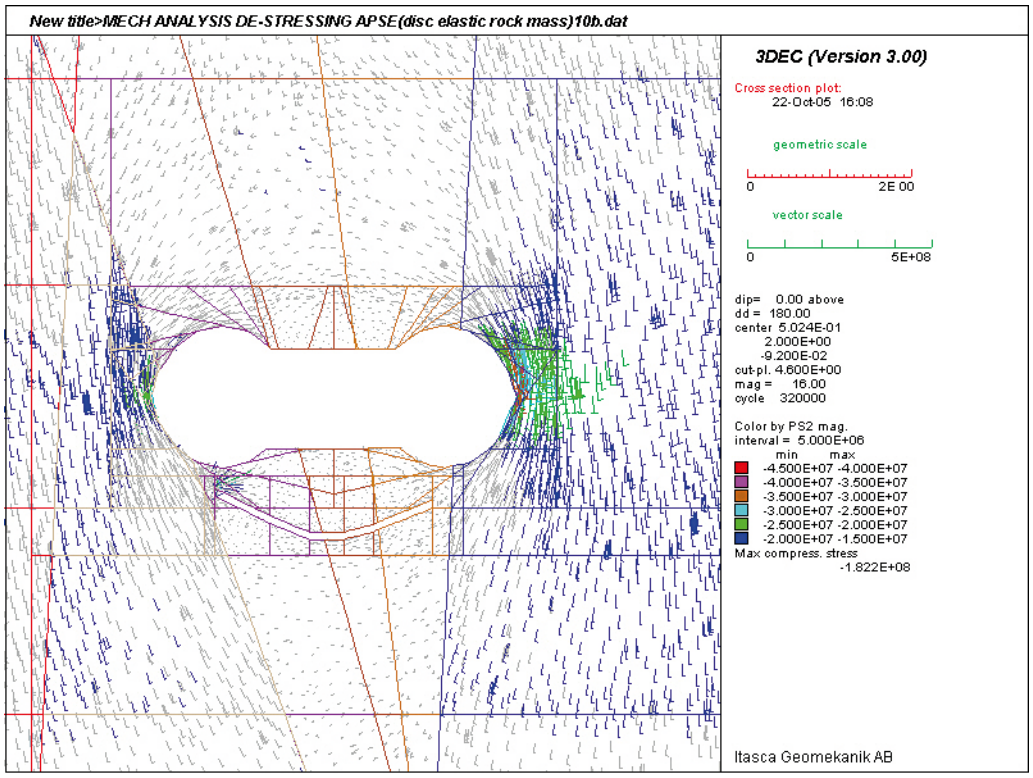

Figure A-23. *Horizontal cross-section showing the projected principal stress at 2.6 m depth from the floor of the APSE tunnel after the central pillar has been removed (Colors by magnitude of σ2).*

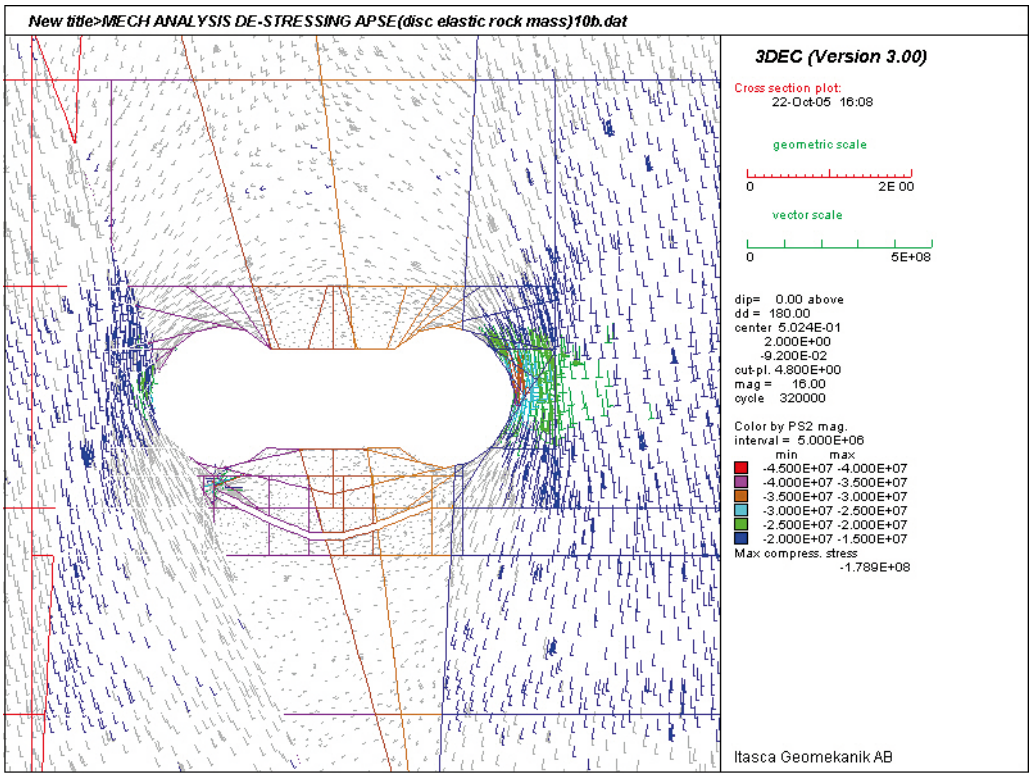

Figure A-24. *Horizontal cross-section showing the projected principal stress at 2.8 m depth from the floor of the APSE tunnel after the central pillar has been removed (Colors by magnitude of σ2).*

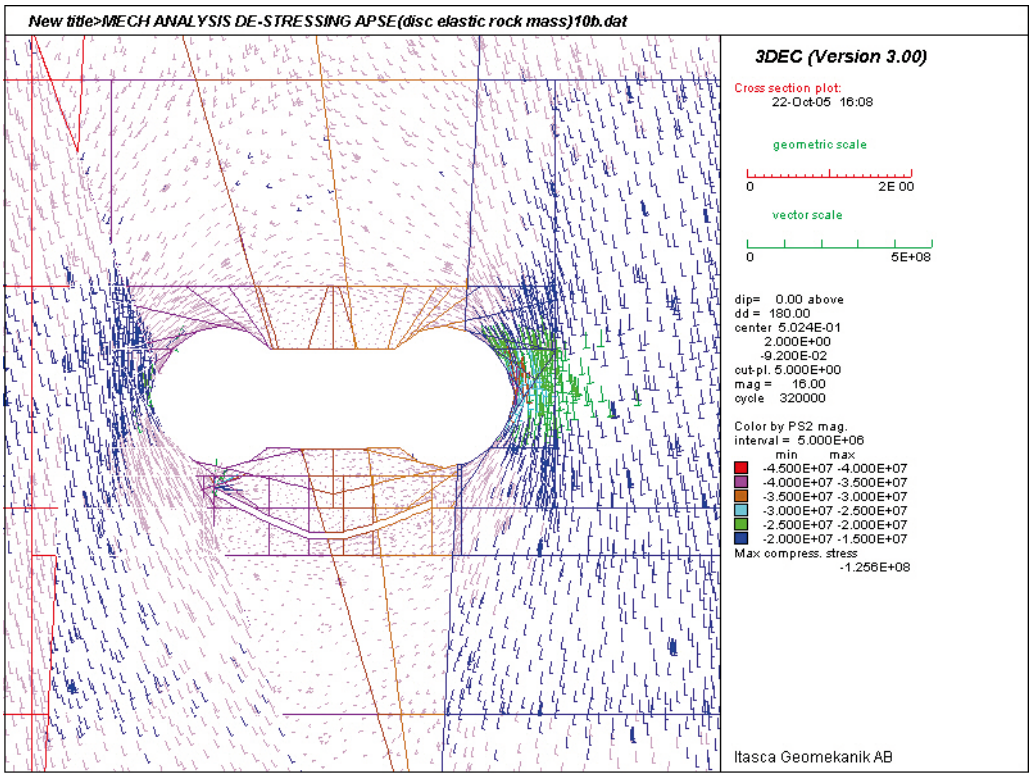

Figure A-25. *Horizontal cross-section showing the projected principal stress at 3 m depth from the floor of the APSE tunnel after the central pillar has been removed (Colors by magnitude of σ2).*

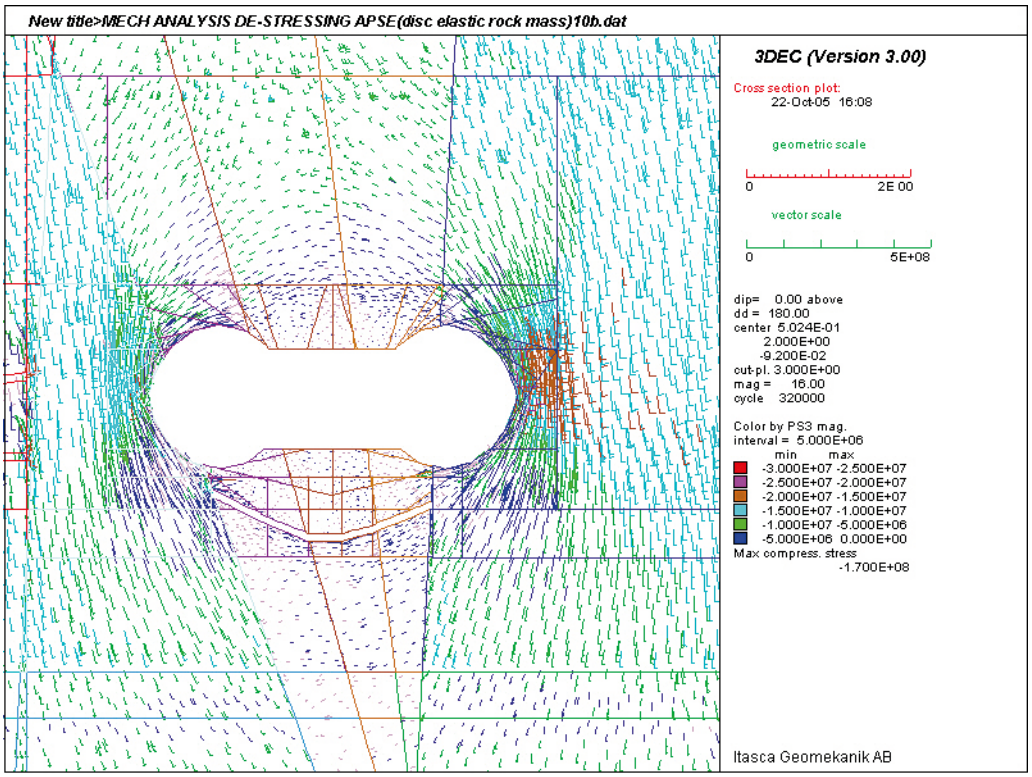

Figure A-26. *Horizontal cross-section showing the projected principal stress at 1 m depth from the floor of the APSE tunnel after the central pillar has been removed (Colors by magnitude of σ3).*

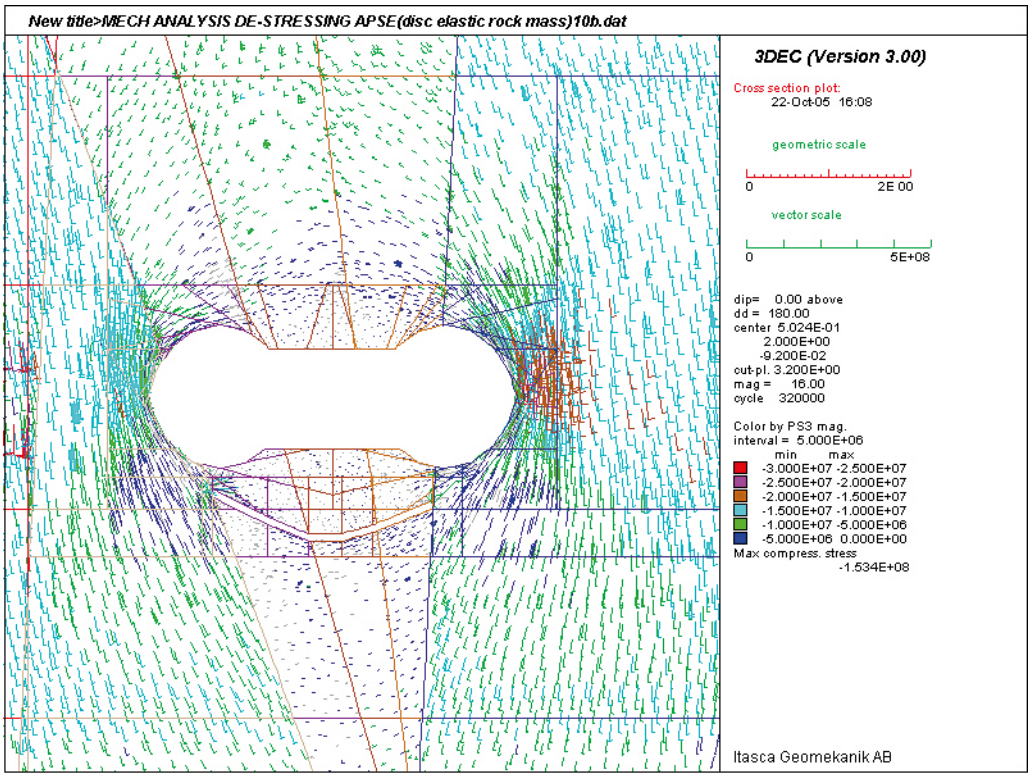

Figure A-27. *Horizontal cross-section showing the projected principal stress at 1.2 m depth from the floor of the APSE tunnel after the central pillar has been removed (Colors by magnitude of σ3).*

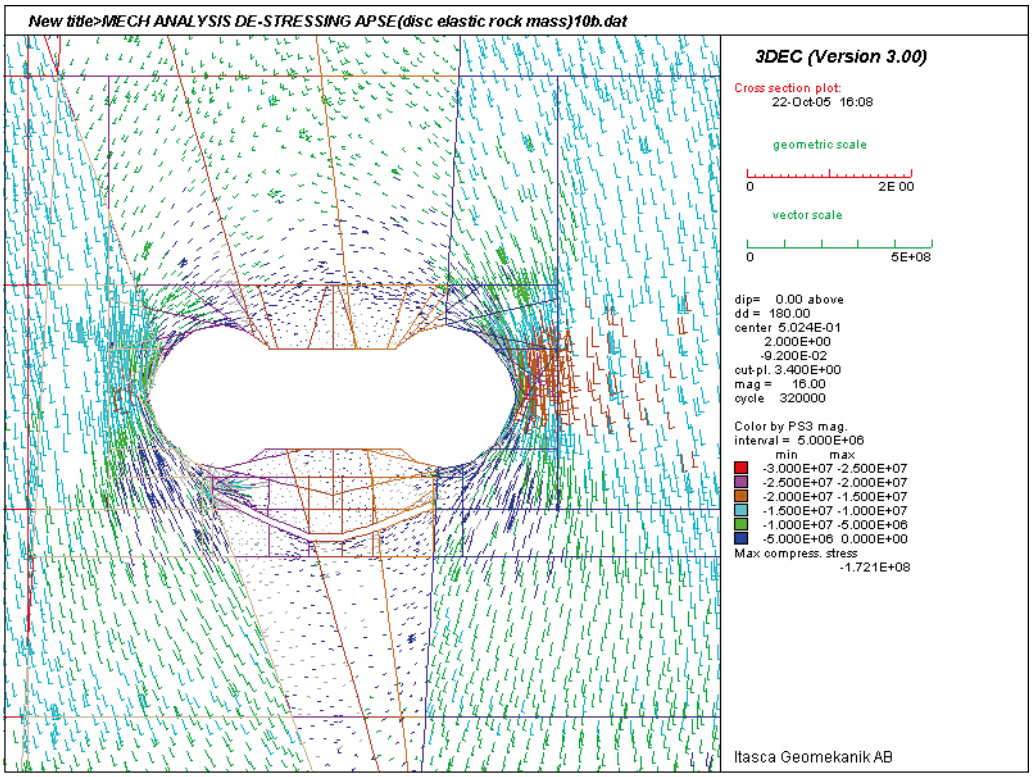

Figure A-28. *Horizontal cross-section showing the projected principal stress at 1.4 m depth from the floor of the APSE tunnel after the central pillar has been removed (Colors by magnitude of σ3).*

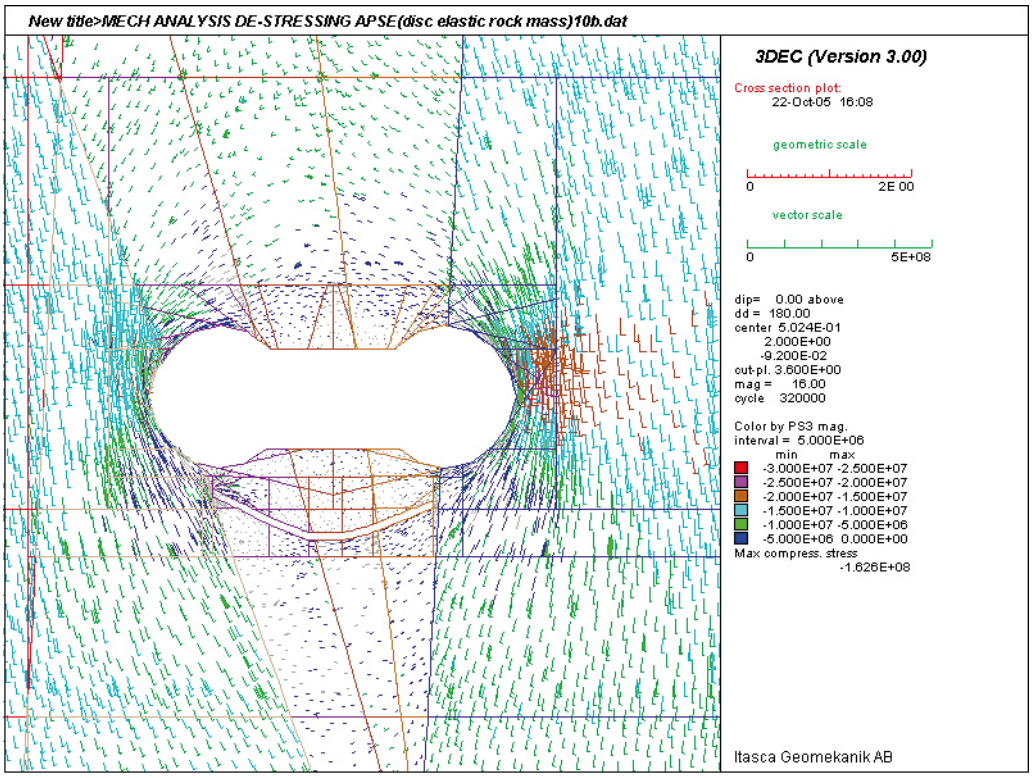

Figure A-29. *Horizontal cross-section showing the projected principal stress at 1.6 m depth from the floor of the APSE tunnel after the central pillar has been removed (Colors by magnitude of σ3).*

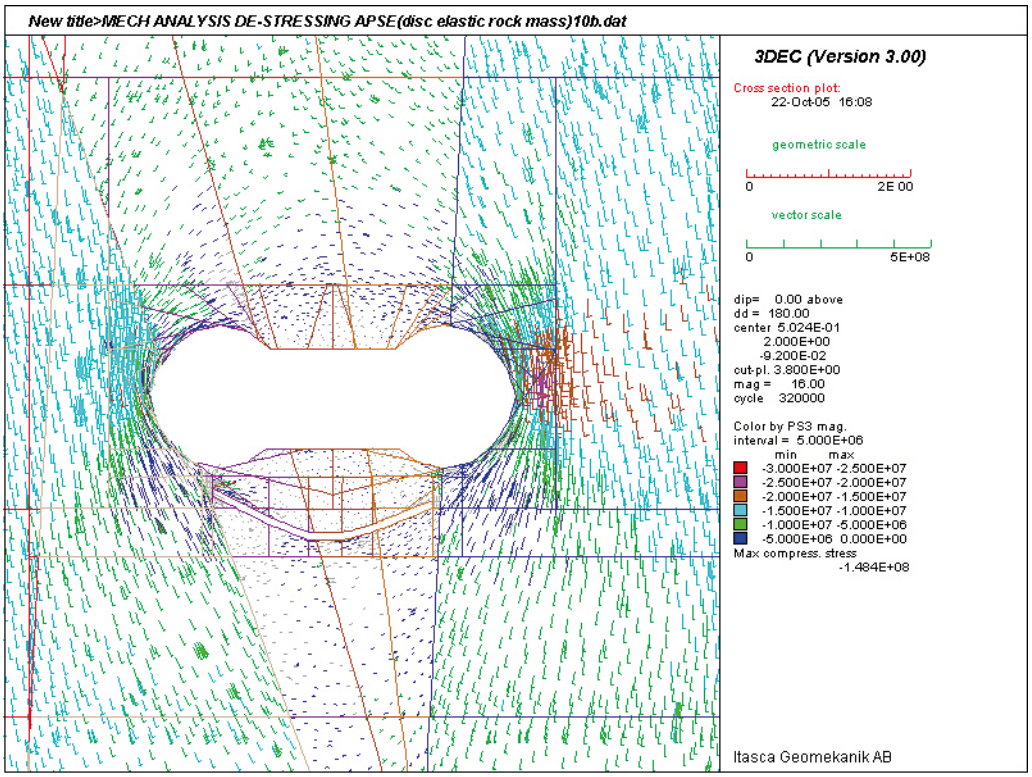

Figure A-30. *Horizontal cross-section showing the projected principal stress at 1.8 m depth from the floor of the APSE tunnel after the central pillar has been removed (Colors by magnitude of σ3).*

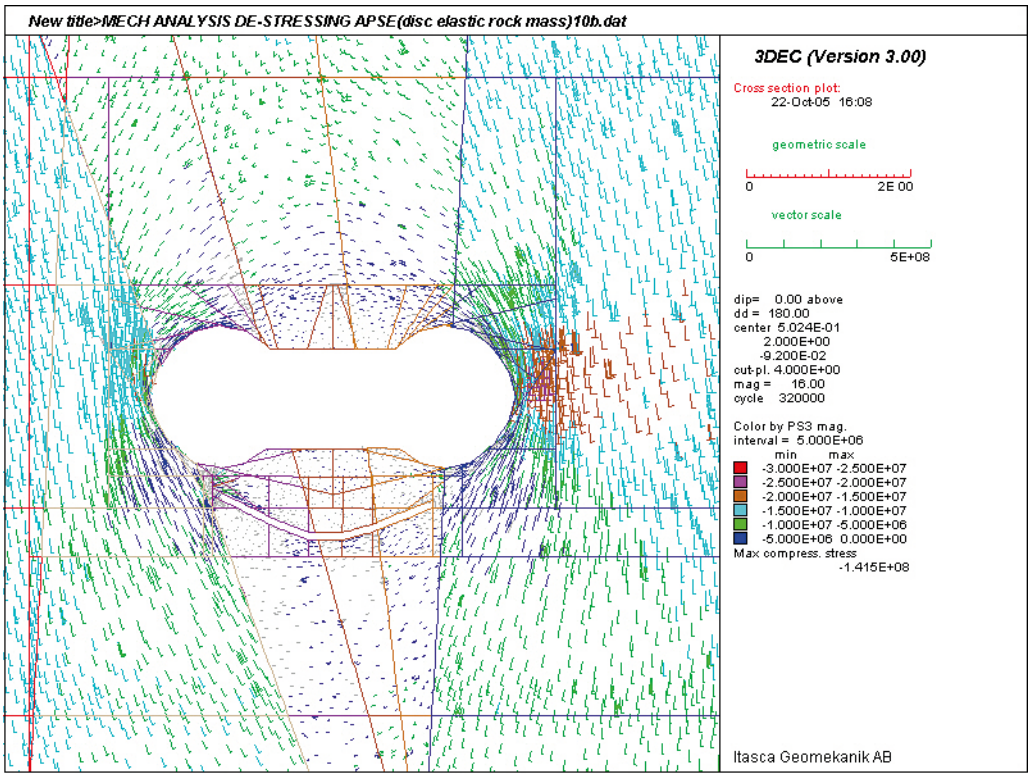

Figure A-31. *Horizontal cross-section showing the projected principal stress at 2 m depth from the floor of the APSE tunnel after the central pillar has been removed (Colors by magnitude of σ3).*

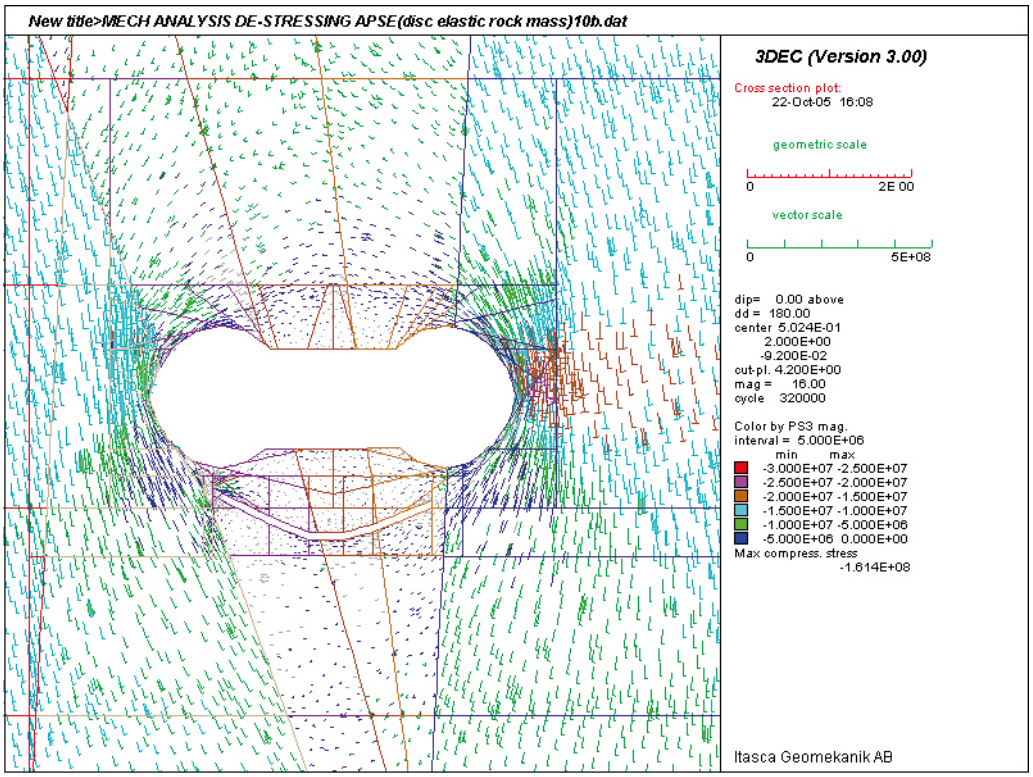

Figure A-32. *Horizontal cross-section showing the projected principal stress at 2.2 m depth from the floor of the APSE tunnel after the central pillar has been removed (Colors by magnitude of σ3).*

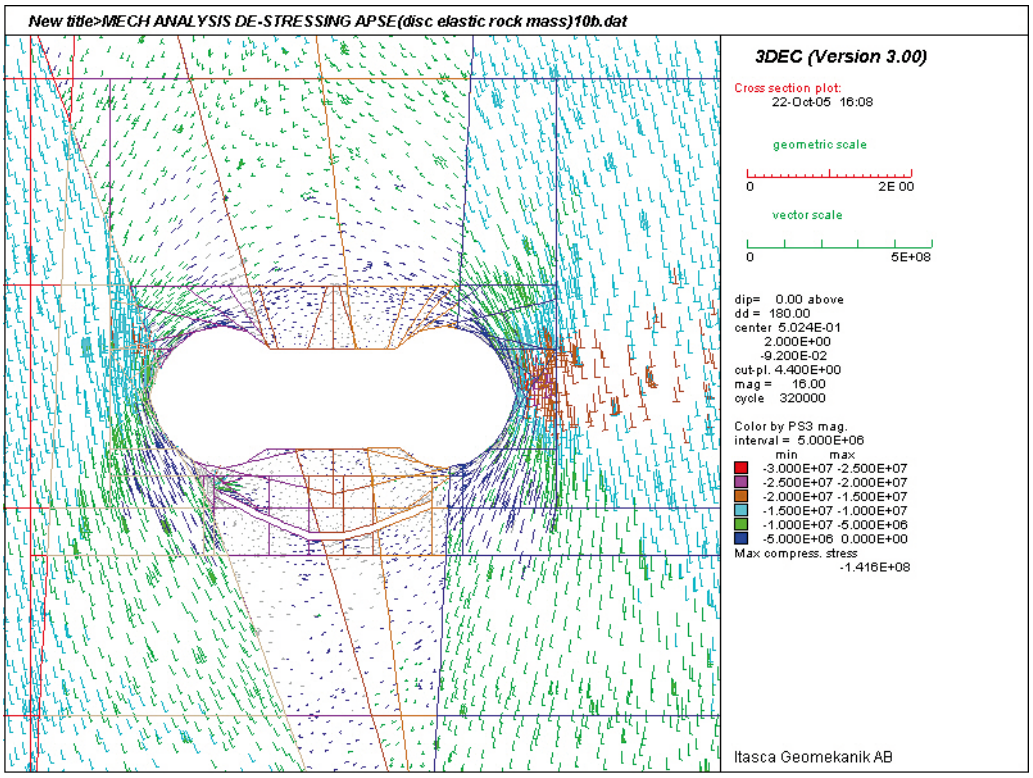

Figure A-33. *Horizontal cross-section showing the projected principal stress at 2.4 m depth from the floor of the APSE tunnel after the central pillar has been removed (Colors by magnitude of σ3).*

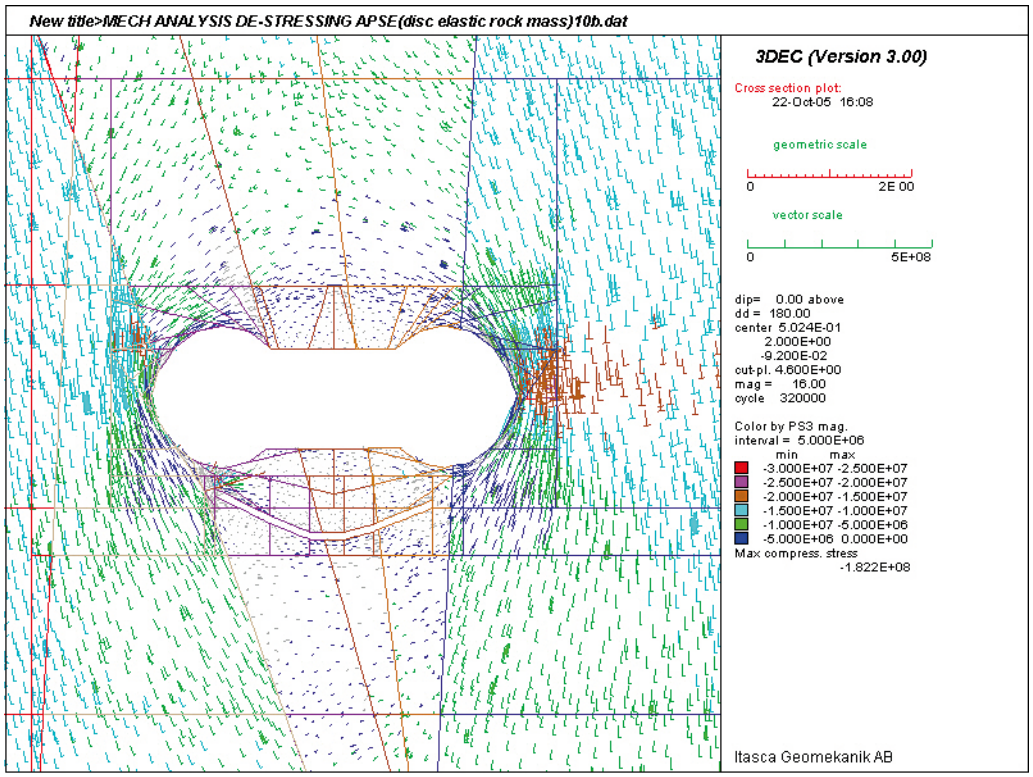

Figure A-34. *Horizontal cross-section showing the projected principal stress at 2.6 m depth from the floor of the APSE tunnel after the central pillar has been removed (Colors by magnitude of σ3).*

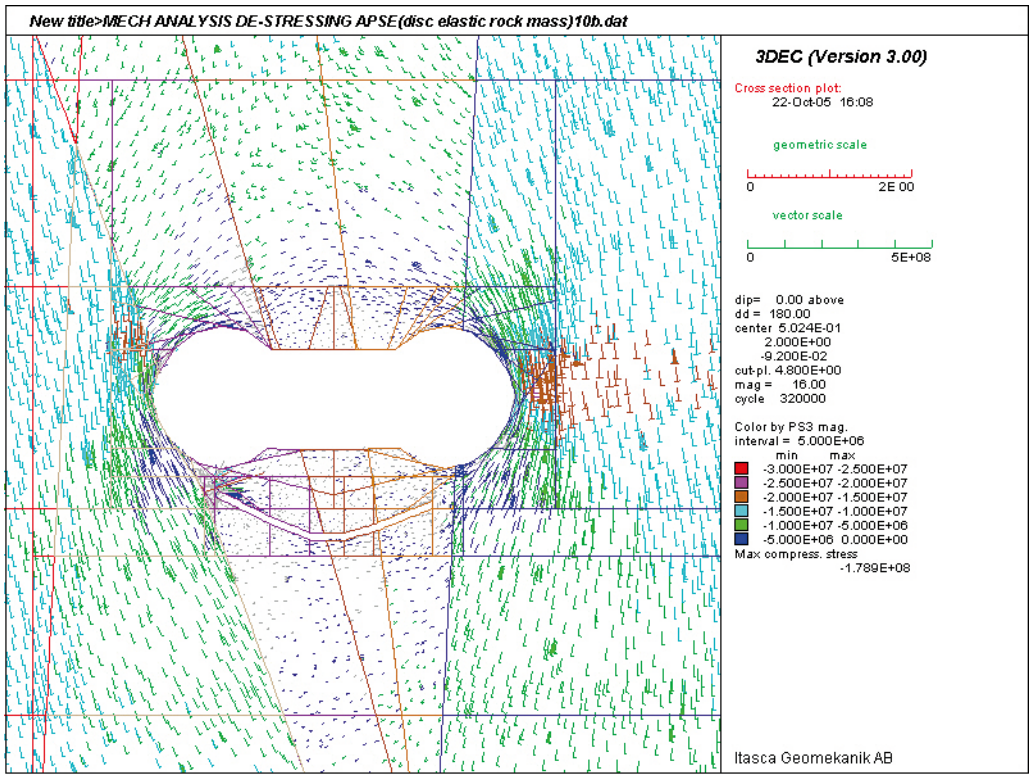

Figure A-35. *Horizontal cross-section showing the projected principal stress at 2.8 m depth from the floor of the APSE tunnel after the central pillar has been removed (Colors by magnitude of σ3).*

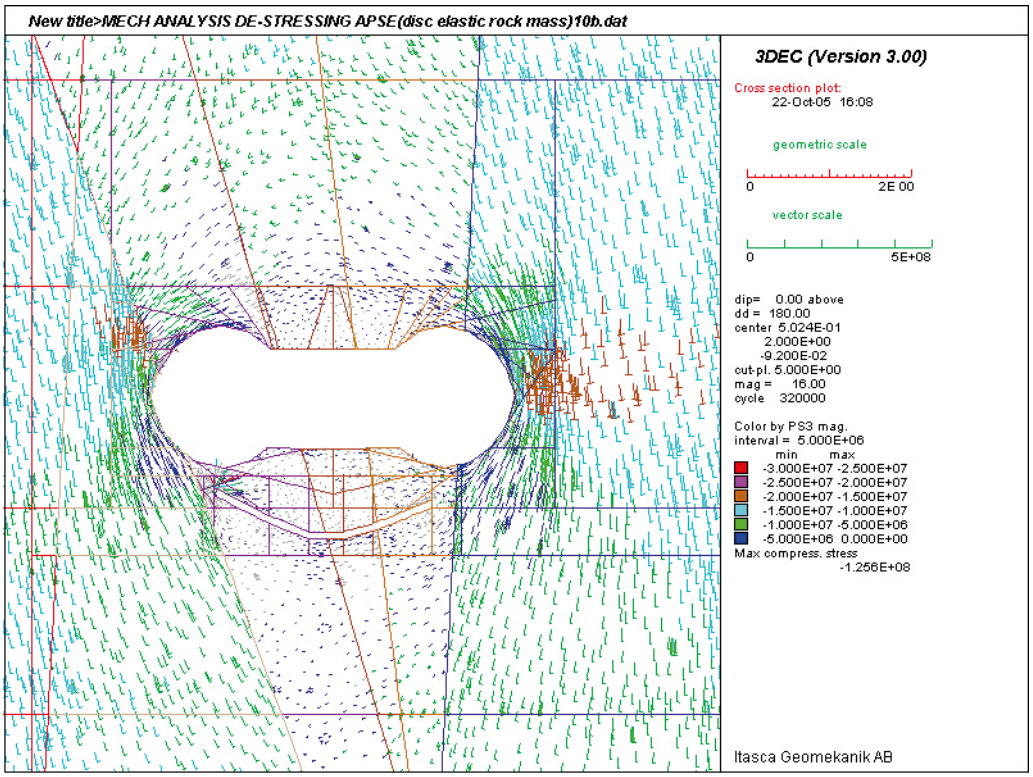

Figure A-36. *Horizontal cross-section showing the projected principal stress at 3 m depth from the floor of the APSE tunnel after the central pillar has been removed (Colors by magnitude of σ3).*

Arkitektkopia AB, Bromma, 2020

SKB is responsible for managing spent nuclear fuel and radioactive waste produced by the Swedish nuclear power plants such that man and the environment are protected in the near and distant future.

skb.se